



AALBORG UNIVERSITY
DENMARK

Aalborg Universitet

Optimal design of passive power filters for gridconnected voltage-source converters

Beres, Remus Narcis

DOI (link to publication from Publisher):
[10.5278/vbn.phd.engsci.00112](https://doi.org/10.5278/vbn.phd.engsci.00112)

Publication date:
2016

Document Version
Publisher's PDF, also known as Version of record

[Link to publication from Aalborg University](#)

Citation for published version (APA):
Beres, R. N. (2016). *Optimal design of passive power filters for gridconnected voltage-source converters*. Aalborg Universitetsforlag. <https://doi.org/10.5278/vbn.phd.engsci.00112>

General rights

Copyright and moral rights for the publications made accessible in the public portal are retained by the authors and/or other copyright owners and it is a condition of accessing publications that users recognise and abide by the legal requirements associated with these rights.

- Users may download and print one copy of any publication from the public portal for the purpose of private study or research.
- You may not further distribute the material or use it for any profit-making activity or commercial gain
- You may freely distribute the URL identifying the publication in the public portal -

Take down policy

If you believe that this document breaches copyright please contact us at vbn@aub.aau.dk providing details, and we will remove access to the work immediately and investigate your claim.

**OPTIMAL DESIGN OF PASSIVE POWER
FILTERS FOR GRIDCONNECTED
VOLTAGE-SOURCE CONVERTERS**

**BY
REMUS NARCIS BERES**

DISSERTATION SUBMITTED 2016



AALBORG UNIVERSITY
DENMARK

OPTIMAL DESIGN OF PASSIVE POWER FILTERS FOR GRID- CONNECTED VOLTAGE-SOURCE CONVERTERS

by

Remus Narcis Beres



AALBORG UNIVERSITY
DENMARK

Dissertation submitted

Dissertation submitted: May 24, 2016

PhD supervisor: Prof. Frede Blaabjerg
Aalborg University

Assistant PhD supervisor: Prof. Marco Liserre
Kiel University

PhD committee: Associate Professor Tomislav Dragicevic (chairman)
Aalborg University, Denmark

Dr. Vladimir Blasko
United Technologies Research Center, USA

Professor Detlef Schulz
Helmuth-Schmidt-Universität, Germany

PhD Series: Faculty of Engineering and Science, Aalborg University

ISSN (online): 2246-1248
ISBN (online): 978-87-7112-712-6

Published by:
Aalborg University Press
Skjernvej 4A, 2nd floor
DK – 9220 Aalborg Ø
Phone: +45 99407140
aauf@forlag.aau.dk
forlag.aau.dk

© Copyright: Remus Narcis Beres

Printed in Denmark by Rosendahls, 2016

ACKNOWLEDGEMENTS

This thesis is part of the Harmony project, which is a 5 year project founded by the European Research Council, under the guidance and supervision of Prof. Frede Blaabjerg. The main focus of the project is the harmonic identification, mitigation and control in power electronics based power systems. A small part of the project is related to the passive filter design for power electronics based systems under the nomenclature “Optimal Design of Passive Power Filters for Grid-Connected Voltage-Source Converters”, which I have been responsible for.

With this occasion, I would like to thank everyone who contributes to the outcome of this thesis in one way or another. Especially, I want to express my deepest gratitude for my supervisor Prof. Frede Blaabjerg who always find the patience and gave me continuously guidance and support for the three year period.

Prof. Claus Leth Bak, who proposed me to the Cigre working group C4/B4.38 on network modeling for harmonic studies, where I have learnt a lot about passive filter design from a system level perspective. I want to thank him for his positive remarks, not only about my work, but also life in general.

For Prof. Marco Liserre, who was the initiator of my project and as a supervisor, gave me the opportunity to work in such an interesting and developing topic, that of the passive filter design.

Greetings to all Harmony members for many fruitful discussions, especially to Xiongfei Wang, Jun Bum, Miquel (for his programming skills and his friendship), Min Huang, Esmail, Haofeng and so on.

I would like to thank Prof. Toshihisa Shimizu, which welcomed me to his laboratory. He has been like a spiritual father to me, always showing support and interest in my research topic and life. Very good memories I shared also with his student Hiroaki Matsumori. Also not to forget about Prof. Keji Wada or Mr. Bizen, who helped me to replace many MOSFETs, which I have broken many times during my experimental measurements.

I am grateful to all staff and people at Department of Energy Technology. Especially, Prof. Remus Teodorescu, Tamas Kerekes, Dezso Sera and Sergiu Spataru, who helped me to develop as an individual during my master studies. I also want to mention Hamid, Gohil (for his valuable comments in improving the thesis), Amir, Cristian Santamarean, Cristian Busca and Adrian Hasmasan, which I will never forget. For Anna Miltersen and Casper Jørgensen, who gave me the opportunity to enjoy good times at the Amsterdam marathon.

I want to thank Prof. Mihai Cernat for his support during my BSc studies. He also guided me towards a PhD degree, from early days. I want to thank Prof. Corneliu Marinescu for the projects we have been working together.

At last but not least, I want to thank my closest friends who I made during the PhD period, Changwoo Yoon and his increasing family, Casper Vadstrup, Catalin Ciontea and Ionela Grigoras. we shared many good times together, not only at the university, but also outside the university.

I would like to thanks my family, which always encouraging me to do my best, with positive advice, supporting me and my choices in life.

To my very dear fiancé Celina, who always gave me support and tried to decouple me from the academic life. Once she told me that there is some kind of resonance between us. From my point of view, resonance is needed, not only in passive filters to save size and cost, but also in real life, to make things more beautiful and interesting. Anatol I. Zverev, known as one who “actually design filters that worked in practice” was repeating many times to his friends:

“... the whole world is a filter”

ENGLISH SUMMARY

Passive filters are a key component, which links power electronics based generation or electrical loads with the power system. For example, a voltage-source converter needs an output filter inductor in order to be able to be operated and controlled. The size of the inductance dictates the amount of current harmonics and thereby influence on the cost, size and efficiency of the overall converter system. A very large inductance, results in an efficient, but a bulky and costly passive filter. On the other hand, a lower inductance implies increased power losses (as a result of increased harmonic current), but at reduced size and cost. However, it became difficult to comply with harmonic regulations by simply adopting a filter inductor. Therefore, an additional inductive-capacitive low pass filter can be adopted with the aim of reducing the high frequency ripple corresponding to the switching device operation. Such filter structure is known as the *LCL* filter. In summary, a voltage-source converter produces current harmonics which causes voltage drops across the system impedances, resulting in increased levels of voltage distortions.

Proper performance specifications of voltage distortion limits has a consequent impact on the passive filter design. Stringent harmonic specifications could demand for bulky and costly passive filters, while more permissible specifications could turn into harmonic stability problems, as result of not sufficient filtering and reduced damping. Harmonic stability problems are caused by series and parallel resonances that exist in the passive filters and the grid impedance. It is found that the inappropriate selection of the passive filter parameters and the processing delay in the control system are the key aspects that may lead to harmonic instability.

To optimize the output behavior of the converter with the aim of reduced risk of harmonic interactions between the converter and the grid impedance, the passive filter design is investigated from the component to the system level. It is found that the main losses in a high-order passive filter, occurs in the converter side inductor. Different magnetic materials are evaluated, which reveals that significant losses may occur, especially under high current ripple condition. The high-ripple condition is found predominantly in optimized filters with low rated filter inductors. A careful selection of the core materials is needed in this situation. However, these aspects are related to the performance specification of the converter and the passive filter.

At the system level, high-order passive filters have detrimental effects due to their inherent resonant behavior for specific frequencies. And the resistive damping from the filter or control system is often ignored or disregarded when designing passive filters. Then, the loss information of the filter inductors are used to account more optimally for the inherent damping that exist in the filter. An optimized passive damping design method is proposed which offers optimal damping (minimum resonance) with reduced rating of passive components and consequently reduced

power losses. Under certain situations, it is possible to design a stable converter without any damping, by proper selection of the filter resonance frequencies. To establish a robust system, it is possible to do so with low rated and low loss passive components.

DANSK RESUME

Passive filtre er en central komponent, der forbinder effektelektronik baserede generatorer eller elektriske belastninger med elsystemet. For eksempel har en spændingskildekonverter behov for en udgangsfilterspole for at kunne fungere og styres. Størrelsen af induktansen dikterer mængden af harmoniske strømme og har derved indflydelse på omkostningerne, størrelsen og effektiviteten af det samlede konvertersystem. En meget stor induktans resulterer i et effektivt, men også omfangsrigt og dyrt passivt filter. På den anden side betyder en lavere induktans et øget effekttab (som følge af øget harmoniske strøm), men med reduceret størrelse og pris. Men blev det vanskeligt at overholde de harmoniske regler ved blot at anvende en filterspole. Derfor kan et ekstra induktiv-kapacitiv lavpasfilter anvendes med henblik på at reducere den højfrekvente ripple, der kommer fra de switchende komponenter. Sådant filter struktur er kendt som et LCL filter. Kort fortalt, en spændingskilde konverter producerer strømharmoniske der forårsager spændingsfald over systemets impedanser, hvilket resulterer i forhøjede niveauer af spændingsforvridninger.

Korrekte specifikationer af spændingsforvrængnings grænser har en konsekvens for det passive filters design. Strenge harmoniske specifikationer kan kræve for pladskrævende og dyre passive filtre, mens flere tilladte specifikationer kan udvikle sig til harmoniske stabilitetsproblemer, som følge af en ikke tilstrækkelig filtrering og reduceret dæmpning. Harmoniske stabilitetsproblemer er forårsaget af serier og parallelle resonanser, der findes i de passive filtre og i elnettets impedans. Det konstateres, at den u hensigtsmæssige udvælgelse af de passive filterparametre og procesforsinkelse i kontrolsystemet er de vigtigste aspekter, der kan føre til harmonisk ustabilitet.

For at optimere outputtet opførsel af konverteren med henblik på at reducere risikoen for harmonisk interaktioner mellem konverteren og elnettet impedans, er det passive filter design undersøgt fra komponent til systemniveau. Det konstateres, at de primære tab i et højere ordens passivt filter, forekommer i konverter sidens spole. Forskellige magnetiske materialer evalueres, hvilket afslører, at betydelige tab kan forekomme, især under højt strømrripple tilstand. Den høje ripple tilstand findes overvejende i optimerede filtre med lave nominel størrelse filter spoler. Der er behov for en omhyggelig udvælgelse af de centrale materialer i denne situation. Men disse aspekter er relaterede til kravspecifikation af konverteren og det passivt filter.

På systemniveau, høj-ordens passive filtre har negative virkninger på grund af deres indbyggede resonans adfærd overfor bestemte frekvenser. Derefter er tabsoplysningerne af filterspolerne brugt til mere optimalt at tage højde for den indbyggede dæmpning, der findes i filteret. Der foreslås en optimeret passiv dæmpet designmetode, som giver optimal dæmpning (minimum resonans) med reduceret

nominel størrelse af passive komponenter og dermed reduceret effekttab. Under visse situationer er det muligt at designe en stabil konverter uden nogen dæmpning, ved passende valg af filter resonansfrekvenser. Det er muligt at etablere et robust system med passive komponenter, der har lave nominelle værdier og med lavt tab.

TABLE OF CONTENTS

Chapter 1. Introduction.....	1
1.1. Project Motivation.....	1
1.2. Background to Harmonic Filtering	2
1.2.1. System Damping	2
1.2.2. Harmonic Filtering	2
1.2.3. Passive Filters for VSC	3
1.2.4. Issues with Passive Filters in VSC.....	4
1.2.5. Previous Contributions to the Research Topic	5
1.3. Problem Formulation	6
1.4. Research Objectives	7
1.5. Limitations	8
1.6. Thesis Outline	8
1.7. List of Publications	10
Chapter 2. Specifications and Requirements for Harmonic Filters Design	13
2.1. System Description	13
2.2. Harmonic Specifications at PCC.....	14
2.2.1. Harmonic Standards	14
2.2.2. Measurement of Harmonics	15
2.3. VSC Characterization.....	16
2.3.1. Harmonic Spectrum from PWM	16
2.3.2. VSC Operation Mode.....	18
2.3.3. Influence of the Measurement Sensors	19
2.4. A.C. Grid Characterization	20
2.4.1. Grid Specifications.....	20
2.4.2. Worst Case Harmonic Grid Impedance.....	21
2.4.3. Grid Impedance Modelling	22
2.5. Virtual Admittance of Harmonic Filters	24
2.6. Summary	26

Chapter 3. Characterization of Passive Filter Topologies	27
3.1. Design Considerations of Passive Filters	27
3.2. Passive Filters for VSC	28
3.2.1. Classification of Passive Filters	28
3.2.2. Frequency Response of Passive Filters	29
3.3. Damping Considerations	32
3.3.1. Shunt Passive Damped Filters for the <i>LCL</i> Filter	32
3.3.2. Shunt Passive Damped Filters for the <i>Trap</i> Filter	34
3.3.3. Series Passive Damped Filters	36
3.4. Impedance Characterization of Passive Components	36
3.4.1. Equivalent Models of Passive Components	37
3.4.2. Impact of the Inductor Model on the Frequency Response of the Passive Filter	37
3.5. Summary	39
Chapter 4. Characterization of Inductive Components	41
4.1. Introduction	41
4.2. Characterization of Magnetic Materials	43
4.2.1. Overview of Magnetic Materials	43
4.2.2. Bias Characteristics of Inductors	44
4.2.3. Energy Storage Capability of Inductors	45
4.3. Design and Description of AC Inductors	47
4.3.1. Converter Side Inductors	47
4.3.2. Shunt Inductor	49
4.3.3. Series Inductor	50
4.4. Evaluation of Core Losses in PWM Converters	50
4.4.1. Description of the Measurement Method	50
4.4.2. Core Losses under Sinusoidal Excitation	51
4.4.3. Core Losses under Rectangular Excitation without DC Bias	53
4.4.4. Core Losses under Rectangular Excitation and DC Bias	53
4.5. Specific Inductor Design	55
4.5.1. Inductor Specifications	55
4.5.2. Loss Map of the Magnetic Materials	56

4.5.3. Evaluation of Power Loss in Inductors	56
4.6. Summary	60
Chapter 5. Parameter Selection and Optimization of High-Order Passive Damped Filters	61
5.1. Stability Considerations of Grid-Connected VSC with <i>LCL</i> Filter	61
5.1.1. Generalized Stability Regions for High-Order Passive Filters.....	62
5.1.2. VSC Output Admittance	64
5.2. Conventional and Optimal <i>LCL</i> Filter Design	67
5.2.1. Conventional <i>LCL</i> Filter Design	67
5.2.2. Optimal <i>LCL</i> Filter Design with Minimization of the Stored Energy....	68
5.2.3. Experimental Results	70
5.3. Optimal Design of <i>Trap</i> Filters	71
5.3.1. Conventional Design of the Individual Traps based on the Trap Quality Factor	71
5.3.2. Improved Design Method based on Individual Functions of the Multi-Split Capacitors	73
5.4. Optimal Design of Passive Dampers.....	76
5.4.1. Proposed Design Method	76
5.4.2. Robust Passive Damping Design	78
5.4.3. Loss Optimized Passive Damping Design	81
5.5. Improved Passive Damped Trap Filter.....	83
5.5.1. Operating Principle of the Proposed Filter.....	84
5.5.2. Design of the Proposed Passive Damped Filter	85
5.6. Summary	86
Chapter 6. Conclusions	89
6.1. Summary	89
6.2. Main Contributions	90
6.3. Future Work	91
References.....	93
Appendices.....	105

TABLE OF FIGURES

Figure 1.1: The end feeder of a distribution benchmark used for integration of distributed energy resources in the utility grid [15].	3
Figure 1.2: Single-phase diagram of a grid-connected VSC with LCL filter.	4
Figure 2.1: One phase schematics of a grid-connected VSC with a generalized passive filter.	13
Figure 2.2: One phase simulated waveforms for a two-level three-phase VSC with $m_f = 21$ and $m_a = 0.9$ for SPWM and $m_a \sim 1$ for SVM and THI-PWM: (a) Pulse generation; (b) Line to line VSC output voltage for THI-PWM; (c) Voltage harmonic content.	17
Figure 2.3: Four quadrant capability of a VSC.	18
Figure 2.4: Vector diagram of the VSC for different operating conditions: (a) Inverter mode with PF = 1; (b) Rectifier mode with PF = -1; (c) Capacitive reactive power support with PF = 0; (d) Inductive reactive power support with PF = 0.	18
Figure 2.5: Vector diagram of the VSC in inverter operation mode for different positions of the measurement sensors [50]: (a) Voltage sensed on the PCC and current sensed on the grid side; (b) Voltage sensed on the filter capacitor and current sensed on the grid side; (c) Voltage sensed on the PCC and current sensed on the converter side; (d) Voltage sensed on the filter capacitor and current sensed on the converter side.	19
Figure 2.6: One phase schematics of a grid-connected VSC with passive filter (model valid above the fundamental frequency).	20
Figure 2.7: Network impedance envelopes modeled by: (a) Discrete polygons; (b) Circle diagrams [52].	23
Figure 2.8: Filter virtual admittance for $m_f = 21$ and $m_a = 0.9$ for: (a) VDE-4105 standard; (b) IEEE 519 standard.	24
Figure 2.9: Filter virtual admittance for $m_f = 201$ and $m_a = 0.9$ for: (a) 0.3 % individual harmonic current limit (IEEE 519-1992 standard); (b) 0.05 % limit (BDEW standard).	25
Figure 3.1: Conventional passive filters used in grid-connected VSCs: (a) Single inductance (L filter); (b) Second-order low pass (LC filter); (c) Third-order low pass (LCL filter); (d) Shunt trap configuration (LLCL filter); (e) Series trap configuration.	28
Figure 3.2: Four-terminal network of high-order passive filters [29].	29
Figure 3.3: Transfer admittance Y_{21} of conventional passive filters used in grid-connected VSCs, provided the same ratings of passive components with $f_0=2.5$ kHz and $f_r=10$ kHz.	31
Figure 3.4: Configuration of passive dampers in high-order filters: (a) Shunt configuration; (b) Series configuration.	32
Figure 3.5: Shunt passive damped filters in LCL configuration: (a) Series resistor R; (b) Shunt RC damper (first order); (c) Shunt RLC damper (second order); (d) Series RLC damper (resonant damper); (e) Third-order damper; (f) Single tuned damper.	33

Figure 3.6: Transfer admittance Y_{21} of the LCL filter with shunt passive dampers, providing the same ratings of passive components and $f_0 = 2.5$ kHz.	34
Figure 3.7: Shunt passive damped filters in trap configuration: (a) Shunt RC damper for one trap; (b) Shunt RC damper for two traps; (c) C-type damper; (d) 2 single tuned dampers; (e) Double tuned damper.	35
Figure 3.8: Transfer admittance Y_{21} of the trap filter with shunt passive dampers, provided the same ratings of passive components with $f_0 \approx 4$ kHz and $f_r = 10$ kHz.	35
Figure 3.9: Series passive damped filters in LCL configuration: (a) Shunt resistor; (b) Shunt RL damper.....	36
Figure 3.10: Equivalent models of passive components: (a) resistors; (b) inductors; (c) capacitors [78].	37
Figure 3.11: Inductor characterization: (a) Inductance dependence with current where L_{rated} is 1.7 mH (Inductor 1), 1.8 mH (Inductor 2), 3.9 mH (Inductor 3) and 1 mH (Inductor 4); (b) Frequency dependence of the winding resistance, where R_{rated} is 1.9 Ω (Inductor 1), 1.65 Ω (Inductor 2), 1.65 Ω mH (Inductor 3) and 0.6 Ω (Inductor 4) at 2.5 kHz.....	38
Figure 3.12: Influence of the actual winding resistance and variable inductance on the frequency response of the LCL filter.	39
Figure 4.1: Characterization of inductors in grid-connected VSC with high-order filters.	41
Figure 4.2: B-H dependence of laminated Fe-Si and Fe powder, measured with 50 Hz sinusoidal excitation.	44
Figure 4.3: Dc bias characteristics of magnetic materials measured with a Magnetic Precision Analyzer PMA 3260B: (a) Laminated steel, amorphous and ferrite materials; (data not available in datasheets); (b) Powder materials with distributed gap (within ± 10 % deviation from the datasheet values).	45
Figure 4.4: Buck chopper circuit for core loss measurement with a B-H analyzer SY-8232 [21].	51
Figure 4.5: Operating waveforms for core loss measurement: (a) Inductor waveforms in dc chopper circuit; (b) Major hysteresis loop due to low frequency sinusoidal excitation voltage (blue line) and dynamic minor loop due to high frequency rectangular excitation voltage (red line) [21].	52
Figure 4.6: Core loss under sinusoidal excitation voltage (50 Hz) for different magnetic materials.	53
Figure 4.7: Core loss versus frequency for rectangular voltage excitation (duty 50 %) and no dc bias ($H_0 = 0$) for: (a) Powder materials; (b) Laminated steel, amorphous and ferrite materials.	54
Figure 4.8: Core loss versus dc bias for rectangular voltage excitation (duty 50 % and 10 kHz switching frequency) with constant magnetic field induction ($\Delta B = 0.09$ T) for powder materials.....	55
Figure 4.9: Core loss map under constant magnetic field induction ($\Delta B=0.09$ T) for: (a) MPP core; (b) High flux core; (c) Sendust core; (d) Mega flux core.....	57
Figure 4.10: Loss multiplication factor as function of frequency for: (a) MPP core; (b) High flux core; (c) Sendust core; (d) Mega flux core.	57

Figure 4.11: Simulated inductor waveforms with $L=2.25$ mH, $N=140$, $f_{sw}=10$ kHz and $\Delta i_{pk}=5$ %	58
Figure 4.12: Power loss due to dc winding resistance and total core losses as function of frequency for: (a) MPP core; (b) High flux core; (c) Sendust core; (d) Mega flux core	59
Figure 4.13: Experimental B-H waveforms for the inductor ($L = 2.25$ mH) with Mega Flux core at 5 kHz, 10 A _{pk} output current and $m_a = 0.5$	60
Figure 5.1: Single-phase equivalent diagram of a grid-connected VSC with LCL filter	61
Figure 5.2: Control block diagram of the closed loop system with converter ($x=1$) and grid current feedback ($x=2$) [90].	62
Figure 5.3: Bode diagram of G_{ol1} and G_{ol2} , for $L_1 = 2$ mH (4 %), $L_2 = 1.5$ mH (3%), $C = 20$ μ F (10 %), $R_d = 1.6$ Ω (0.3 %), $k_p = 5$ and $k_i = 250$	63
Figure 5.4: Generalized stability regions for VSC with high-order passive filters, provided that $T_d = 1.5 T_s$ [98].	64
Figure 5.5: The decoupled canonical control block diagram of the closed loop current control [101]	65
Figure 5.6: Impedance-based equivalent model of the VSC with high-order output filter [101]	66
Figure 5.7: Bode diagram of VSC output admittance with different passive filters and current control feedback.	67
Figure 5.8: Simulated LCL filter parameters variation ($C_b=199\mu$ F and $L_b =51$ mH) for $f_s = 5$ kHz as function of:(a) High frequency attenuation, Y_{21} at ($mf - 2$); (b) Characteristic frequency, f_0	69
Figure 5.9: Measurements for a designed LCL filter showing the output current harmonics response compared with IEEE 1547 and BDEW limits for a 10 kVA VSC with converter current control and $V_{dc} = 700$ V, $f_s = 5$ kHz: (a) Conservative approach; (b) Optimized filter.	70
Figure 5.10: Per phase schematics of a multi-tuned trap filter.	71
Figure 5.11: Characteristic impedance of the series tuned traps: (a) Provided same inductance/resistance and $Q_{t1} = 50$, $Q_{t2} = 25$; (b) Definition of the bandwidth parameter	72
Figure 5.12: Filter admittance around the tuned frequency of the first trap for different X/R values (or Q factors).	73
Figure 5.13: Examples of a 2 trap filter admittances Y_{21} for different trap capacitances (C_t) and split factors (t_1).	74
Figure 5.14: Measured current waveforms and harmonic spectrum of 2 trap filter with the proposed design method: (a) First trap; (b) Second trap; (c) Grid current.	75
Figure 5.15: Passive filter configurations with multi-split capacitors and/or inductors: (a) LCL with shunt RC damper; (b) Trap with shunt RC damper; (c) 2 traps with shunt RC damper.	76
Figure 5.16: Optimum quality factor and frequency for passive filters with split capacitors and/or inductors.	77

Figure 5.17: Optimal quality factor of the LCL filter and trap filter with shunt RC damper.	78
Figure 5.18: Root loci of the closed loop current control under ideal and worst case conditions for the trap filter with shunt RC damper (grid current control feedback).	79
Figure 5.19: Optimal selection of the capacitors ratio for an LCL filter with shunt RC damper as a trade-off between the resonance peak, damping losses and grid current harmonics at the most dominant harmonic frequency.	80
Figure 5.20: Damping losses in the filter at rated current as function of switching frequency for converter (i_1) and grid current control (i_2).	82
Figure 5.21: Filter size evaluation for converter (i_1) and grid current control (i_2) by total relative stored energy in inductors (relative to the LCL + series R damper working at $f_s = 1.05$ kHz).	83
Figure 5.22: Proposed passive damped filter topology, which is a C-type filter.	84
Figure 5.23: Transfer admittance of the proposed filter with optimum damping resistor (red line), zero damping resistor (LCL filter) and infinite damping resistor (trap filter).	85
Figure 5.24: Measured grid current waveforms and harmonic spectrum of the proposed filter, with $L_1 = 1.5$ mH (3 %), $L_2 = 0.5$ mH (1 %), $C_f = 4.7$ μ F (2.3 %), $P_d = 0.07$ % ($S_{VSC} = 10$ kVA, $f_{sw} = 10$ kHz).	86

CHAPTER 1. INTRODUCTION

The introduction of this thesis includes project motivation, background in harmonic filtering, a short review of stability interactions related to Voltage-Source Converters (VSCs), problem formulation, project objectives and limitations of this work.

1.1. PROJECT MOTIVATION

The use of multiple grid-connected VSCs may create harmonic interactions between the multiple harmonic sources and the passive components tuned for different frequencies [1]. The results are harmonic resonances in a wide frequency spectrum, which may lead to amplification of individual harmonics in certain operating conditions, leading to harmonic instabilities [2]. This phenomenon is currently increasing with the spread of power electronics based harmonic sources, e.g. HVDC stations or VSCs based power generation [3]. It has been shown that in a grid-connected VSC, the harmonic instability is influenced by the design of passive filter, tuning of current controller parameters and the time delay associated with the digital computation. In addition, the harmonic analysis of a grid connected VSC should consider the influence of the grid impedance, which depends on the grid configuration and may also include other parallel-connected VSCs.

The Impedance Based Stability Criterion (IBSC) can be used to distinguish between VSC output impedance and the grid impedance [4]. The ratio between the two impedances (called minor loop gain), can be used to individually assess the harmonic interactions at the point of common coupling (PCC) of the respective VSC. To ensure the harmonic stability, the VSC output impedance should be lower than the grid impedance. If otherwise occurs, then the phase difference between the two impedances should be lower than 180° in order to maintain stability [2]. Therefore, for given VSC output impedance, it can be imposed limits on the grid impedance to ensure harmonic stability. Otherwise, for known harmonic grid impedance, the VSC output impedance can be designed in such a way to ensure harmonic stability.

However, there is rather limited information about the output impedance of a VSC because of the passive filter characteristics. Especially, the filter inductors exhibit non-linear dependence of their equivalent inductance and resistance with the operating current, frequency or temperature. And it has been shown [5], that the filter inductor, which is used on the output of the converter may have significant higher losses than expected, as result of the high frequency excitation voltage given by the Pulse Width Modulation (PWM). Then, the equivalent power loss of the

inductor contributes to the inherent damping from the filter and it is dependent on the flux density ripple, dc bias magnetic field and the frequency of the excitation signal. Therefore, several aspects concerning the passive filter influence on the VSC output impedance and may include:

- In-depth characterization of passive components under PWM excitation to describe their inherent damping
- Passive filter topologies and their output characteristics (including the current controllers)
- Parameter selection of passive filters to meet performance criteria (effective design)

1.2. BACKGROUND TO HARMONIC FILTERING

1.2.1. SYSTEM DAMPING

New HVDC connections [6], integration of renewable energy sources [7] in modern power systems or the use of Distributed Generation (DG) [8] at distribution levels, increase the share of power electronics based conversion systems. An example of a low voltage feeder with DG is illustrated in *Figure 1.1*. The presence of DG, decrease the total power loss associated with the transfer of electrical energy in such a way that the equivalent damping in the system continuously decreases. At the user end, the efficiency also progressively increases with the spread of power electronics based loads [9], and less damping is expected [10]. One consequence of decreased damping in the power grid is that current and voltage harmonic distortions are increasing in a wide frequency spectrum.

1.2.2. HARMONIC FILTERING

The key practice to limit harmonics is to place a filter in shunt configuration [11], [12] close to the harmonic source by providing low impedance to dominant harmonics. If the filter is passive, then it is the most cheapest and effective solution to reduce harmonic distortions from the non-linear loads [13]. On the other hand, an active filter or a hybrid combination of the active and passive solutions can prove to be a more effective solution in situations that requires for reduced footprint or in the case when the harmonic emissions vary in a wide range of frequencies and magnitudes [13], [14]. Experience from industry shows that existing installations and demand for active filters are still limited and the cost is still the most significant design constraint, rather than the size or flexibility of the electrical installation [14]. Therefore, this thesis focuses on the design of passive filters and their use, in connection with VSCs.

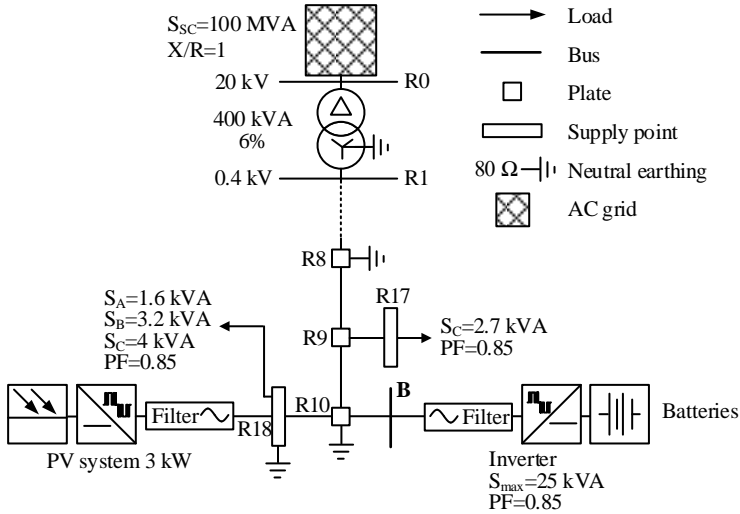


Figure 1.1: The end feeder of a distribution benchmark used for integration of distributed energy resources in the utility grid [15].

1.2.3. PASSIVE FILTERS FOR VSC

The passive filter is a key component to link harmonic sources given by power electronics based loads or sources with the utility grid [16]. It is a critical component in power electronics, which significantly impact on the cost, size, weight and efficiency of the power electronics based conversion systems [5]. In general, it may use around 30 % of the total space or it may dissipate around 2 % of the total power in a power electronics conversion system [5], [16]. The passive filter directly influences on the harmonic specifications at the PCC and also on the controllability of the power converter system [17].

Explicitly, typical power electronics conversion units consist of a VSC, which needs an inductance on the ac output in order to be able to be operated and to reduce the harmonic distortion (see *Figure 1.2*). The inductance limits the high frequency harmonics related to the switching device operation in such a way that output current and voltage fulfills the grid connection regulations. Instead of a simple inductance, it is possible to use a low pass filter configuration such as the *LCL* filter, which can bring the size and cost down significantly [18], [19]. Then at low frequencies the sum of the inductances in the filter influences the bandwidth and the controllability of electrical power, while at the switching frequencies, the harmonic magnitudes are effectively suppressed by the low pass filter [20].

However, such low pass filter configuration uses lower inductances which result in higher ripple current in the converter side inductance. Since the inductance on the converter side of the filter is driven by rectangular voltage excitation from PWM, with a frequency much higher than the fundamental frequency, it increases the losses in the inductance [21], [22]. A VSC with an LCL filter is illustrated in *Figure 1.2*, where the following notations are adopted and used extensively throughout this thesis: L_1 is the inductance on the converter side of the filter (PWM inductor); L_2 is the inductance on the grid side of the filter (line inductor); C is the shunt capacitor of the filter; Z_g is the grid impedance; v_{dc} , v_{VSC} and v_{PCC} are the dc-link, converter and PCC voltages, respectively; i_1 , i_2 and i_3 are the converter, grid and capacitor current, respectively; the PCC is the electrical connection point which delimit the VSC installation from the utility grid.

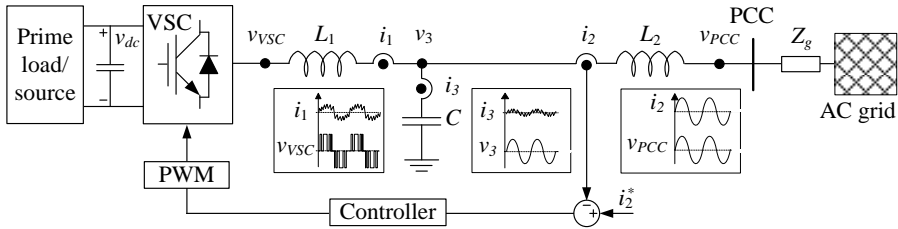


Figure 1.2: Single-phase diagram of a grid-connected VSC with LCL filter.

The filter arrangement illustrated in *Figure 1.2* has the particular drawback that creates series and/or parallel resonances between the filter and the grid impedance. A damping circuit may be required in order to minimize the risk of harmonic instabilities [18]. The need of damping may be dictated in accordance with:

- Passive filter design
- Grid impedance profile and its corresponding X/R ratio at the respective dominant harmonic frequencies of the resonances [23]
- Control system delay given by the zero-order hold (ZOH) from the PWM and computation delay
- Current controller design

1.2.4. ISSUES WITH PASSIVE FILTERS IN VSC

In grid-connected VSC, the controllers are designed depending on the filter topology, and its corresponding output admittance should be well separated from the equivalent admittance of the grid in order to ensure the system stability [4], [24]. Then, it is not unusual that the filter itself is the main cause of harmonic instabilities.

For example, the damping resistors in the shunt filter burned because of increased 17th and 19th harmonic orders in a wind power plant (WPP) in Dongmafangxiang (Province of Shanxi, China) [25]. In Naomaohuzhen (Province of Xinjiang, China), weak grid condition and large capacitance of the filters in the wind turbines as result of cost optimized filters triggered harmonic instabilities due to low resonance (around 2.5th order harmonic) [25]. The capacitance in the filter was reduced in order to decrease the current and loss in the resistor and to decrease the harmonic amplification factor. In Germany and Denmark, offshore wind turbines have been disconnected from the main grid due to interactions between VSCs and large connection cables [26]. As result of high frequency resonances, a milking machine actually stopped working after the installation of photovoltaic (PV) inverters in the neighborhood area [10]. It is expected the same kind of interaction to happen by the spread of electric vehicles connected to the grid [10]. In a Dutch distribution network, photovoltaic inverters switched-off undesirably and exceed harmonic regulations for certain operating conditions, even all PV individually have satisfied the harmonic regulations [27]. However, these harmonic interactions are rather isolated to situations with high share of power electronics and there is still limited evidence and documentation about such kind of harmonic instabilities.

1.2.5. PREVIOUS CONTRIBUTIONS TO THE RESEARCH TOPIC

As many publications exist in this field, several main contributions related to harmonic filtering and some key issues to passive filters design and characterization can be summarized but not limited to:

1948 – E.W. Kimbark publishes in “Power System Stability” the rules of system stability (low frequency oscillations) based on the conventional motor – generator (two-machine system) power system. It gives an understanding of the operation, control and design of the traditional power system [28].

1967 – A. I. Zverev work “Handbook of Filter Synthesis”, includes a comprehensive collection of passive filters, which are analyzed for different design conditions with the main features of the filters (asymptotes and corner frequencies) tabulated in tables [29].

1971 – “Direct Current Transmission” of E.W. Kimbark references the use of power electronics for dc power transmission, which is required for a more economical interconnection of high power ac systems. It provides practical information about converters, harmonic filter design, network harmonic impedance etc [23].

1976-1978 – R.D. Middlebrook proposes the fundamental impedance inequality to address the controller stability (high frequency oscillations) of dc-dc converters

with input filter [30]. The load and source impedance inequality, which is the basis of IBSC [4], can ensure that the current regulator of power converters is not influenced by the filter. Additionally, it proposes explicit design guidelines of the quality factor, resonance frequency and optimal damping parameters of the passive filters, which can avoid possible oscillations in the control system [24].

2001-onwards – The *LCL* filter design is explicitly addressed in literature. The parameters selection of the passive components based on a conceptual approach is introduced in [31]; the minimization of the stored energy in passive components is given in [17], while an optimization of the filter ratings based on the physical design of passive components with detailed loss characterization is addressed in [32].

2003-onwards – T. Shimizu at Tokyo Metropolitan University (TMU) conducts several works [21], [22], [33], [34] in which address explicitly the core loss of inductors under PWM excitation. The method proposed by TMU, namely “loss map” is based on actual measurements of the core losses by using the two winding method. Once the core losses are measured, the loss map enables an accurate characterization of the core loss for any configuration and design of the inductor, otherwise rather difficult to be done under practical operating conditions. The use of the loss map method facilitates the calculation of the equivalent damping from the loss of inductive components.

1.3. PROBLEM FORMULATION

In a grid-connected VSC, the duty cycle is changing according to the modulation index, which results into high-frequency rectangular excitation voltage at the input of the converter side inductance of the filter. It is not clear how significant are the power losses in the converter side inductance or how significant it may influence on the equivalent damping of the filter. Inaccurate models of the passive components under PWM excitation is one of the main reasons why the design of passive filters is not yet fully understood. For a low-pass filter, is not clear how to choose the low-pass filter parameters in such a way to avoid the resonance interactions. As a consequence, the design and stability evaluation of grid-connected inverters cannot be fully explored and the consequent resonance conditions with negative effects on the power grid operation are spreading around the world. To avoid misoperation of power electronics based systems, new and more complete design methods of the passive filters are needed. These must be updated to actual operating conditions of modern power systems, which are very different than decades ago.

1.4. RESEARCH OBJECTIVES

The main goal of this project is to evaluate the stability of a grid-connected VSC, from the filter design point of view. The question is no longer limited to how much penetration of renewables (and implicitly the use of VSC with passive filters) can be achieved. The question is how to avoid the interaction between paralleled connected VSCs (with output filters) and the system impedance, which causes harmonic instabilities. To answer this, it is required to solve a set of interdisciplinary studies:

- It is possible to develop a more complete model of the filter components with more accurate damping information?

Regardless of the VSC specifications, recent works show that the efficiency of the energy conversion system is finally limited by the choice of the converter side inductance, used to suppress the switching harmonics from the PWM. As the ac inductor is excited with rectangular voltages with much higher frequency than the fundamental grid frequency, significant loss occurs in the VSC and the filter. In addition, the loss highly depends on the adopted ripple current in the filter inductance, which further depends on the PWM method and magnetic material specifications. Then, there is limited evidence on how this loss influence on the equivalent model and damping of the passive filter. Another problem consists in the frequency dependence of the ac filter inductor. Its equivalent inductance depends on the magnetic core and air gap reluctances, and the adopted number of turns. Its equivalent resistance depends mainly on the length and cross-section area of the winding, and the equivalent wire resistivity, which accounts for the skin effect. For example, the inductance varies with current (dc bias) and is approximatively constant with changing frequency. On the other hand, the equivalent resistance of inductors is approximatively constant with changing current, while it varies with increasing frequency due to the skin effect in the winding. A second research question is:

- For a given passive filter topology of a grid-connected VSC, can be identified stability regions or stability-based design guidelines which minimize the interaction of the VSC with the grid impedance?

It is desirable that stability interactions of passive filters with the grid impedance and VSC control system to be minimized. That is, the VSC controllers and the passive filter should be designed robust, in order to account for changes in the grid impedance. The IBSC allows decoupling the impedance of the passive filter from the grid impedance, which makes it possible to evaluate afterwards, the system stability of respective VSC at the PCC. However, an alternative stability criterion also exists and needs to be investigated, such as the frequency-domain passivity

theorem. Accounting all available evaluation methods, it is required to systematically identify the cause of harmonic instabilities in dominant power electronics based power systems from the passive filter design point of view. A third research question, which can be formulated, is:

- Can new design guidelines be defined for power filters depending on the power application?

Different power applications have different requirements. For low power, damping from the grid impedance or from the loss of inductive components and control system may suffice the stability requirements. However, at high power levels, damping is more limited and the use of additional damping circuits may be mandatory. Then, new design guidelines taking into account the damping capability of passive filters are needed. Existing literature is rather limited from a damping design point of view, and the system stability is again questionable. Passive filter topologies and their corresponding design methods should be investigated, which should ensure low damping losses and at the same time achieve high sensitivity to filter or grid impedance parameters variations.

1.5. LIMITATIONS

The discussions in this thesis are limited to two-level VSC, with an operating switching frequencies ranging from 1 to 15 *kHz*. Additionally, low power levels (reduced scale) of the VSC and passive filters (up to 10 *kW*) such as those found in standard photovoltaic (PV) systems are used to develop new models and design methods of the passive filters. A Per Unit (PU) rating is used for an easy adaptation to larger scale platforms. Still, the methodology and principles adopted throughout this thesis it can appropriately be valid regardless of the power level or voltage levels of the VSC.

1.6. THESIS OUTLINE

This thesis deals with the mitigation of harmonic instabilities related to the interactions between the converter output impedance and the grid impedance, in grid-connected applications. The main cause of such instabilities is an inappropriate design of the passive filter and its corresponding tuned frequencies in addition to the current control loops. For example, the passive filter is excited with rectangular pulses from the PWM method with high frequency, which results into power losses in the range of 1–2 %. The non-linear characteristics of inductors such as saturation (or inductance variation with current due to permeability dependence of the magnetic material) complicate even more the design of the passive filter.

Similar effect is obtained from the frequency dependence of the equivalent resistance in the inductor windings. The variation of the grid impedance and its influence on the stability of grid-connected VSCs is another aspect, which is often disregarded. An inappropriate filter topology for a given power grid configuration also contributes to an increased risk of instability. Therefore, in this research work, the passive filters, their physical characterization and design are systematically approached based on state-of-the-art techniques in the following way.

The introduction of this thesis is made in Chapter 1 and includes motivation of the research topic, background in harmonic filtering, a review of stability interactions problems related to VSCs, problem formulation, objectives and limitations of this work.

In *Chapter 2*, several specifications and requirements of the passive filters are given at system level. By considering the passive filter as a black-box model, it is possible to establish a set of design prerequisites by inspection of the filter operating conditions from the converter and grid side, independently. For instance, the dependencies of the output harmonic voltage of the converter with different operation modes of the VSC are considered. Then, the influence of the worst case harmonic grid impedance on the filter and some methods to describe the frequency dependent grid impedance are given. The concept of the filter virtual admittance is introduced afterwards, which can facilitate the choice of a suitable passive filter topology.

In *Chapter 3*, several passive filters and a comprehensive selection of passive damping circuits for use in VSC applications are classified together with their pros and cons. A methodology to derive the passive filters frequency response, which can describe the filters behavior at low and high frequency is given afterwards. Finally, the influence of the non-linear inductance and frequency dependent resistance of inductors on the frequency response of the passive filter is measured and reported.

The characterization of inductive components is presented in *Chapter 4*. It is shown how in a high-order filter, the inductor on the converter side of the VSC is the limiting factor, when is to be decided about the passive filter size, cost and efficiency. Several magnetic materials are compared in terms of power losses, and their non-linear characteristics are fully explored. Using a dc chopper and a B-H analyzer, the core loss is measured for each operating point, and then stored in a loss map for the respective core material. Then, by using an electrical circuit simulation software, different inductor designs can be analyzed together with the loss information. The role of different inductors in passive filters is also highlighted, together with their corresponding sizing considerations.

In Chapter 5, generalized stability conditions for grid-connected VSC with *LCL* filter are presented, which can be used to minimize the interactions of the inverter with the grid impedance. Afterwards, the main focus is the design of filters with passive damping, which are well known for their simplicity and robustness. An optimal design method is also proposed, which simplifies the passive damping design and which ensures maximum damping performance by using lower rated damping components. To differentiate between the features of different passive filter topologies, an in-depth comparison and analysis is completed. Based on the performed comparison, a new passive damped filter is presented which offers a good trade-off in terms of size and loss compared with the traditional *LCL* filter and *trap* filter.

The second part of the thesis contains papers that have been published during the PhD period. It supports the main outcome of this research in the form of new or improved design methods, comprehensive evaluations, simulation or experimental results.

1.7. LIST OF PUBLICATIONS

Journal papers:

- I. R. Beres, X. Wang, F. Blaabjerg, M. Liserre, and C. L. Bak, "Optimal Design of High-Order Passive-Damped Filters for Grid-Connected Applications," *IEEE Trans. Power Electron.*, vol. 31, no. 3, 2016, pp. 2083–2098.
- II. R. Beres, X. Wang, M. Liserre, F. Blaabjerg, and C. L. Bak, "A Review of Passive Power Filters for Three Phase Grid Connected Voltage-Source Converters," *IEEE Journal of Emerging and Selected Topics in Power Electronics*, vol. 4, no. 1, 2016, pp. 54–69.
- III. C. Yoon, H. Bai, R. Beres, X. Wang, C. L. Bak, and F. Blaabjerg, "Harmonic Stability Assessment for Multi-Paralleled, Grid-Connected Inverters", *IEEE Trans. Sustainable Energy*, Early Access, 2016.

Conference papers:

- I. R. Beres, X. Wang, F. Blaabjerg, C. L. Bak, and M. Liserre, "A Review of Passive Filters for Grid-Connected Voltage Source Converters," in *Proc. of the 29th Annual IEEE Applied Power Electronics Conference and Exposition, APEC 2014*, pp. 2208-2215.

- II. R. Beres, X. Wang, F. Blaabjerg, C. L. Bak, and M. Liserre, “Comparative analysis of the selective resonant LCL and LCL plus trap filters,” in Proc. International Conference on Optimization of Electrical and Electronic Equipment (OPTIM), 2014, pp. 740–747.
- III. R. Beres, X. Wang, F. Blaabjerg, C. L. Bak, and M. Liserre, “Comparative evaluation of passive damping topologies for parallel grid-connected converters with LCL filters,” in Proc. of the 2014 International Power Electronics Conference (IPEC-Hiroshima 2014 - ECCE-ASIA), 2014, pp. 3320-3327.
- IV. R. Beres, X. Wang, F. Blaabjerg, C. L. Bak, and M. Liserre, “New optimal design method for trap damping sections in grid-connected LCL filters,” in Proc. of the 2014 IEEE Energy Conversion Congress and Exposition (ECCE), 2014, pp. 3620-3627.
- V. R. Beres, X. Wang, F. Blaabjerg, C. L. Bak, and M. Liserre, “Improved Passive-Damped LCL Filter to Enhance Stability in Grid-Connected Voltage-Source Converters,” in Proc. of the 23rd International Conference on Electricity Distribution (CIRED), 2015, pp. 1–5.
- VI. X. Wang, R. Beres, F. Blaabjerg and P. C. Loch, “Passivity-Based Design of Passive Damping for LCL-Filtered Voltage Source Converters,” in Proc. of the 2015 IEEE Energy Conversion Congress and Exposition (ECCE), 2015, pp. 3718-3725.
- VII. R. Beres, H. Matsumori, T. Shimizu, X. Wang, F. Blaabjerg and C. L. Bak, “Evaluation of Core Loss in Magnetic Materials Employed in Utility Grid AC Filters,” in Proc. of the 31st Annual IEEE Applied Power Electronics Conference and Exposition, APEC 2016, pp. 3051-3057.

CHAPTER 2. SPECIFICATIONS AND REQUIREMENTS FOR HARMONIC FILTERS DESIGN

In this chapter, several specifications and requirements for passive filters are given at a system level. By considering the passive filter as a black-box model, it is possible to establish a set of filter design prerequisites by inspection of the filter behavior from the converter side and grid side, independently. For instance, the dependencies of the output harmonic voltage of the converter with different operation modes of the VSC are considered. Then, the influence of the worst case harmonic grid impedance on the filter and some methods to describe the frequency dependent grid impedance are given. The concept of the filter virtual admittance is introduced afterwards, which can facilitate the choice of suitable passive filter topologies.

2.1. SYSTEM DESCRIPTION

Power quality compliant voltages or currents at the PCC in terms of their harmonic content are mandatory in order to ensure a safe, secure and reliable operation of the utility grid. In this regard, the VSC can be seen as a voltage harmonic source, whose harmonic spectrum is highly dependent on the PWM method and operation mode of the VSC. A single-phase representation of a three-phase VSC is illustrated in *Figure 2.1* and it includes a passive filter of a *T-type* structure [20], where: Z_1 is the impedance of the converter side of the filter; Z_2 is the filter impedance on the grid side; Z_3 is the shunt impedance of the filter; v_{VSC} is the VSC output line to neutral voltage; v_{PCC} is the PCC line to neutral voltage and v_1 , v_2 and v_3 are the voltage drops across the converter side impedance, grid side impedance and shunt impedance, respectively. By replacing the filter impedances with L_1 , L_2 and C accordingly, the overall passive filter become an *LCL* filter, which is well-known for its cost-effectiveness and it is widely used in practice [35].

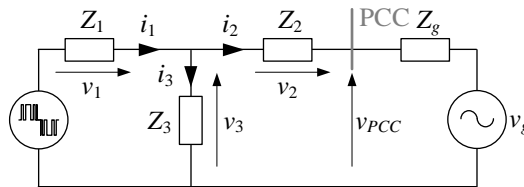


Figure 2.1: One phase schematics of a grid-connected VSC with a generalized passive filter.

2.2. HARMONIC SPECIFICATIONS AT PCC

At the PCC, both voltage and current harmonics should be limited according to some standards. The specifics of the grid or the nature of the harmonic source directly influence on the specified harmonic limits. In general, current harmonics should be limited by the VSC, while the voltage harmonics are within the utility operator responsibility. Both of them are explicitly specified in grid connection standards or the power quality standards.

2.2.1. HARMONIC STANDARDS

The harmonic voltages transferred to low voltage levels are very low with increasing frequency due to the characteristics of power transformers and loads at these frequencies. Therefore, power quality standards include harmonic orders up to 50 as it is illustrated in *Table 2.1* and *Table 2.2*. The grid connection standards [33], [34] impose more stringent harmonic current limits and are defined for an extended frequency range (up to 9 kHz), and whose values are dependent on the network Short Circuit Ratio (SCR). Hence, for grid connection standards, the limits presented in *Table 2.1* become more stringent with decreasing the SCR.

Table 2.1: Harmonic current limits (% of rated current) for several power quality/interconnection standards [36]–[40]

Harmonic order h	IEEE 519 ⁽¹⁾ [LV & MV]	EN 61000-3-2 ⁽²⁾ [LV]	EN 61000-3-12 [LV]	VDE-AR-N ⁽³⁾ 4105 [LV]	BDEW ⁽⁴⁾ [MV]
3	4	14.4	–	4.16	–
5	4	8.8	10.7	2.08	2.06
7	4	4.8	7.2	1.39	2.84
11	2	2	3.1	0.69	1.8
13	2	1.3	2	0.55	1.32
17	1.5	7.5/ h	–	0.42	0.76
19	1.5	7.5/ h	–	0.35	0.62
23	0.6	7.5/ h	–	0.28	0.42
25	0.6	7.5/ h	–	0.21	0.32
29-33	0.6	7.5/ h	–	5.2/ h	8.67/ h
35-37	0.3	7.5/ h	–	5.2/ h	8.67/ h
41-49	0.3	–	–	6.24/ h	6.24/ h
53-179	–	–	–	6.24/ h	6.24/ h

⁽¹⁾ grid SCR < 20, in addition the limits are adopted also by IEEE1547 [41], IEC 61727 [42] and UL1741 [43];

⁽²⁾ grid SCR not specified and it applies for a rated base current of 16 A;

⁽³⁾ grid SCR = 20;

⁽⁴⁾ calculated for 400 V and an SCR of 20.

Table 2.2: Harmonic voltage limits (% of rated voltage) for several power quality/interconnection standards

Harmonic order h	EN 61000-2-2 [LV]	EN 50160 [LV]	BDEW [MV]
3	5	5	–
5	6	6	0.5
7	5	5	1
11	3.5	3.3	1
13	3	3	0.85
17	2	2	0.65
19	1.8	1.5	0.6
23	1.4	1.5	0.5
25	1.3	1.5	0.4
29-37	38.6/h-0.25	–	0.4
41-49	38.6/h-0.25	–	0.3
53-179	–	–	0.3

The SCR is defined as the ratio between the short circuit power of the grid (S_{SC}) and the VSC dc power (S_{VSC}).

2.2.2. MEASUREMENT OF HARMONICS

In general, the Total Harmonic Distortion (THD) of the current (I_{THD}) should be limited to less than 5 %, measured at rated output of the VSC. The limits should be calculated excluding the effect of background voltage distortion that may lead to an enhanced current distortion. Therefore, harmonic measurements can be made with the VSC delivering 100 % of its rated power, while supplying a resistive load [43]. If individual harmonic currents are below 0.05 % of the fundamental rated current, no harmonics are needed to be considered [40]. Hence, a 0.05 % individual harmonic current limit can be imposed for harmonic orders, where the limits are not specified. The time interval for measurement of parameter magnitudes (supply voltage, harmonics, interharmonics and unbalance) can be chosen as 10-cycles for 50 Hz nominal frequency [44]. The range can be extended to 3 s interval, 10 min. interval or 2 h interval for some specific applications.

Harmonic measurement techniques are defined for a frequency range of up to 9 kHz in [45]. In general, for verifying the standard compliance, the measured currents (I_m), voltages (V_m) and power (P_m) should be measured with a maximum error as presented in Table 2.3. The error is calculated from the nominal value of the measurement instrument (I_{nom} , V_{nom} or P_{nom}) [45].

Table 2.3: Accuracy specifications for current, voltage and power measurement for compliance with power quality standards [45]

Measurement	Conditions	Maximum error
Voltage	$V_m < 1 \% V_{nom}$	$\pm 0.05 \% V_{nom}$
	$V_m \geq 1 \% V_{nom}$	$\pm 5 \% V_{nom}$
Current	$I_m < 3 \% I_{nom}$	$\pm 0.15 \% I_{nom}$
	$I_m \geq 3 \% I_{nom}$	$\pm 5 \% I_{nom}$
Power	$P_m < 150 \text{ W}$	$\pm 1.5 \text{ W}$
	$P_m \geq 150 \text{ W}$	$\pm 1 \% P_{nom}$

2.3. VSC CHARACTERIZATION

The operation mode of the VSC and its harmonic output directly influences on the size of the filter and filter topology [46]. In general, a grid-connected VSC should provide reactive power support in a range of around 40% of the rated active power, e.g. given by a power factor (PF) of 0.9, both inductive and capacitive. It may provide grid-feeding or grid-supporting features [47] to support the voltage at the PCC (which may vary between 0.9 and 1.1 PU) and/or the grid frequency (which may vary within ± 0.1 Hz).

2.3.1. HARMONIC SPECTRUM FROM PWM

Depending on the operating range of the VSC and its modulator signal (PWM method), the harmonic output can be calculated or simulated with relatively high accuracy [48]. For a given PWM method, the harmonic content is dependent on the modulating signal and the carrier wave used for duty cycle generation. In addition, the output THD content, increases with decreasing the amplitude modulation index m_a (for the linear range of m_a), which can be written as a function of the modulating voltage V_m and the carrier wave V_{cr} as:

$$m_a = \frac{\hat{V}_m}{\hat{V}_{cr}} \quad (2.1)$$

The frequency modulation index (m_f) can be written as function of the carrier frequency (f_{cr}) and fundamental output frequency (f_1) as:

$$m_f = \frac{f_{cr}}{f_1} \quad (2.2)$$

Therefore, high modulation index is needed in grid-connected applications in order to limit the harmonic content. In general, for a grid-connected VSC, m_a is between 0.7 and 1 depending on the adopted PWM method. For example, a conventional

space vector PWM (SVM) provides lower THD and better dc-link voltage utilization (by a factor of 1.15) compared with the conventional sinusoidal PWM (SPWM) method [13]. In *Figure 2.2*, the duty cycle generation, the output line to line voltage and the harmonic content are given for SPWM, SVM and $\frac{1}{4}$ third harmonic injection PWM (THI-PWM), assuming the same dc-link voltage utilization. In this thesis, the THI-PWM is adopted for the filter design.

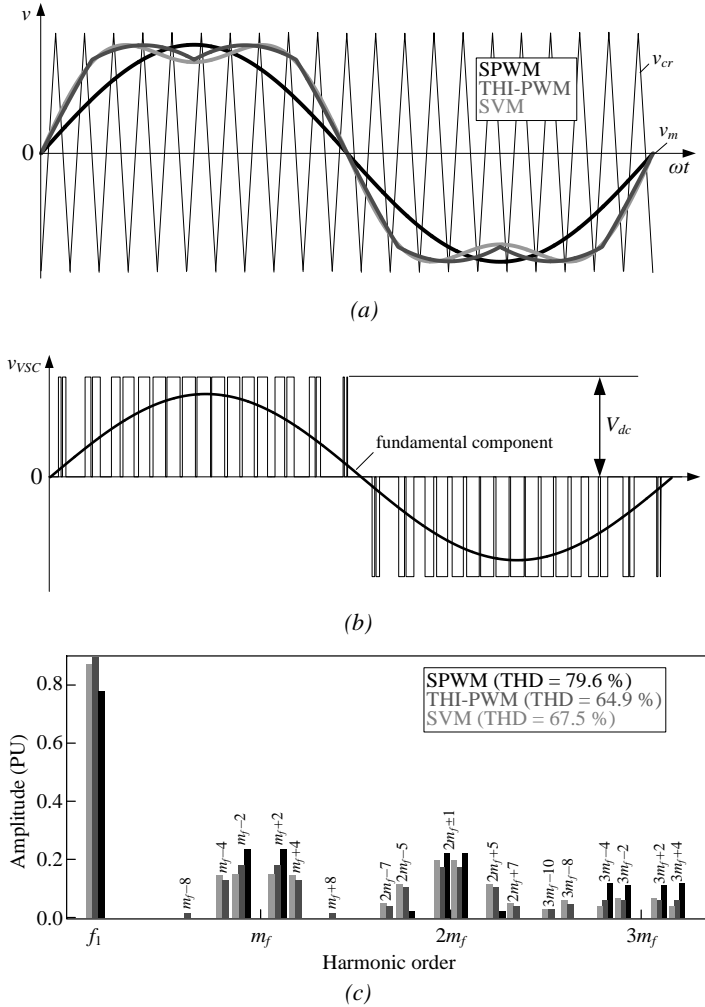


Figure 2.2: One phase simulated waveforms for a two-level three-phase VSC with $m_f = 21$ and $m_a = 0.9$ for SPWM and $m_a \sim 1$ for SVM and THI-PWM: (a) Pulse generation; (b) Line to line VSC output voltage for THI-PWM; (c) Voltage harmonic content.

2.3.2. VSC OPERATION MODE

From *Figure 2.2* it can be noticed how for the same dc-link voltage utilization, with different PWM methods, different fundamental voltage magnitudes can be obtained. Nevertheless, the output fundamental voltage changes dependent upon the operation mode of the VSC. Recalling *Figure 2.1* and considering that the voltage at the PCC is fixed by the utility grid, it follows that the voltage drop across the filter will change the fundamental converter voltage. Therefore, the voltage THD at the converter terminals will also change since the amplitude of the output phase to phase voltage of the VSC is equal with the dc-link voltage V_{dc} as illustrated in *Figure 2.2*.

The four quadrant capability of a VSC is illustrated in *Figure 2.3*, which shows how the VSC can be operated in inverter or rectifier mode and it may provide at the same time different reactive power set-points, such that the Power Factor (PF) may be different than unity.

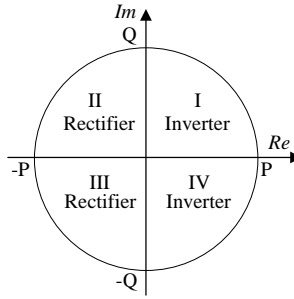


Figure 2.3: Four quadrant capability of a VSC.

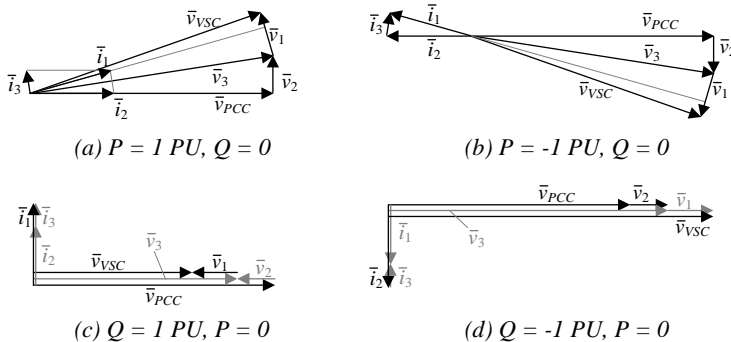


Figure 2.4: Vector diagram of the VSC for different operating conditions: (a) Inverter mode with PF = 1; (b) Rectifier mode with PF = -1; (c) Capacitive reactive power support with PF = 0; (d) Inductive reactive power support with PF = 0.

The vector diagram of the VSC for four limiting operating conditions is illustrated in *Figure 2.4*. It results that the amplitude of the v_{VSC} is minimum while supplying the negative reactive power and is maximum while supplying the positive reactive power.

2.3.3. INFLUENCE OF THE MEASUREMENT SENSORS

The sensor position used for the current reference and grid synchronization also influences on the magnitude of the converter voltage [49]. Using the VSC terminology from *Figure 2.1* it may be seen that both converter and grid current can be used for the current control reference. By sensing the converter current, the hardware implementation will be simpler. Sensing the grid current, it will increase the complexity in implementation since the sensor must be placed after the shunt branch of the filter. For grid synchronization, both the voltage across the shunt impedance v_3 and voltage at PCC v_{PCC} can be used with similar complexity in implementation. Then, there are four possible sensing scenarios, all illustrated in *Figure 2.5*, considering that the VSC is in the inverter operation mode and that controlled current is in phase with the synchronized voltage [50]. It reveals that the v_{VSC} is lowest when sensing the grid current. By adopting the voltage across the shunt filter for grid synchronization, it shifts the PF at the PCC depending upon the voltage drop across the grid side impedance v_2 . Therefore, excepting the case when the grid current is controlled to be in phase with the voltage at PCC, it is required to compensate in the control system for the voltage drop across the corresponding filter impedance in order to ensure unity PF.

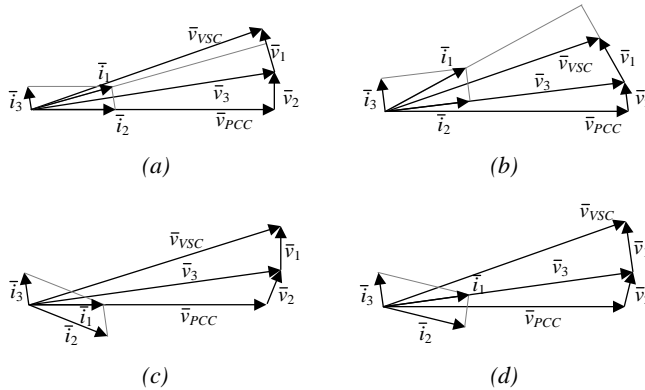


Figure 2.5: Vector diagram of the VSC in inverter operation mode for different positions of the measurement sensors [50]: (a) Voltage sensed on the PCC and current sensed on the grid side; (b) Voltage sensed on the filter capacitor and current sensed on the grid side; (c) Voltage sensed on the PCC and current sensed on the converter side; (d) Voltage sensed on the filter capacitor and current sensed on the converter side.

2.4. A.C. GRID CHARACTERIZATION

The frequency dependence of the grid impedance can significantly influence on the power quality at PCC due to multiple resonances that may exist in the grid [51]. Additionally, the actual impedance of the grid plays a significant role to suffice the damping requirements of the filter and to reduce the insulation requirements in the passive components. In general, damping is more pronounced in LV networks rather than higher voltage networks and the damping increases with the frequency [23]. For an adequate and effective filter design, the harmonic impedance of the grid is required. Unfortunately, the harmonic impedance has no relationship to the fundamental frequency SCR. Lower SCR's implies easier amplification of non-characteristics harmonics of relatively low orders, while during transients, higher overvoltage are expected across the passive filters [52].

In *Figure 2.6*, a single phase schematics of a grid connected VSC with passive filter and grid impedance Z_g is illustrated, which is valid above the grid fundamental frequency. It replicates the conventional filter design problem [23], where for a specific impedance on the grid side of the filter given by Z_2 and for a given harmonic source, the shunt filter Z_3 should ensure the attenuation of harmonic currents from the harmonic source. At the same time, it should avoid the risk of amplification of the individual harmonic voltages (which exists in the voltage across the shunt filter v_3 and the PCC voltage v_{PCC}) due to the parallel resonant circuit given by the shunt filter and the impedance on the grid side of the filter given by Z_2 .

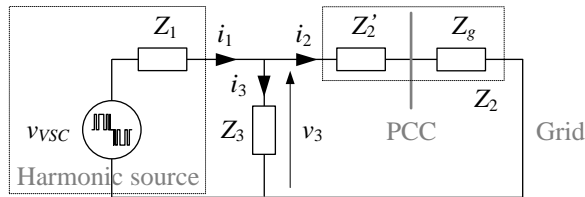


Figure 2.6: One phase schematics of a grid-connected VSC with passive filter (model valid above the fundamental frequency).

2.4.1. GRID SPECIFICATIONS

In general, the grid impedance Z_g is continuously changing and some reasonable assumptions of the worst case grid impedance must be considered by the filter designer. Especially, there will be an optimum quality factor of the filter, which minimizes the harmonic content in the PCC voltage, which is dependent on the grid impedance [23]. Therefore, several design prerequisites of the passive filter in connection with the a.c. grid may include [23], [53]:

1. Preexisting harmonic levels
2. Variation of the supply grid voltage
3. Unbalance of the grid voltage
4. Fundamental power frequency and its variation
5. Impedances at harmonic frequencies:
 - a. For various load conditions (light and heavy loads)
 - b. With various outages of lines and equipment
 - c. Limiting phase angle
6. System interaction with harmonic emissions

The key issue is that some of the critical design data are not readily available for the filter designer, including the level of existing harmonic distortions (which is difficult to measure or predict), or tolerance to harmonics of the existing or future equipment connected to the power system itself [14]. Simulations of the grid impedance for various operating conditions may lead to satisfactory harmonic distortion levels and some critical impedance information can be obtained for the filter design. However, in general, it is not obvious to what extent the passive filters in some instances may have been over-designed, and that a more economical design might have been possible [14].

2.4.2. WORST CASE HARMONIC GRID IMPEDANCE

In *Figure 2.6*, the grid impedance Z_g and the grid side impedance of the filter Z_{f2} , form the equivalent impedance on the grid side of the filter, namely Z_2 . Z_2 is connected in parallel with Z_3 , resulting in a harmonic voltage v_3 across Z_3 , which is dependent on all aforementioned variables, given by:

$$v_3 = \frac{Z_3 Z_2 i_1}{Z_3 + Z_2} = \frac{i_1}{Y_3 + Y_2} \quad (2.3)$$

The harmonic grid current i_2 and the shunt filter current i_3 , can be derived as:

$$i_2 = \frac{v_3}{Z_2} = \frac{Z_3 i_1}{Z_3 + Z_2} = \frac{Y_2 i_1}{Y_3 + Y_2} \quad (2.4)$$

$$i_3 = \frac{v_3}{Z_3} = \frac{Z_2 i_1}{Z_3 + Z_2} = \frac{Y_3 i_1}{Y_3 + Y_2} \quad (2.5)$$

Several worst case grid impedances can be identified as [23]:

1. If Z_2 is zero, v_3 is zero as $i_3 = i_2$ and the shunt filter would have no filtering effect with all current harmonics passing from the VSC to the grid. Perfect

filtering of v_3 is obtained, while i_2 is limited only by the converter impedance Z_1 .

2. If Z_2 is infinite, $i_2 = 0$ and $i_1 = i_3$, that is, all current harmonics from the VSC are passing through the shunt filter. Therefore, a perfect filtering of i_2 is obtained, while v_3 is limited by the shunt filter impedance Z_3 .
3. The grid and the shunt filter impedances are in a parallel resonance, which means that the harmonic components of both i_2 and v_3 could be increased by the presence of the filter.

The first two scenarios are not practical, but they reveal how the filter operates for low and high grid impedance. Solutions to reduce i_2 and v_3 include addition of more filters or de-tuning the filter resonance away from the existing harmonics in order to shift the resonances far away from each other. De-tuning can be defined as a relative measure of how much the actual resonance frequency of the filter ω_{res} is shifted from the initial tuned frequency of the filter ω_t :

$$\delta = \frac{\omega_{res} - \omega_t}{\omega_t} \quad (2.6)$$

2.4.3. GRID IMPEDANCE MODELLING

The frequency dependent grid impedance can be modeled using impedance envelopes [52]. Typical impedance envelopes include:

1. Sector diagrams: this is the simplest to use method when information about the grid impedance is limited. It provides the maximum grid impedance value together with maximum and minimum phase angle.
2. Circle diagrams: a better fitting of the grid impedance can be obtained by providing the minimum resistance of the grid for given harmonics orders. The largest value of the grid impedance defines the radius of a circle which characterizes the grid impedance range.
3. Discrete polygons: for different frequencies of interest, especially for lower order harmonics (e.g. h lower than 20) discrete impedance polygons can be used to provide better accuracy of the grid impedance representation. Thereby, a filter overdesign can be avoided.

In *Figure 2.7*, two examples of grid impedance envelopes are illustrated. In general, the grid impedance is inductive for low order harmonics, while with increasing frequency, it can be either inductive or capacitive, depending on the particular grid configuration. Depending on the grid impedance, the filter has different influence on the power quality. For very low grid impedance, the PCC voltage harmonics are good, while the grid current harmonics are limited by the series impedances of the filter. For very high grid impedance, the grid voltage harmonics are limited by the

shunt filter, while the grid current is free of harmonics. However, these two scenarios are not very likely to occur in practical situations, and the grid impedance will be somewhere between the two extreme cases.

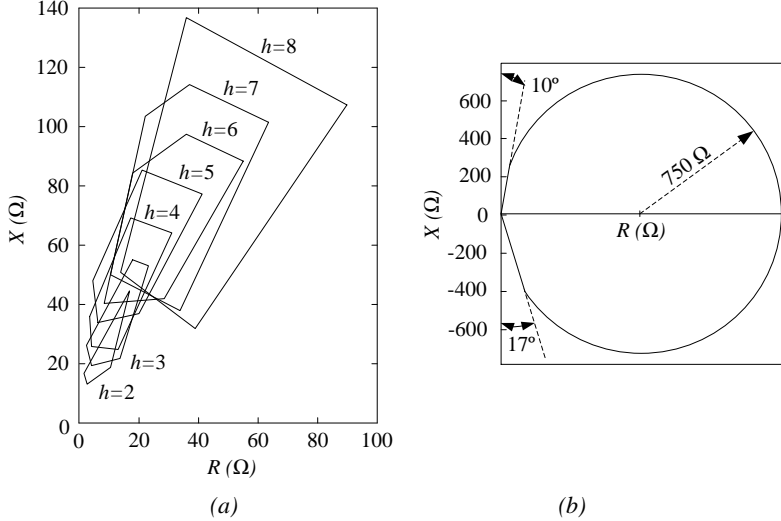


Figure 2.7: Network impedance envelopes modeled by: (a) Discrete polygons; (b) Circle diagrams [52].

For a given grid impedance, one should avoid the harmonic amplification given by the parallel resonance between the filter and the grid impedance. Therefore, a magnification factor which describes the harmonic amplification can be derived as:

$$k_v = \frac{i_2}{i_1} = \frac{v_3}{v_{3(0)}} = \frac{Y_2}{Y_3 + Y_2} \quad (2.7)$$

where $v_{3(0)}$ is the voltage across the shunt filter when there is no shunt passive filter.

For optimum filter design, the minimum or maximum grid impedance and its equivalent damping that contributes to harmonic filtering should be taken correspondingly into account. The influence of the grid impedance to both grid current and voltage must be considered altogether. However, the converter impedance is also needed for correct resonance analysis. The response of the converter control system can cause a negative resistance for low order harmonics [52], as it will be explained in a later section.

2.5. VIRTUAL ADMITTANCE OF HARMONIC FILTERS

Since the individual harmonics of the current at the PCC are limited by grid connection standards or other applicable standards (see *Table 2.1*), then it is possible to estimate the required filter admittance needed for a VSC with a given PWM method. The ratio between the harmonic current limit at PCC (i_{limit}) and the harmonic voltage corresponding to the PWM method is defined as the virtual admittance of the harmonic filter, namely Y_{vhf} :

$$Y_{vhf} = \frac{i_{\text{limit}}(h)}{v_{VSC}(h)} \quad (2.8)$$

An illustrative example of Y_{vhf} calculated for the three PWM methods shown in *Figure 2.2*, is illustrated in *Figure 2.8*, considering different applicable standards and a switching frequency of 1.05 kHz.

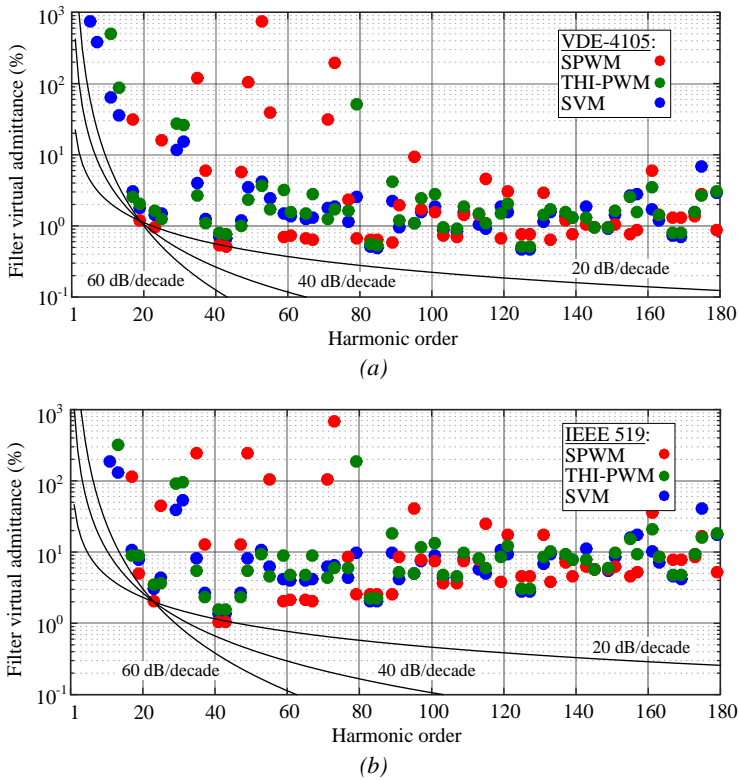


Figure 2.8: Filter virtual admittance for $m_f = 21$ and $m_a = 0.9$ for: (a) VDE-4105 standard; (b) IEEE 519 standard.

Additionally, three different ideal filter characteristics tuned for the SPWM method, and which have an attenuation of 20, 40 and 60 dB/decade, are drawn. It reveals

that with different harmonic standards, different filter design approaches and topologies are needed. For example, for the VDE-4105 recommendations, it can be seen that a first order filter tuned around the first switching harmonics can suffice the attenuation requirements of the high order harmonics. However, for the IEEE 519 recommendations, a first order filter should be tuned around twice the switching harmonics ($h \approx 41$) in order to ensure a proper attenuation off all the switching harmonics. In turn, a second order filter can be tuned for the first switching harmonics. Very different results in terms of filter ratings would result for the two standards, since around the switching frequency, VDE-4105 impose twice more stringent harmonics limits than the IEEE519 counterpart. At higher frequencies, the difference is even higher.

Similarly, Y_{vhf} is illustrated in *Figure 2.9* for a switching frequency of 10.05 kHz.

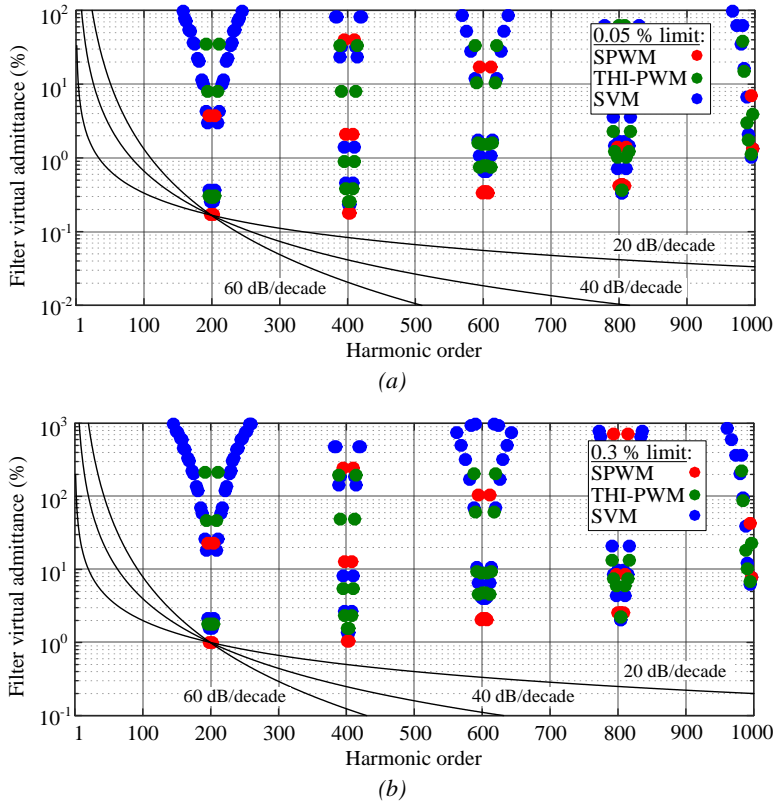


Figure 2.9: Filter virtual admittance for $m_f = 201$ and $m_a = 0.9$ for: (a) 0.3 % individual harmonic current limit (IEEE 519-1992 standard); (b) 0.05 % limit (BDEW standard).

Since at high frequencies, there is no clear applicable harmonic standard to date, two scenarios are considered. The first, considers the 0.05 % limit recommended by

BDEW standard and which can be extended for use at higher frequencies. The second scenario considers a fixed 0.3 % limit as it is recommended by the old IEEE-519 standard (1992 edition) and is widely adopted in literature [54]–[56].

Figure 2.8 and *Figure 2.9* reveal that at high frequencies, a first order filter (or 20 dB/decade) could provide sufficient attenuation of the switching harmonics. Since Y_{vhf} is used only for individual current harmonic compliance, the THD of the current is another aspect which should be taken into account. However, in general, following Y_{vhf} will result in lower current THD than the recommended limits.

2.6. SUMMARY

In this chapter, the concept of the virtual harmonic admittance of the filter has been presented. At the converter side of the filter, the voltage harmonics are known from the PWM method; on the grid side of the filter, the individual current harmonics limits are known from the harmonic standards. Then, the resulting harmonic admittance can simplify the choice of the filter topology, which ensures the required attenuation of switching harmonics. In addition, limitations on the passive filter size and ratings can be determined based on the considerations given for the operation mode of the converter and that of the grid impedance. However, for harmonic interactions and resonance analysis, the full VSC models including the control loops need to be considered.

CHAPTER 3. CHARACTERIZATION OF PASSIVE FILTER TOPOLOGIES

In this chapter, several passive filters and a comprehensive selection of passive damping circuits for use in VSC applications are categorized together with their pros and cons. A methodology to derive the passive filters frequency response, which can describe the filters behavior at low and high frequency, is given. To simplify the derivations, it is neglected the influence of the grid impedance on the passive filter frequency response. Finally, the influence of the non-linear inductance and frequency dependent resistance of inductors on the frequency response of the passive filter is measured and reported.

3.1. DESIGN CONSIDERATIONS OF PASSIVE FILTERS

Passive filters should ensure two main features when they are used in grid-connected VSC applications [50]. They should provide an inductive behavior at the fundamental frequency in order to ensure a proper operation of the VSC. Then, the passive filters should limit the harmonic content related to the PWM in order not to interact with other devices connected to the same grid. Other undesirable effects of increased levels of harmonics may include overheating of electrical apparatus, instability of the VSC controllers or interference with the telecommunication systems [23]. There are several options for the passive filter topology, which may fulfill the aforementioned requirements. In general, it is desirable for the chosen passive filter topology to have the following features [29]:

1. High efficiency
2. Low cost
3. Negligible sensitivity to parameter tolerances
4. Reduced number of components
5. Simplicity in manufacturing
6. Small physical dimensions and weight
7. Long life-time

Since the passive filter topologies are application specific, it may not be possible to achieve all the desirable features at the same time. Typical applications of passive filters may include integration of renewable sources in the power grid [49], HVDC systems [6], railway systems [57], electromagnetic interference filtering (EMI) [58], power conditioning units [59] or aircraft power systems [48].

3.2. PASSIVE FILTERS FOR VSC

3.2.1. CLASSIFICATION OF PASSIVE FILTERS

Typically, a low-pass filter, a band-stop filter topology or combination of both can be chosen to limit the harmonic content to the grid effectively. In *Figure 3.1*, several common passive filters are illustrated on a per-phase basis.

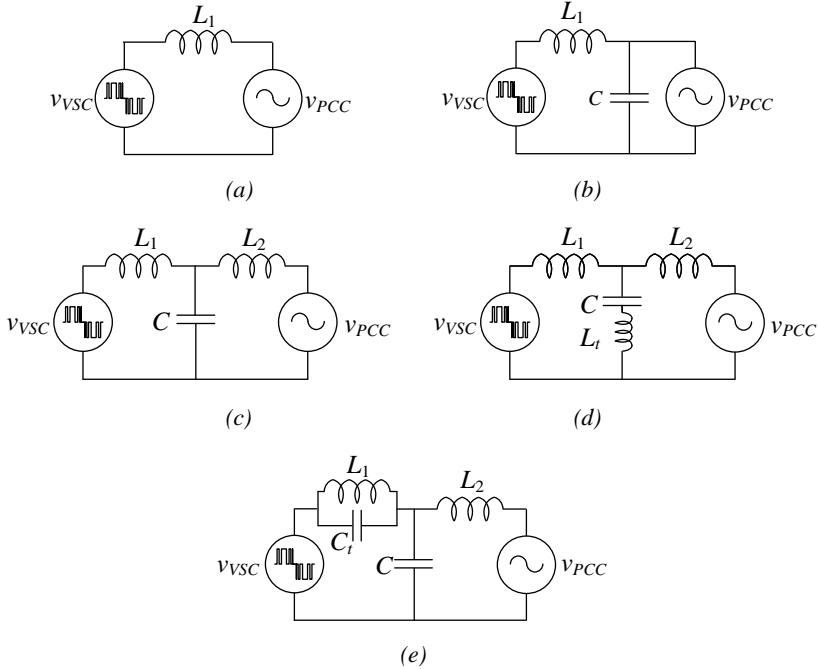


Figure 3.1: Conventional passive filters used in grid-connected VSCs: (a) Single inductance (L filter); (b) Second-order low pass (LC filter); (c) Third-order low pass (LCL filter); (d) Shunt trap configuration ($LLCL$ filter); (e) Series trap configuration.

A simple inductor (L filter), which is illustrated in *Figure 3.1 (a)* is the simplest filtering solution. The resonance of this type of filter with the system impedance is avoided since the utility grid is inductive in most applications. However, a large inductance in the L filter is required to limit the high frequency switching ripple from the PWM, which results in a bulky and expensive passive filter. The low ripple condition leads to a high efficiency as a result of lower core losses, similar to the 50/60 Hz utility transformers. The drawbacks are very high cost and excessive voltage drop across the inductor, which limits the use of this solution for applications above several kW [19], unless interleaved [60] or multi-level VSCs [61] are employed.

On the other hand, a low-pass LC or an LCL filter, which are illustrated in *Figure 3.1 (b)-(c)* provide two or three times more attenuation (dB/decade) depending on the adopted cut-off frequency. Hence, a reduced size and cost of the filter can be obtained. On the assumption that the grid impedance is inductive, the LC filter can be perceived as an LCL filter. Two-stage LC filters in a cascaded configuration can also be used to limit both the current ripple and EMI noise [62].

Recently, a *trap* filter [63] was proposed as well for VSCs, as an alternative filter solution which can suppress the switching harmonics even better than the LCL filter. It uses single or multiple shunt LC -traps with close to zero impedance around the switching harmonics, which makes it possible to decrease the size of the filter [56], [64]–[67]. In [55], a *trap* filter was proposed for single-phase inverters as the $LLCL$ filter, which is illustrated in *Figure 3.1 (d)*.

The *trap* filter can be adopted in a series configuration as shown in *Figure 3.1(e)* [68]. In this case it can suppress the switching harmonics around the first carrier and can release in part the converter side inductance from the losses associated to the high frequency ripple. It provides a better trade-offs between size and power loss than the shunt *trap* configuration. However, at the fundamental frequency, the series *trap* consumes reactive power, while the shunt *trap* it produces reactive power [23]. The drawbacks of *trap* filters are the sensitivity to inductance and/or capacitance variation with the operating conditions, as well as the change of its impedance characteristic during life-time.

In general, the LCL filter is the most adopted solution since it provides the best trade-offs between the different features listed previously. The grid side inductance L_2 , in the LCL filter can be in some cases replaced by a step up or isolation transformer, which can be modeled by a fixed leakage inductance in series with a frequency dependent resistance [23].

3.2.2. FREQUENCY RESPONSE OF PASSIVE FILTERS

The LCL filter [18] can be seen to some extent as a generalized interfaced filter model (T equivalent circuit) as illustrated in *Figure 3.2*.

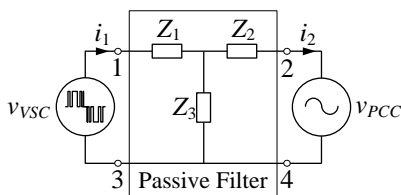


Figure 3.2: Four-terminal network of high-order passive filters [29].

Except the L filter, all other passive filter topologies can be simplified in a similar way to the LCL filter using the four-terminal network. The transfer admittances of the four-terminal network can be used to evaluate the frequency response of the passive filters and to establish basic design criteria.

For example, the input i_1 and output current i_2 of the filter can be expressed as a function of the admittance system as:

$$\begin{bmatrix} i_1(s) \\ i_2(s) \end{bmatrix} = \begin{bmatrix} Y_{11}(s) \\ Y_{21}(s) \end{bmatrix} v_{VSC}(s) + \begin{bmatrix} Y_{12}(s) \\ Y_{22}(s) \end{bmatrix} v_{PCC}(s) \quad (3.1)$$

where Y_{11} and Y_{22} are the primary and secondary short-circuit admittances, respectively, while Y_{12} and Y_{21} are the transfer short-circuit admittances.

From *Figure 3.2*, the short-circuit admittances can be derived as:

$$\begin{bmatrix} Y_{11}(s) \\ Y_{12}(s) \\ Y_{21}(s) \\ Y_{22}(s) \end{bmatrix} = \begin{bmatrix} \left. \frac{i_1(s)}{v_1(s)} \right|_{v_2=0} \\ \left. \frac{i_1(s)}{v_2(s)} \right|_{v_1=0} \\ \left. \frac{i_2(s)}{v_1(s)} \right|_{v_2=0} \\ \left. \frac{i_2(s)}{v_2(s)} \right|_{v_1=0} \end{bmatrix} = \frac{1}{Z_1(s)Z_2(s) + Z_1(s)Z_3(s) + Z_2(s)Z_3(s)} \begin{bmatrix} Z_2(s) + Z_3(s) \\ Z_3(s) \\ Z_3(s) \\ Z_1(s) + Z_3(s) \end{bmatrix} \quad (3.2)$$

It should be mentioned that the impedance on the grid side of the filter may or may not include the equivalent impedance of the grid, depending on the actual purpose of the study. If only the passive filter is to be investigated, then the grid impedance is not included. For stability analysis, it is often required to account for the influence of the grid impedance. In this case, the grid impedance can be included in Z_2 as long as there are no significant voltage harmonics at PCC for the frequency range of interest.

In a current controlled VSC, the filter transfer admittance Y_{21} can be used to evaluate the harmonic attenuation performance of the filter, *i.e.* indicates how the harmonic voltages specific to a given PWM method propagates into the grid current. In *Figure 3.3*, Y_{21} is shown for several passive filters.

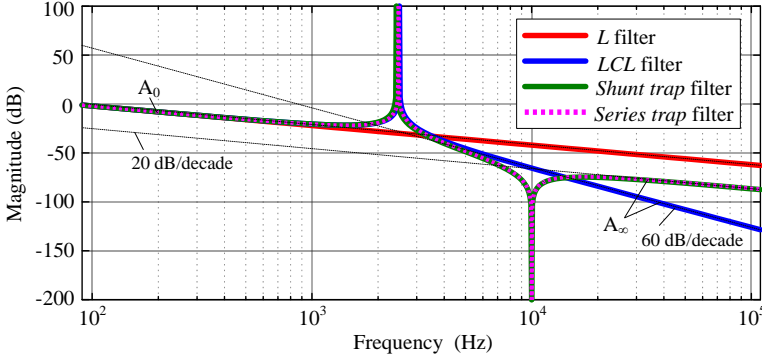


Figure 3.3: Transfer admittance Y_{21} of conventional passive filters used in grid-connected VSCs, provided the same ratings of passive components with $f_0=2.5$ kHz and $f_t=10$ kHz.

The transfer admittance of the LCL filter can be derived as [69]:

$$Y_{21(LCL)}(s) = A_0 \frac{1}{\frac{s^2}{\omega_0^2} + 1} = A_\infty \frac{1}{\frac{\omega_0^2}{s^2} + 1} \quad (3.3)$$

where $A_0 = 1/[s(L_1 + L_2)]$ is the low frequency asymptote; $A_\infty = 1/(s^3 L_1 L_2 C)$ is the high frequency asymptote resulted from the inverted pole arrangement of the filter transfer admittance; $\omega_0 = \sqrt{(L_1 + L_2)/(L_1 L_2 C)}$ is the characteristic frequency of the filters (the resonance frequency assuming no resistance in the passive filter).

Similarly, the transfer admittance of either of the *trap* filters can be derived as:

$$Y_{21(trap)}(s) = A_0 \frac{\frac{s^2}{\omega_t^2}}{\frac{s^2}{\omega_0^2} + 1} = A_\infty \frac{\frac{\omega_t^2}{s^2}}{\frac{\omega_0^2}{s^2} + 1} \quad (3.4)$$

where $A_0 = 1/[s(L_1 + L_2)]$; $A_\infty = L_t/[s(L_1 L_2 + L_1 L_t + L_2 L_t)]$; $\omega_t = \sqrt{(L_t C)^{-1}}$ and $\omega_0 = \sqrt{[L_1 L_2/(L_1 + L_2) + L_t] C}^{-1}$.

Following the previous representations of the passive filter transfer admittances, it simplifies the design of the passive filter. For example, A_0 can be used to design the passive filters based on the controllability of the VSC [70], while A_∞ can be used to design the attenuation of switching harmonics. In a *trap* filter, ω_t is used to tune the filter in such a way that the attenuation of the most dominant harmonics is achieved.

3.3. DAMPING CONSIDERATIONS

Similarly, as with any high-order passive filter (order equal or higher than two), the consequent resonance of the filter is one of the main reasons, which can threaten the stability of the network and may increase the harmonic distortions levels above the recommended limits. Damping is needed to limit the risk of instability in the control system of the VSC. Depending on the equivalent damping from the filter, the passive filters can be classified as:

1. Passive filters with inherent damping from the control system, grid impedance and/or equivalent resistance of the passive components
2. Passive filters with damping from additional passive damping circuits

The first category comprehends the most efficient filter solutions, since the use of additional passive components and the consequent power losses are avoided. However, in many of the practical situations, this solution cannot deal with all stability and/or sensitivity requirements. Therefore, the use of additional passive damped circuits may often be needed. Fortunately, there are several passive filter topologies, which can limit the power losses associated with damping [20]. Typical configuration of passive dampers in high-order filters are illustrated in *Figure 3.4*.

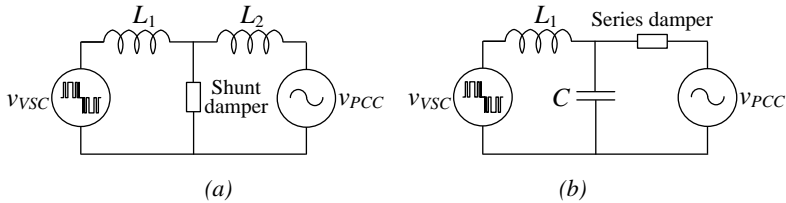


Figure 3.4: Configuration of passive dampers in high-order filters: (a) Shunt configuration; (b) Series configuration.

3.3.1. SHUNT PASSIVE DAMPED FILTERS FOR THE LCL FILTER

Shunt passive damped filters are preferred in general, due to lower ratings and higher damping performance compared with series damped filters. In *Figure 3.5*, several shunt passive filters for the LCL filter are illustrated.

A damping resistor in series with the filter capacitor is one of the most adopted passive damping solutions due to its simplicity in design and implementation as illustrated in *Figure 3.5 (a)* [19]. This solution is suitable, when the switching frequency is relatively high, case in which the filter capacitance is typically low, resulting in low fundamental current in the resistor.

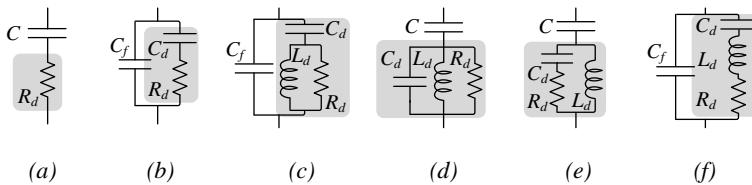


Figure 3.5: Shunt passive damped filters in LCL configuration: (a) Series resistor R ; (b) Shunt RC damper (first order); (c) Shunt RLC damper (second order); (d) Series RLC damper (resonant damper); (e) Third-order damper; (f) Single tuned damper.

The damping resistor can also be placed in parallel with the filter capacitor, but this solution is not practical since a high ripple current will flow into the resistor [71].

An improved damping solution can be the shunt RC damper illustrated in *Figure 3.5 (b)*. The main benefit of this filter is that the high frequency attenuation of the filter is retained to 60 dB/decade. Additionally, the power losses in the resistor can decrease with a proper selection of the split capacitor ratio [72]. More details about this filter topology can be found in [69].

A good high frequency attenuation and lower damping loss can be obtained by the second order damped filter (RLC circuit in parallel with the filter capacitor) as illustrated in *Figure 3.5 (c)* [73], since the fundamental current in the resistor is bypassed by the additional damping inductance L_d .

Similar benefits can be obtained by the use of a selective resonant circuit (parallel RLC circuit connected in series with the filter capacitor) as proposed in [46] and illustrated in *Figure 3.5 (d)*. The damping inductor and capacitor selectively bypasses the damping resistor below and above the resonance frequency of the filter.

The RLC circuit can be configured also as an conventional third-order damper [23], which is illustrated in *Figure 3.5 (e)*. It can be tuned both as a *trap* filter or resonant damper. It can ensure very low damping losses as in the previous two cases.

The *single tuned* damper illustrated *Figure 3.5 (f)* resonates around the characteristic frequency of the filter and can ensure both higher resonance damping and low damping loss. Since all the passive filters with RLC dampers provide similar functionalities, the main differences between them consist in different ratings and impulse voltage levels across the damping inductors and different sensitivities towards the parameter variation of passive components [14]. Thus, the insulation requirements are different with different passive dampers.

Under the presence of damping, the filter transfer admittance becomes dependent on the quality factor, which reduces the resonance magnitude and shifts the

resonance frequency of the filter. For example, for the LCL filter with series damping resistor, the transfer admittance can be derived as:

$$Y_{21(LCL+R)}(s) = A_0 \frac{\frac{Qs}{\omega_0} + 1}{\frac{s^2}{\omega_0^2} + \frac{Qs}{\omega_0} + 1} \quad (3.5)$$

where $A_0 = 1/[s(L_1 + L_2)]$; $A_\infty = R_d/(s^2 L_1 L_2)$; $\omega_0 = \sqrt{(L_1 + L_2)/(L_1 L_2 C)}$ and $Q = R_d/\sqrt{L_1 L_2}/[(L_1 + L_2)C]$. For shunt passive damped filters, the low frequency asymptote is always given by the sum of the converter and grid side inductances. However, the high frequency asymptote changes with the different passive filters. The transfer admittance of the LCL filter with shunt passive dampers is illustrated in *Figure 3.6*. The main difference between the shunt dampers is the resonance attenuation characteristics and the associated losses to achieve the required damping.

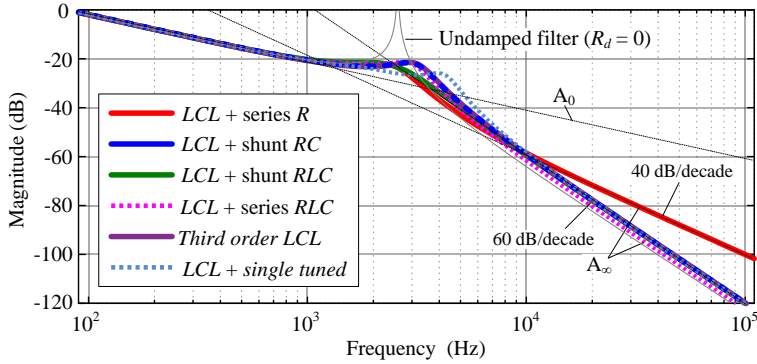


Figure 3.6: Transfer admittance Y_{21} of the LCL filter with shunt passive dampers, providing the same ratings of passive components and $f_0 = 2.5$ kHz.

3.3.2. SHUNT PASSIVE DAMPED FILTERS FOR THE TRAP FILTER

For the *trap* filter, several passive damped circuits are illustrated in *Figure 3.7*. The shunt RC damper can be used for one *trap* and two *traps* filters as indicated in *Figure 3.7 (a)-(b)*, similar as for the LCL filter. However, the RC damper used in connection with *trap* filters improves the high frequency attenuation of the filters by 20 dB/decade [69].

The *C-type* damper illustrated in Figure 3.7 (c) is tuned in such a way that the switching harmonics voltages of the VSC are to be cancelled from the grid current and the damping losses due to switching harmonics are also reduced.

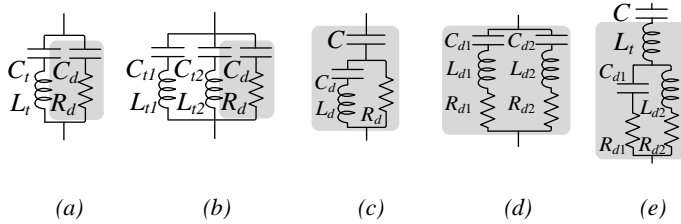


Figure 3.7: Shunt passive damped filters in trap configuration: (a) Shunt RC damper for one trap; (b) Shunt RC damper for two traps; (c) *C-type* damper; (d) 2 single tuned dampers; (e) Double tuned damper.

The *two single tuned dampers* illustrated in Figure 3.7 (d) and its alternative *double tuned damper*, which is shown in Figure 3.7 (e) can be used in situations where the harmonic limits are very low and a very high attenuation is required from the filters. Compared with *two single tuned dampers*, the *double tuned damper* can provide less power loss at fundamental frequency and only one inductor, instead of two is subjected to the full impulse voltage [23]. Additionally, it provides better sensitivity towards the tolerance of passive components if designed properly, e.g. they are less susceptible to de-tuning.

The transfer admittance of the *trap* filter with shunt passive dampers is illustrated in Figure 3.8.

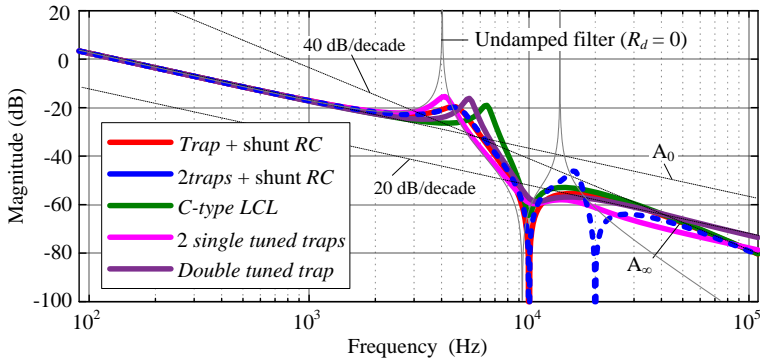


Figure 3.8: Transfer admittance Y_{21} of the trap filter with shunt passive dampers, provided the same ratings of passive components with $f_0 \approx 4$ kHz and $f_i = 10$ kHz.

$$Y_{21(C\text{-type})}(s) = A_0 \frac{\frac{s^3}{\omega_0 \omega_t^2 Q} + \frac{s^2}{\omega_t^2} + (n+1) \frac{s}{\omega_0 Q} + 1}{\frac{s^4}{\omega_0^2 \omega_t^2} + \left(\frac{n}{\omega_0^3} + \frac{1}{\omega_0 \omega_t^2} \right) \frac{s^3}{Q} + \left(\frac{1}{\omega_0^2} + \frac{1}{\omega_t^2} \right) s^2 + (n+1) \frac{s}{\omega_0 Q} + 1} \quad (3.6)$$

where $A_0 = 1/[s(L_1 + L_2)]$; $A_\infty = R_d/(s^2 L_1 L_2)$; $\omega_0 = \sqrt{(L_1 + L_2)/(L_1 L_2 C)}$; $\omega_t = \sqrt{1/(L_d C_d)}$ and $Q = \sqrt{L_1 L_2 / [(L_1 + L_2) C]} / R_d$.

3.3.3. SERIES PASSIVE DAMPED FILTERS

In some situations like damping of EMI filters [74] it is possible also to adopt series passive damped filters as those shown in *Figure 3.9*. In general, these solutions are not preferred since the design of such topologies is more complicated because of their series connection with the varying grid impedance. The damping resistor in parallel with the grid side inductance of the filter is illustrated in *Figure 3.9 (a)*. This filter provides lower size and loss than the shunt RL damper illustrated in *Figure 3.9 (b)* [74]. The series damped filters can be also used together with the shunt filters in a composite solution, which can result in damping methods that are less sensitive to grid impedance variations [75].

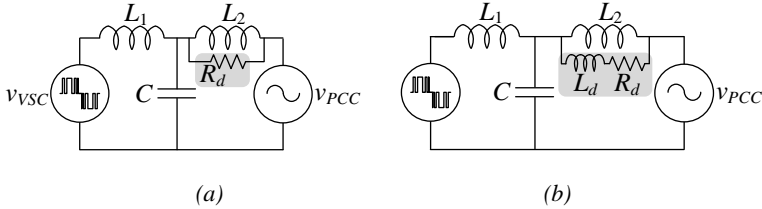


Figure 3.9: Series passive damped filters in LCL configuration: (a) Shunt resistor; (b) Shunt RL damper.

3.4. IMPEDANCE CHARACTERIZATION OF PASSIVE COMPONENTS

In the previous analysis, it has been considered that all passive components have ideal characteristics, that is, they exhibit linear relationship with the operating current and frequency. However, in practice, the ratings of passive component may change with the operating and environmental conditions, or they may be susceptible to aging. Depending on the application, it may drastically affect the frequency response of the passive filter. In addition, the passive components are subject to manufacturer tolerances. In general, the tolerance in commercial high voltage capacitors is $\pm 20\%$ while for inductors, they are $\pm 5\%$ [53]. In industrial

applications, the tolerances are in the range of + 5 % for capacitors and ± 2 % for inductors [53]. For kW range applications, the tolerances in capacitors are in the range of ± 20 % while for inductors ± 30 % [69].

3.4.1. EQUIVALENT MODELS OF PASSIVE COMPONENTS

Simplified equivalent models of the passive components are illustrated in *Figure 3.10*. Resistors employed in the passive filters to damp the oscillations, can be selected according to the power handling capability and their capacity to withstand high voltage surges [76]. Connecting two resistors with the same power rating in series increase the power handling capability by a factor of 2, while the connection in parallel by a factor of 4. Another important aspect is the reliability of power resistors, which is often far from acceptable. Shunt capacitors requires short cabling since the equivalent series inductance (ESL) may create resonances as low as few kHz, as it is observed in [77].

Since damping resistors have negligible influence on the high frequency impedance characteristics [76] and the capacitance can be considered relatively constant with the applied voltage, the key factor, which can influence on the passive filter frequency response, is represented by the inductors. The equivalent model of inductors contains a frequency and current dependent inductance, a series resistor corresponding to the loss in magnetic material (if a magnetic core is used), namely R_c , and a series resistor which corresponds to the inductor winding, namely R_w .

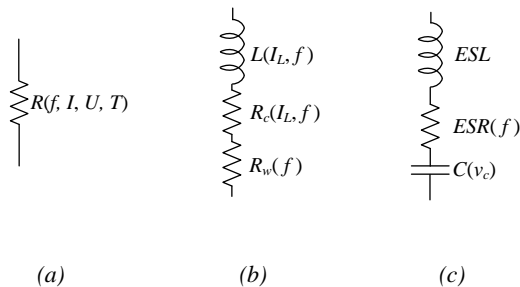


Figure 3.10: Equivalent models of passive components: (a) resistors; (b) inductors; (c) capacitors [76].

3.4.2. IMPACT OF THE INDUCTOR MODEL ON THE FREQUENCY RESPONSE OF THE PASSIVE FILTER

The equivalent inductance of inductors depends on the magnetic core and air gap reluctances, and the adopted number of turns, while the equivalent dc resistance

depends mainly on the length and cross-section area of the winding, and the equivalent wire resistivity. Some examples of L , R characteristics of different single-phase commercial inductors used for PV inverters (10 kHz range) and which are measured with a Magnetic Precision Analyzer PMA 3260B, are shown in *Figure 3.11*.

It can be seen that the initial inductance (at 0 current) is about 20-40 % higher than the rated inductance (L_{rated}) due to the characteristics of the magnetic material. On the other hand, the winding resistance increase linearly with frequency, and at 2.5 kHz it is about 3 to 10 times higher than the dc component. The frequency at 2.5 kHz is of particular interest and is chosen as reference value for the rated resistance (R_{rated}), as at this frequency it affects the damping of the passive filter (if an LCL filter is selected). The winding resistance is measured at zero current, in order to avoid changes in the wire resistivity due to changes in the operating temperature.

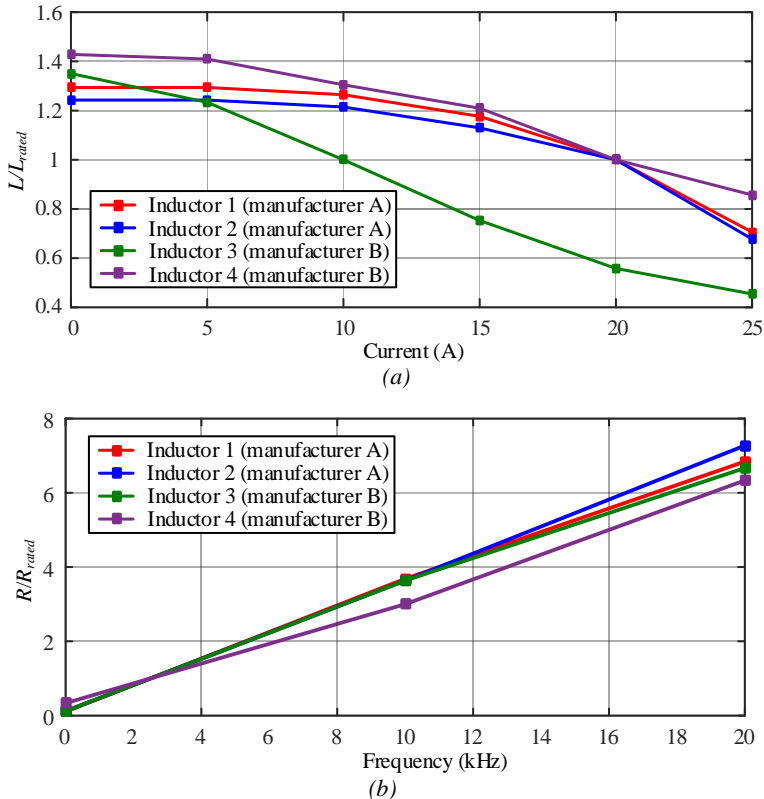


Figure 3.11: Inductor characterization: (a) Inductance dependence with current where L_{rated} is 1.7 mH (Inductor 1), 1.8 mH (Inductor 2), 3.9 mH (Inductor 3) and 1 mH (Inductor 4); (b) Frequency dependence of the winding resistance, where R_{rated} is 1.9 Ω (Inductor 1), 1.65 Ω (Inductor 2), 1.65 Ω (Inductor 3) and 0.6 Ω (Inductor 4) at 2.5 kHz.

The impedance of the inductors is not significantly changed compared with the ideal inductor, since the inductive reactance is much larger than the resistance, resulting in a phase angle of about 86-88 degrees, for the frequency range of interest. However, it affects the damping of the passive filter, as it is shown in *Figure 3.12*. The ideal filter uses only the inductance information of the *Inductor 2*, for the converter side inductance and of the *Inductor 1*, for the grid side inductance. The frequency response of the actual filter @ 20 A, adds the 2.5 kHz corresponding winding resistance information, which results in dampening the filter resonance. The actual filter @ 0 A considers also the variation in the filter inductance, so the inductances are increased with 25 % and 30 %, respectively, which result in shifting the resonance frequency of the filter. For this particular case, only the influences of the inductance variation and winding resistance were illustrated. The effect of the series resistance corresponding to the loss in magnetic material should also be considered for more detailed analysis.

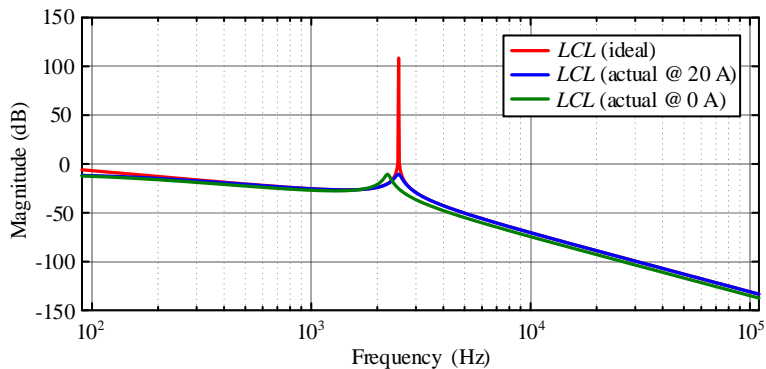


Figure 3.12: Influence of the actual winding resistance and variable inductance on the frequency response of the LCL filter.

3.5. SUMMARY

In this chapter, several passive filters and a comprehensive selection of passive damping circuits for use in VSC applications have been categorized. It was shown how a high-order filter, like the *LCL* or *trap* filters can provide reduced size as consequence of high filtering attenuation. However, the drawback denoted by the presence of resonances in the filter frequency response, may require the use of an additional damping circuit. Different passive filter solutions to damp the filter resonances are given. However, the best suited topology is to be decided depending on the intended application, since with passive damping, there is no significant influence on the low and high frequency behavior of the filter. It is also shown, how the winding resistance of the inductors can contribute to the damping of the filter and can significantly reduce the resonant peaks in the frequency response. The

inductance dependence with current plays a role in lowering the filter resonance frequency with decreasing operating current. However, the effect of the series resistance corresponding to the loss in magnetic material should also be considered for more detailed analysis.

CHAPTER 4. CHARACTERIZATION OF INDUCTIVE COMPONENTS

The characterization of inductive components, which are the main part of the passive filters used in VSC applications, is presented in this chapter. It is shown how in a high-order filter, the inductor on the converter side of the VSC is the limiting factor, when is to be decided about the passive filter size, cost and efficiency. Several magnetic materials are compared in terms of power losses, and their non-linear characteristic is fully explored. Using a dc chopper and a B-H analyzer, the core loss is measured for each operating point, and then stored in a loss map for the respective core material. Then, by using an electrical circuit simulation software, different inductor designs can be analyzed together with the loss information. The role of different inductors in passive filters is also highlighted, together with their corresponding sizing considerations.

4.1. INTRODUCTION

The efficiency of a high-order filter is limited by the choice and design of the AC filter inductor adopted on the output of the VSC to cancel the switching harmonics due to PWM [5], [21]. For example, the operating waveforms of different inductors employed in a high-order filter are illustrated in *Figure 4.1*.

The inductor in the PWM filter is excited with rectangular voltages from the PWM, which have a considerable higher frequency than the fundamental grid frequency, resulting in significant power losses [78]. The loss highly depends on the adopted current ripple in the filter inductance, which further depends on the excitation voltage and magnetic material specifications. Unfortunately, appropriate guidelines on how to choose the current ripple in the inductor in order to limit the power loss are not common yet.

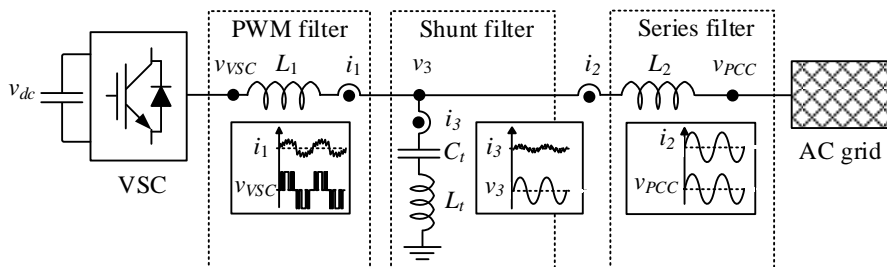


Figure 4.1: Characterization of inductors in grid-connected VSC with high-order filters.

A trade-off between efficiency versus size or cost dictates on the final choice of the inductor main parameters. In [79], an improved Generalized Steinmetz Equation (iGSE) is used to investigate the loss of the filter with the aim to minimize the weight of a 2 ~ 6 kHz power filter used in a 1.2 MVA VSC. A Pareto front optimization of the power loss of inductors and semiconductors reveal only a small range variation of the inductor and semiconductor losses (20 – 30 %) with changing the modulation method, core material (laminated Fe-Si vs. Amorphous) or winding material (Cu vs. Al). The weight of the filter can be decreased by a factor of 4 by increasing the total VSC losses with 50 %. Power loss of inductors are in the range of 0.1 ~ 0.2 % while the semiconductor losses are in the range of 0.8 ~ 1.5% depending on the aforementioned variables. However, these results are open for interpretation since the iGSE method cannot accurately describe the inductor core loss under PWM excitation and dc-bias magnetic field strength [21].

In [80], the power loss in the *LCL* filter and VSC are evaluated at no load condition using the Natural Steinmetz Extension method (NSE). Here, the core loss results in the range of 0.3 ~ 0.5 % for a switching frequency of 2~12 kHz. The power loss in the semiconductors are 0.5 ~ 1 %, depending on the modulation method and dc-link voltage. However, the evaluation of instantaneous iron loss in the inductors in [22] show that under load conditions the core loss can be significantly higher. Therefore, different optimized designs of the *LCL* filter are performed for the grain-oriented Fe-Si material in [5] using more accurate loss models. It is shown that adopting around 20 % maximum ripple in the converter side inductance, the total filter loss is in the range of 1.2 ~ 2.2 % depending on the adopted volume and switching frequency of the filter. The *LCL* filter prototype built in [5] yields around 1.8% total power loss, out of which ~ 80 % of the loss is related to the converter side inductance only. In *Table 4.1*, a summary of the power losses in the VSC (semiconductor and switching loss) and losses in the passive filter is made. Therefore, for accurate core loss calculation, a loss mapping approach is considered in this thesis.

Table 4.1: Power loss in the VSC and LCL filter with laminated Fe-Si inductors

Reference	Frequency range	VSC loss	Filter loss	Core loss calculation method	Verified
[79]	2~6 kHz	0.8~1.5 %	0.1~0.2 %	iGSE	–
[80]	2~12 kHz	0.5~1 %	0.3~0.5 %	NSE	–
[5]	3~12 kHz	0.5~1.2 %	1.2~2.2 %	i ² GSE +loss mapping	yes

4.2. CHARACTERIZATION OF MAGNETIC MATERIALS

The key criteria for designing inductors are on the selection of the core material, corresponding air gap and of the windings [50].

4.2.1. OVERVIEW OF MAGNETIC MATERIALS

The main properties of common core materials are illustrated in *Table 4.2*. The magnetic cores can be divided in two main categories: with distributed gap (powder cores) or with discrete gap (cut cores). The cheapest cores from the two categories are the laminated Fe-Si and iron powder, but they also exhibit the highest core loss. Ferrites and Sendust materials are two alternatives that offer better cost/loss tradeoffs. In general, the magnetic cores with discrete gaps have linear B-H dependence for $B < B_{sat}$ (constant permeability) and exhibits hard saturation, while the powder cores have a non-linear B-H dependence for $B < B_{sat}$ (decreased permeability with increased excitation) and exhibits soft saturation. This fact can be seen from the B-H curves of the cheapest materials from the two categories, which are illustrated in *Figure 4.2*, together with the main parameters of the magnetic cores (where B_{max} is the maximum magnetic induction, B_r is the remanent induction, H_{max} is maximum magnetic field strength, H_c is the coercitive magnetic field strength, P_{cv} are the volumetric core losses and μ_a is the amplitude permeability).

Table 4.2: Comparison of different magnetic core materials [81]

Materials	μ	B_{sat} (T)	Core Loss	DC Bias	Relative Cost	Temp. Stability	Curie Temp.(°C)	
Powder	MPP (Ni-Fe-Mo)	14-200	0.7	Lower	Better	High	Best	450
	High Flux (Ni-Fe)	26-160	1.5	Low	Best	Medium	Better	500
	Sendust (Fe-Si-Al)	26-125	1	Low	Good	Low	Good	500
	Mega Flux (Fe-Si)	26-90	1.6	Medium	Best	Low	Better	700
	Iron (Fe)	10-100	1	High	Poor	Lowest	Poor	770
Strip	Silicon Steel (Fe-Si)		1.8	High	Best	Lowest	Good	740
	Amorphous (Fe-Si-Bo)	Up to 10000	1.5	Low	Better	Medium	Good	400
	Ferrite (Mn-Zn)		0.45	Lowest	Poor	Lowest	Poor	100~300

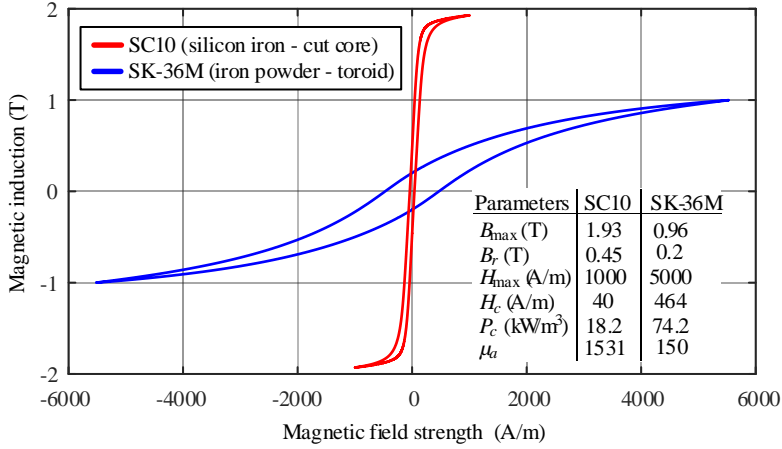


Figure 4.2: B-H dependence of laminated Fe-Si and Fe powder, measured with 50 Hz sinusoidal excitation.

4.2.2. BIAS CHARACTERISTICS OF INDUCTORS

The permeability μ dependence (or inductance decrease) as function of the dc-bias magnetic field H_0 are illustrated in *Figure 4.3* for magnetic core samples of equal volume (except the ferrite which is 1.5 times larger than others). The powder materials are toroidal cores, the silicon steel and amorphous are U cores, while the ferrite is of an E structure. The inductance factor A_L or the permeance of the core samples is defined as:

$$A_{L@0A} = \frac{L_0}{N^2} = \frac{\mu A_c}{l_e} = \frac{1}{\mathfrak{R}_{tot}} = \frac{1}{\mathfrak{R}_g + \mathfrak{R}_c} \quad (4.1)$$

$$A_{Lrated} = \frac{L_{rated}}{N^2} = \frac{L_0}{N^2} \frac{\mu\%}{100} \quad (4.2)$$

where L_0 and L_{rated} are the inductances of the core at zero and rated current, A_c is the cross-section area of the magnetic core, l_e is the effective length of the magnetic core path, l_g is the gap length specific to one leg of the magnetic core, N is the number of turns and \mathfrak{R}_t is the total reluctance of the core including air gap (given by the core reluctance \mathfrak{R}_c and gap reluctance \mathfrak{R}_g). The number of turns is dependent on H , l_e and the inductor current I as given by Ampere law:

$$N = \frac{H l_e}{I} \quad (4.3)$$

For designing inductors, it is reasonable to assume that 70 % of the initial permeability is achieved at rated current for powder cores, in order to “fully”

exploit the stored energy capability $L_{rated}I^2$. For gapped cores it can be considered to be around 95-100% of the initial permeability in order to avoid saturation.

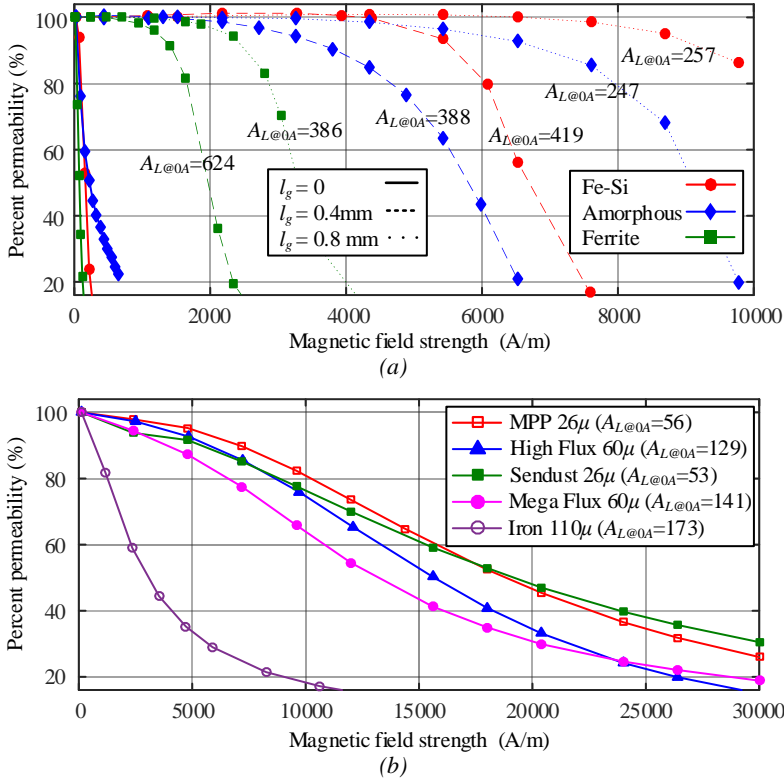


Figure 4.3: Dc bias characteristics of magnetic materials measured with a Magnetic Precision Analyzer PMA 3260B: (a) Laminated steel, amorphous and ferrite materials; (data not available in datasheets); (b) Powder materials with distributed gap (within ± 10 % deviation from the datasheet values).

4.2.3. ENERGY STORAGE CAPABILITY OF INDUCTORS

By considering a 1 mm diameter round wire for the inductor windings (with a current density of 5 A/mm^2) and considering a fixed H which avoids saturation of the core, the number of turns is readily available from the Ampere law. Since the inductance factor is fixed for a given material, the inductance value is given only by the number of turns, assuming a fixed current and H . By using the inductance factor from Figure 4.3, the inductance value can be calculated as function of N .

In Table 4.3, L , N and the energy storage capability LI^2 of the high permeability materials are shown, considering a H_{max} that corresponds to 95 % of the percentage

permeability at rated current. For the powder cores, 70 % percentage permeability is chosen in the design (including 95 % and 50 % for the Mega Flux core) and the results are shown in *Table 4.4*.

Due to the distributed air gap, powder cores can reach a maximum magnetic field strength H_{max} in the range of 10-80 kA/m. On the other hand, the ungapped laminated steel or ferrites materials can reach 1 kA/m. By adding air gap, the range of H can be increased, leading to higher storage capability.

In *Table 4.3* and *Table 4.4*, the window utilization factor k_u has been assumed 0.45. However, the number of turns that lead to $k_u = 0.45$ is exceeded for some inductor designs. In order to avoid excessive temperature rise in inductors, the number of turns should be decreased or a larger core should be adopted.

Table 4.3: Design examples of sample inductor with high permeability core materials

Sample	Fe-Si (SC10)		Amorphous (AMCC10)		Ferrite (E55 N87)	
	0.4	0.8	0.4	0.8	0.4	0.8
l_g (mm)	0.4	0.8	0.4	0.8	0.4	0.8
H_{max} (kA/m)	5	8.7	3	6	1.2	2.3
l_e (mm)	138	138	138	138	124	124
L (mH)	12.2	22	4.06	10.3	0.6	1.95
I_{max} (A)	4	4	4	4	4	4
N	175	300	105	210	32	73
LI^2 (mHA ²)	190	340	60	160	10	30
N ($k_u = 0.45$)	220	220	220	220	185	185

Table 4.4: Design examples of sample inductor with low permeability core materials

Sample	MPP (CM571)	High Flux (CH571)	Sendust (CS571)	Mega Flux (CK571)		Iron (SK-36M)	
	70	70	70	95	70	50	70
H_{max} (kA/m)	13	11	12	3	9	13	1.8
l_e (mm)	125	125	125	125	125	125	142.4
L (mH)	6.67	11	5.41	1.23	8.13	12	0.5
I (A)	4	4	4	4	4	4	4
N	414	350	382	96	287	414	65
LI^2 (mHA ²)	100	170	83	19	125	186	8
N ($K_u=0.45$)	300	300	300	300	300	300	400

From the considered magnetic cores, the silicon steel and amorphous materials offers the best cost/energy storage trade-offs. For the powder cores, it is possible to increase the energy storage capability by adopting lower percentage permeability which in turn will increase the size of the winding and associated cost/loss. Another

drawback is that with lower percentage permeability, the inductance will drop accordingly with the operating current.

4.3. DESIGN AND DESCRIPTION OF AC INDUCTORS

It was shown how the choice of a magnetic material can influence on the variation of the inductance with the operating current (see *Figure 4.3*). In the following, the derivation of the inductance and its corresponding current rating are given for common type of inductors found in high-order filters. The base ratings of the VSC can be used to refer the ratings of the passive components to that of the VSC system, as given by:

$$Z_b = \frac{3V_{PCC}^2}{S_{VSC}} \quad L_b = \frac{Z_b}{\omega_1} \quad C_b = \frac{1}{\omega_1 Z_b} \quad I_b = \frac{S_{VSC}}{3V_{PCC}} \quad (4.4)$$

where Z_b , L_b , C_b and I_b are the base impedance, base inductance, base capacitance and base current, respectively; V_{PCC} is the rms line to neutral voltage at the PCC, S_{VSC} is the apparent power of the VSC and ω_1 is fundamental frequency of the grid.

A high-order passive filter is illustrated in *Figure 4.1*. This filter structure can be used to analyze three different types of inductors, independently. Particularly, the filter inductor on the converter side of the filter is subjected to high frequency rectangular voltage excitation [21], which may lead to significant losses in the core [5] depending on the magnetic material [82] and current ripple specifications [83]. Additionally, shunt or series inductors that exists in the *LCL* or *trap* filters and which are subjected to sinusoidal excitation have different specifications and requirements compared to the inductor on the converter side of the filter as it is explained in the following.

4.3.1. CONVERTER SIDE INDUCTORS

PWM filters are mainly represented by an inductor subjected to rectangular excitation (which depends on the PWM method) of frequencies up to tens of kHz. The time varying switched excitation waveform $F(t)$ of the converter side inductor can be written in the general form as [84]:

$$\begin{aligned}
F(t) &= \frac{A_{00}}{2} + \sum_{n=1}^{\infty} \{A_{0n} \cos(n\omega_1 t) + B_{0n} \sin(n\omega_1 t)\} \\
&+ \sum_{m=1}^{\infty} \{A_{m0} \cos(m\omega_c t) + B_{m0} \sin(m\omega_c t)\} \\
&+ \sum_{m=1}^{\infty} \sum_{\substack{n=-\infty \\ n \neq 0}}^{\infty} \{A_{mn} \cos[(m\omega_c + n\omega_1)t] + B_{mn} \sin[(m\omega_c + n\omega_1)t]\}
\end{aligned} \tag{4.5}$$

where A_{00} is the dc offset of the time varying signal, the first summation term represents the fundamental and baseband harmonics, the second summation term represents the carrier harmonics, while the third summation term represents the carrier sideband harmonics. For a given PWM method, the magnitude of the $[m\omega_c + n\omega_1]$ harmonic voltage components can be found evaluating the double integral Fourier form [84] as:

$$C_{mn} = A_{mn} + jB_{mn} = \frac{1}{2\pi^2} \int_{-\pi}^{\pi} \int_{-\pi}^{\pi} F(x, y) e^{j(mx+ny)} dx dy \tag{4.6}$$

where $F(x, y)$ is the switched waveform for one fundamental period, ω_c is the carrier frequency and $x = \omega_c t$, ω_1 is the fundamental frequency and $y = \omega_1 t$, m is the carrier index (ω_c/ω_1); n is the baseband index. The analytical solutions of the Fourier coefficients for the most known PWM methods for single and three phase inverters are given in [85].

Once the harmonic spectrum of v_{VSC} is known, the inductance and current rating (to avoid saturation) of the PWM reactor can be found. The inductance of the PWM reactor is limited by the current ripple requirement. The inductance L_1 at the rated current is directly proportional with the dc-link voltage V_{dc} and inversely proportional with the maximum current ripple Δi_{1pk} and switching frequency f_s :

$$L_1 = \frac{V_{dc}}{r \Delta i_{1pk} f_{sw}} \tag{4.7}$$

Hence, the current ripple or inductance value depend mainly on the parameter r , which is dependent on the number of levels presented in the excitation voltage [50]. For a two-level three-phase VSC which uses the conventional Space Vector Modulation (SVM) (assuming a modulation index m_a of 0.9), the ripple factor $r = 24$ [69]. However, to evaluate the time varying current ripple, it is required to analyze its harmonic content around the switching frequency and its multiples. Above the characteristic frequency of the filter ω_0 , the individual harmonic current components in the PWM filter that contributes to the current ripple can be found as:

$$I_1(h) = \frac{V_1(h)}{h\omega_1 L_1} \Big|_{h_0 = \frac{\omega_0}{\omega_1}}^{h > h_0} \quad (4.8)$$

Then, the high frequency time varying current ripple waveform results as:

$$i_{1HF}(t) = \sum_{h > h_0}^n I_1(h) \cos(h\omega_1 t) \quad (4.9)$$

The current rating to design the converter side inductor in order to avoid the core saturation can be found as:

$$I_{1pk} = \max(i_{1LF}(t) + i_{1HF}(t)) = \frac{A_c B_{\max} N}{L_1} \quad (4.10)$$

where $i_{1LF}(t) = I_1 \cos(\omega_1 t)$; the maximum flux density of the inductor is chosen lower than the saturation flux density of the magnetic core such as $B_{\max} < B_{\text{sat}}$. The key trade-off in the PWM inductor design is the optimum selection (to minimize core loss) of the ripple current for a given magnetic material. The current ripple creates minor hysteresis loops related to the switching frequency modulation and are the major part of the core losses [22].

4.3.2. SHUNT INDUCTOR

Shunt filters can be used for PF correction, voltage support or harmonic compensation. The common operating frequencies of ac inductors in a harmonic shunt filter can be up to 3 kHz [53]. Shunt filtering can also be used to trap the ripple current from VSCs, especially in *trap* filter configurations [64]. For *trap* filters, the operating frequency of the inductors can reach tens of kHz [56]. The core loss of a shunt filter reactor can be measured with a high frequency (equal to the tuned frequency) and small amplitude sinusoidal voltage. The shunt inductance L_t can be derived as:

$$L_t = \frac{1}{\omega_t^2 C_t} \quad (4.11)$$

The current rating of the shunt inductor must consider the fundamental current given by the impedance of the shunt capacitor C_t and the high frequency ripple current from the converter current:

$$I_{3pk} = \max(i_{3LF}(t) + i_{1HF}(t)) = \frac{A_c B_{\max} N}{L_t} \quad (4.12)$$

where $i_{3LF}(t) = \omega_1 C_t V_1 \cos(\omega_1 t)$ is the fundamental current in the shunt reactor.

A fixed inductance value is desirable in shunt inductors, in order to avoid de-tuning of the filter during operation. For three-phase shunt filters, it is desirable to have three single-phase inductors in shunt configuration in order to avoid inductance mismatch due to mutual couplings. Magnetic cores with discrete gaps such as the amorphous or the laminated silicon steel are recommended for this type of inductors.

4.3.3. SERIES INDUCTOR

Sine wave filters or series inductors are used to smoothen out the grid current. They are driven by sinusoidal voltages at the fundamental grid frequency. Since full current (rated current of the VSC) have to be handled by the series inductors, high energy storage capability and low cost are preferable for this type of filter. Silicon steel is the preferable choice for this type of inductor.

4.4. EVALUATION OF CORE LOSSES IN PWM CONVERTERS

The frequency response of passive filters may be significantly damped as result of the losses in the magnetic core. Therefore, the core losses are measured and reported for different excitation conditions in the following.

4.4.1. DESCRIPTION OF THE MEASUREMENT METHOD

The core loss per volume (P_{cv}) for rectangular excitation voltages are measured with an IWATSU SY-8232 B-H analyzer and a dc-chopper, which is shown in *Figure 4.4*. The dc-chopper is used for the core loss measurement under dc-bias condition [21]. In short, the dc-chopper is operated with a 50 % duty cycle and its frequency can be selected in the range of 5 – 100 kHz. The input dc-link voltage V_{IN} can be varied in order to change the magnetic induction B of the inductor. The magnetic field strength H (dc-bias) is varied by adjusting the output current I_0 through the variable resistor R_0 . Then, the sample inductor has a secondary winding, which is used to detect B according to the two-winding core loss measurement method [86]. Detailed information about the measurement setup can be found in [21], [87]. Similarly, the core loss measurement under sinusoidal excitation voltage and rectangular voltage without dc-bias is measured with a standard B-H analyzer (IWATSU SY-8219).

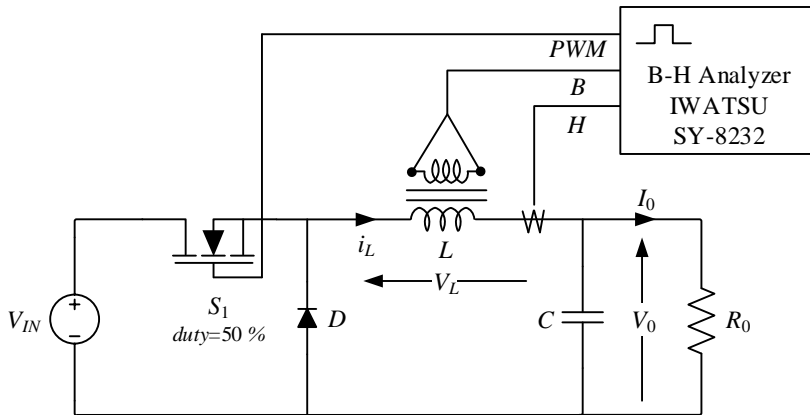


Figure 4.4: Buck chopper circuit for core loss measurement with a B-H analyzer SY-8232 [21].

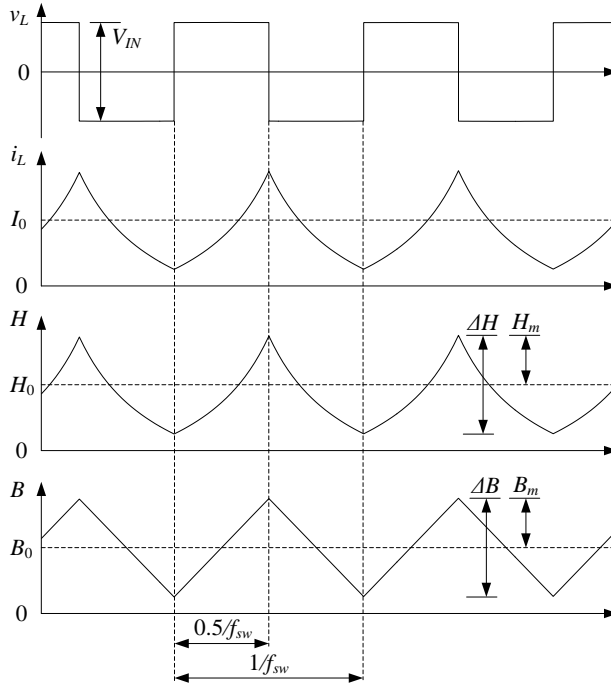
The operating waveforms for the core loss measurement are shown in *Figure 4.5*. In a PWM converter, the core losses in the magnetic material contain two components. One component is a low frequency component given by the area of the major hysteresis loop. Then, there are high frequency components of the excitation voltage, which generates a set of dynamic minor loops along the major hysteresis loop [78] and whose number is equal with the switching frequency of the PWM converter. The dc-chopper circuit is used to generate the minor loops independently, according to the desired operating conditions. Then, the total energy loss per fundamental cycle in the magnetic core is the sum of the areas given by the major hysteresis loop and each of the individual dynamic minor loops.

4.4.2. CORE LOSSES UNDER SINUSIODAL EXCITATION

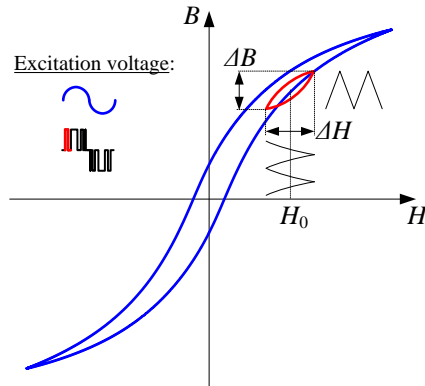
The core loss measured at 50 Hz sinusoidal excitation for the magnetic core samples presented in *Section 4.2.2*, are shown in *Figure 4.6* as function of the applied magnetic field strength. The core loss for materials with discrete gaps does not change significantly with different air gap length (if reported as function of the magnetic induction).

The Ampere law can be used to associate the core loss from *Figure 4.6* to the rated current of a given inductor. The 50 Hz core loss information can be used to design sine wave inductors, such as the inductor on the grid side of the filter. For shunt inductors, the core loss under higher frequency sinusoidal voltage excitation is needed.

Figure 4.6 reveals how the Amorphous, Ferrite, MPP or Sendust materials provides lower core losses, in accordance to the comparison given in Table 4.2.



(a)



(b)

Figure 4.5: Operating waveforms for core loss measurement: (a) Inductor waveforms in dc chopper circuit; (b) Major hysteresis loop due to low frequency sinusoidal excitation voltage (blue line) and dynamic minor loop due to high frequency rectangular excitation voltage (red line) [21].

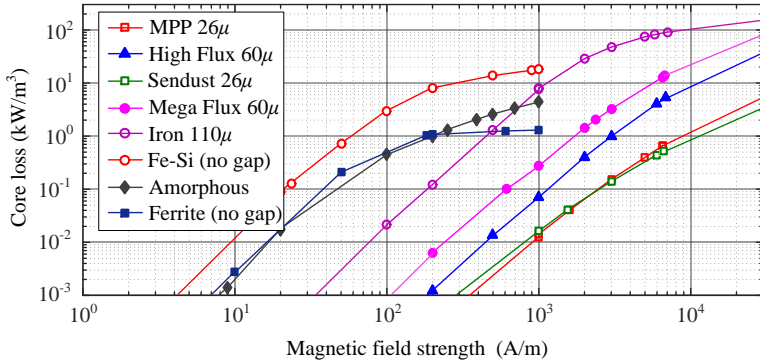


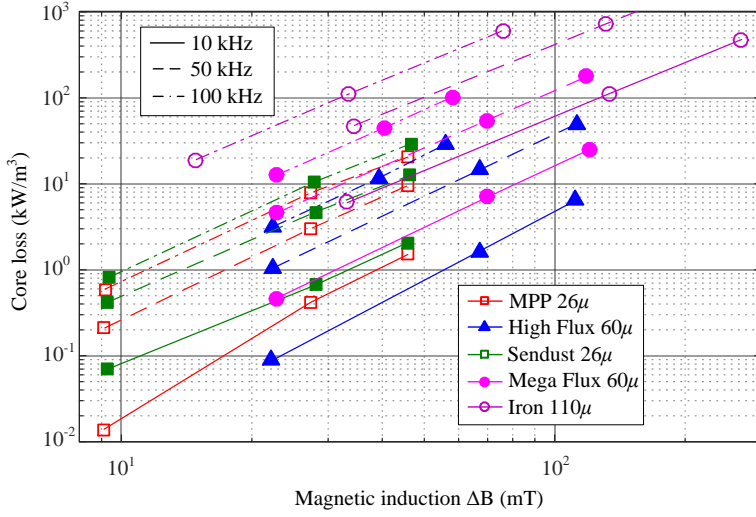
Figure 4.6: Core loss under sinusoidal excitation voltage (50 Hz) for different magnetic materials.

4.4.3. CORE LOSSES UNDER RECTANGULAR EXCITATION WITHOUT DC BIAS

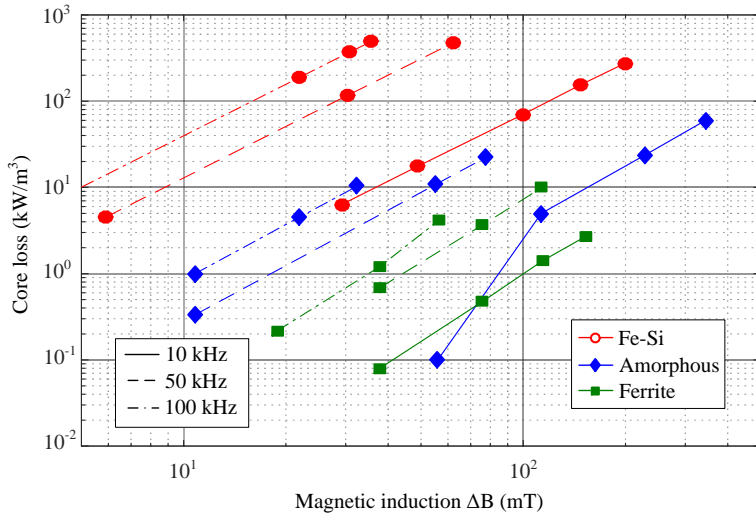
The core losses under rectangular voltage excitation without dc bias, *i.e.* $P_{cv}(f, \Delta B, H_0 = \text{ct.} = 0)$ are reported in *Figure 4.7* as function of the magnetic induction ripple ΔB . It can be followed that the watt loss associated with one dynamic minor loop can easily exceed the loss associated with the major loop given by the fundamental frequency component. That is, the watt losses of the minor loops are the major part of the losses in the inductor. It is for this reason, why the efficiency of high-order filters is dictated by the design of the inductor on the converter side of the filter and which is subjected to rectangular excitation voltage.

4.4.4. CORE LOSSES UNDER RECTANGULAR EXCITATION AND DC BIAS

The dc-bias condition of dynamic minor loops can contribute to increased losses in the core as it is illustrated in *Figure 4.8* for powder cores, *i.e.* $P_{cv}(f, H_0, \Delta B = \text{ct.} = 0.09 \text{ T})$. It follows from *Figure 4.7* and *Figure 4.8*, how the core loss evaluation from *Table 4.2* does not apply well for rectangular voltage excitation. For example, the MPP core does not provide lower core losses compared to other powder materials as it is recommended in *Table 4.2*. Therefore, for a given magnetic core material used in the inductor on the converter side of the filter, the final losses should consider both the low frequency and high frequency core loss components in addition to the loss caused by the winding.



(a)



(b)

Figure 4.7: Core loss versus frequency for rectangular voltage excitation (duty 50 %) and no dc bias ($H_0 = 0$) for: (a) Powder materials; (b) Laminated steel, amorphous and ferrite materials.

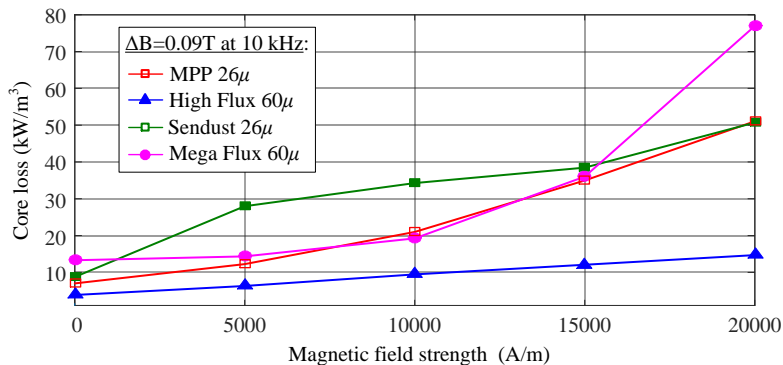


Figure 4.8: Core loss versus dc bias for rectangular voltage excitation (duty 50 % and 10 kHz switching frequency) with constant magnetic field induction ($\Delta B = 0.09$ T) for powder materials.

4.5. SPECIFIC INDUCTOR DESIGN

For a detailed analysis of the losses which occurs in the filter inductors, some specific designs are evaluated in the following. The filter inductors are designed for a 10 kHz single-phase PV inverter, supplying a 5 A_{pk} (Ampere peak) rated current at 230 V output rms voltage. The inverter is working under unipolar PWM with a $m_a = 0.9$.

4.5.1. INDUCTOR SPECIFICATIONS

Since the current ripple is the main design factor when is to be decided about the required inductance, three current ripple levels are selected for the inductor design, *i.e.* 5 %, 10 % and 20 % of the rated peak current, respectively. Four core materials are investigated for this application. The resulted inductor parameters are given in Table 4.5, where l_w is the length of the winding; $R_{w,dc100^\circ}$ is the dc resistance of the winding at 100 °C; $P_{w,dc}$ is the percent loss of the inductor corresponding to the dc resistance of the winding; N is the number of turns; $\mu\%$ is the percentage permeability of the inductor; Δi_{1pk} is the percentage current ripple calculated as half of the peak to peak current ripple at 5 A and L_{rated} is the rated inductance calculated at 5 A. The magnetic core samples are of equal volume of 28600 mm³. The main differences between the different designs are in the winding equivalent dc resistance and percentage of the inductance decrease with the operating current. To simplify the analysis, only the influence of the power loss due to the dc resistance and core loss will be investigated in the following. However, the influence of the frequency dependence of the winding resistance on the passive filter frequency response has been addressed in Section 3.4.2.

Table 4.5: Design example of sample inductor with low permeability core materials

Core	l_w (m)	R_{dc100} (Ω)	$P_{w,dc}$ (%)	N	$\mu\%$	Δi_{1pk} (%)	L_{rated} (mH)
CM571026 (MPP)	17.44	0.38	0.58	218	84	5	2.25
	11.02	0.24	0.37	147	92	10	1.125
	8.85	0.2	0.31	118	96	20	0.75
CH571060 (High Flux)	10.42	0.23	0.35	139	90	5	2.25
	6.79	0.15	0.23	97	93	10	1.125
	5.39	0.12	0.18	77	96	20	0.75
CS571026 (Sendust)	18.64	0.41	0.63	233	78	5	2.25
	11.85	0.26	0.4	158	85	10	1.125
	9.3	0.21	0.32	124	92	20	0.75
CK571060 (Mega Flux)	10.5	0.231	0.35	140	80	5	2.25
	6.65	0.146	0.22	95	88	10	1.125
	5.32	0.12	0.18	76	90	20	0.75

4.5.2. LOSS MAP OF THE MAGNETIC MATERIALS

A loss map of the magnetic material can be created from the core loss information given in *Figure 4.7* and *Figure 4.8*. The loss map is interpolated and extrapolated from the available measurement points using the Matlab function `interp()`, as it is illustrated in *Figure 4.9*. The accuracy of the loss map increases with the number of measurement points, but in general, the loss map is consistent with the operating frequency and magnetic field strength [22]. The loss maps illustrated in *Figure 4.9*, are given for a fixed magnetic field induction ripple $\Delta B = 0.09$ T. Therefore, for different ΔB , loss multiplication factors are created from $P_{cv}(f, \Delta B, H_0 = \text{ct.})$ curves illustrated in *Figure 4.7*. The loss multiplication factors for the four magnetic materials are illustrated in *Figure 4.10* and shows how core losses increases/decreases compared to the core loss measured at $\Delta B = 0.09$ T.

4.5.3. EVALUATION OF POWER LOSS IN INDUCTORS

The inductor operating waveforms obtained with a circuit simulator are shown in *Figure 4.11*. They correspond to the inductor designed with 5 % current ripple and Mega Flux core. The maximum magnetic field strength H is around 5600 A/m which results in around 10 kW/m^3 low frequency core losses as it can be read out from *Figure 4.6*. This would translate to around 0.3 W power loss. However, the high frequency loss is more tedious to be calculated. For given H , ΔB and equivalent frequency of the duty cycle, the corresponding loss for each duty cycle period has to be summed up during one fundamental period using the loss map.

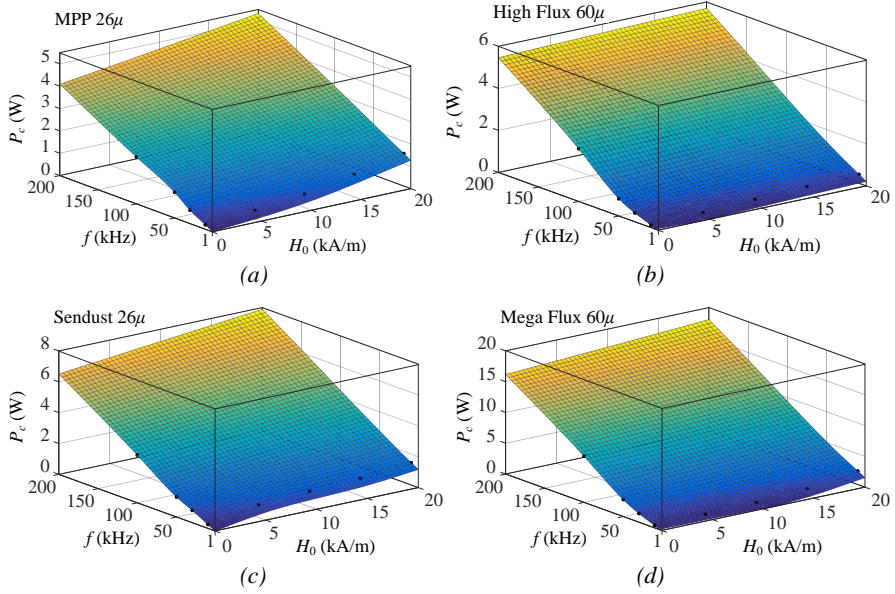


Figure 4.9: Core loss map under constant magnetic field induction ($\Delta B=0.09$ T) for: (a) MPP core; (b) High flux core; (c) Sendust core; (d) Mega flux core.

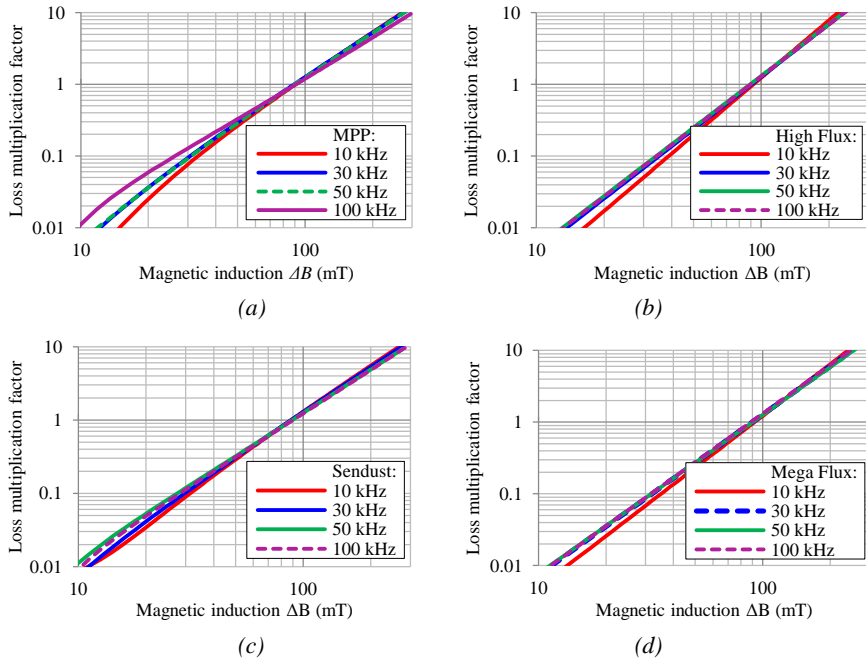


Figure 4.10: Loss multiplication factor as function of frequency for: (a) MPP core; (b) High flux core; (c) Sendust core; (d) Mega flux core.

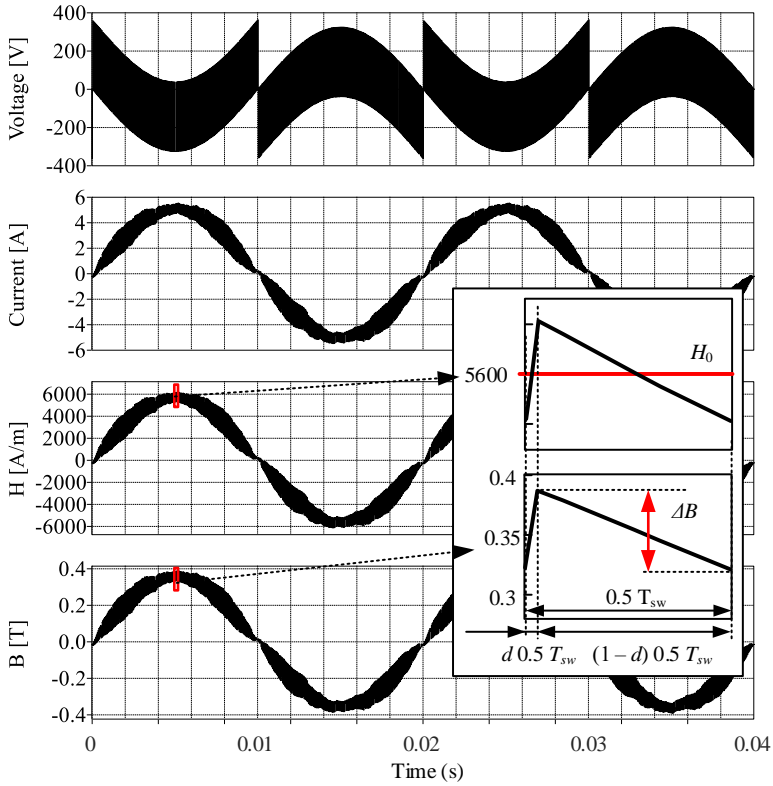


Figure 4.11: Simulated inductor waveforms with $L=2.25$ mH, $N=140$, $f_{sw}=10$ kHz and $\Delta i_{pk}=5$ %.

For example, at the peak current, the duty cycle is very low resulting in an equivalent frequency of 181 kHz for the on switching instance and 22 kHz for the off interval. Then, the dc-bias is around 5600 A/m and $\Delta B = 0.053$ T. From the loss map, the resulted core losses are 1.8 W and 0.14 W, respectively, for the considered half switching period. Summing up the losses for one fundamental period is resulting an average high frequency core loss of 4 W, which is only 13 times higher than the fundamental power loss. The reason is the low ripple condition chosen in the inductor design (5 %). The resulted total core losses are 0.53 %. The total core losses and the losses associated with the dc resistance of the winding, for the designed inductors are shown in Figure 4.12, with changing frequency. Since the inductors are designed for 10 kHz operation, decreasing the switching frequency to 5 kHz will double the maximum current ripple, resulting in around twice higher core losses. Doubling the switching frequency, it will reduce to half the current ripple, resulting in significant decrease of the core losses. It should be pointed out, that the results are shown for the same size of the magnetic cores with the parameters given in Table 4.5.

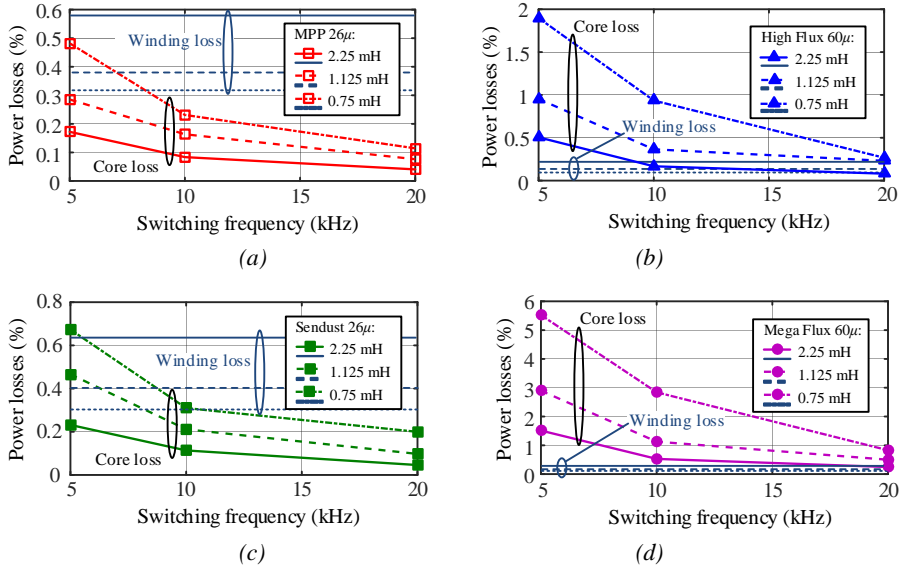


Figure 4.12: Power loss due to dc winding resistance and total core losses as function of frequency for: (a) MPP core; (b) High flux core; (c) Sendust core; (d) Mega flux core.

The results illustrated in Figure 4.12 reveals how a Mega Flux core can lead to significant losses (1-3 %), if a current ripple of 10 - 20 % is adopted in the filter design. The current ripple for typical *LCL* filters is recommended to be around 15 - 25 % [73], while for high-order filters in *trap* configuration, up to 60 % current ripple is suggested [56]. Therefore, the total loss can result significantly higher, which may damp significantly the passive filter frequency response. The equivalent resistance corresponding to the core loss can be derived as:

$$R_c = \frac{2P_c}{I_0^2} = 2P_c \left(\frac{N}{H_0 l_c} \right)^2 \quad (4.13)$$

It results that 1 % power loss is around 0.65 Ω resistor. Therefore, significant damping performance from the loss of inductors can be obtained, similar as with the equivalent resistance of the winding shown in Section 3.4.2.

In Figure 4.13, experimental B-H waveforms for the Mega Flux inductor are shown, considering $L = 2.25$ mH. The low frequency core loss P_{cvLF} is 37.5 kW/m³ and the total core loss P_{cv} is 1000 kW/m³ or 1.75 %. The winding loss is measured around 0.1 %, that is, do not significantly contribute to the total loss. However, if a sine filter has to be designed, the dc resistance will dominate the loss since no significant harmonics flows in sine filters and the low frequency core loss is relatively low.

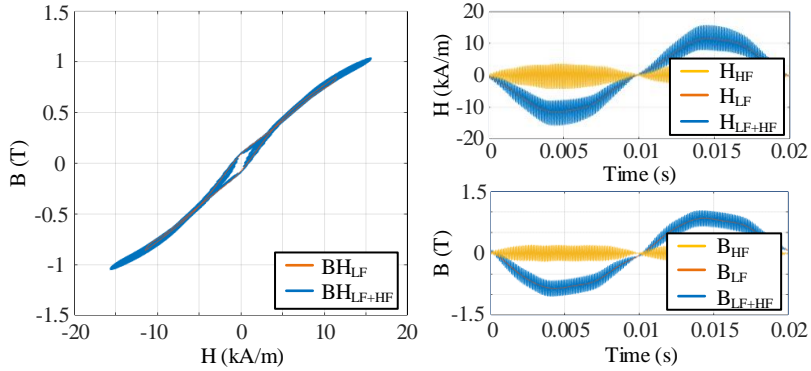


Figure 4.13: Experimental B-H waveforms for the inductor ($L = 2.25$ mH) with Mega Flux core at 5 kHz, 10 A_{pk} output current and $m_a = 0.5$.

4.6. SUMMARY

The physical design of inductive components and their loss characterization have been presented in this chapter. From the investigated core materials, the laminated steel has the best energy storage capability. However, it provides around 10 times higher core loss than the equivalent Mega Flux powder under rectangular voltage excitation. Hence, the laminated steel is the best candidate for sine wave filters applications. The powder materials are good candidates for PWM filters, especially at high ripple current, case in which the Sendust material can offer good cost/loss trade-offs. The Amorphous core can be seen as the material with the best trade-off between size and loss. Ferrites do provide lower core loss, but the energy storage capability is the lowest. In addition, the permeability and loss of ferrites are highly dependent on temperature. For shunt filter applications, magnetic cores with discrete gaps are preferred, in order to keep a fixed inductance value as function of the dc bias. The loss information of inductive components can be used to derive the equivalent loss resistance of inductors, which can be used further to calculate the inherent damping of the filter. The results are valid for low power applications, since in high power applications, the laminated steel material is most likely to be selected.

CHAPTER 5. PARAMETER SELECTION AND OPTIMIZATION OF HIGH-ORDER PASSIVE DAMPED FILTERS

In this chapter, the phase information of passive filters is introduced, in order to assess the stability of grid-connected VSC. It provides additional information to be used in the VSC controller design. A set of generalized stability conditions for grid-connected VSC with *LCL* filter are presented, which can be used to minimize the interactions of the VSC with the grid impedance. Afterwards, the main focus is the design of filters with passive damping, which are well known for their simplicity and robustness. An optimal damping design method is proposed, which ensures maximum damping performance by using lower rated passive components in the damping circuit. To differentiate between the features of the different passive filter topologies, an in-depth comparison and analysis is completed. Based on the performed analysis, a new passive damped filter is presented, which offers a good trade-off in terms of size and loss compared with the traditional *LCL* filter and *trap* filter.

5.1. STABILITY CONSIDERATIONS OF GRID-CONNECTED VSC WITH *LCL* FILTER

Cost-effective filter solutions have detrimental effects on the frequency response of the filter, especially below the switching frequency of the VSC. The response of the converter control system can cause a negative resistance for low order harmonics [52] as result of resonances that exist in the passive filter and the closed loop control system of the VSC [88].

A generalized single-phase diagram of a grid-connected VSC with an output *LCL* filter is illustrated in *Figure 5.1*. The equivalent damping offered by the filter components is neglected. The purpose is to find simple design guidelines, which can address the stability of the specified VSC system from *Figure 5.1*.

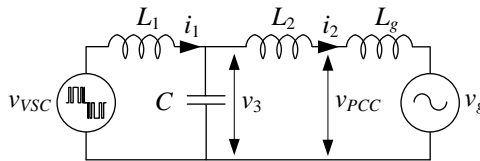


*Figure 5.1: Single-phase equivalent diagram of a grid-connected VSC with *LCL* filter.*

5.1.1. GENERALIZED STABILITY REGIONS FOR HIGH-ORDER PASSIVE FILTERS

A simplified control diagram of the current control closed loop system of the VSC, with either the converter ($x = 1$) or grid current feedback ($x = 2$), is illustrated in *Figure 5.2*.

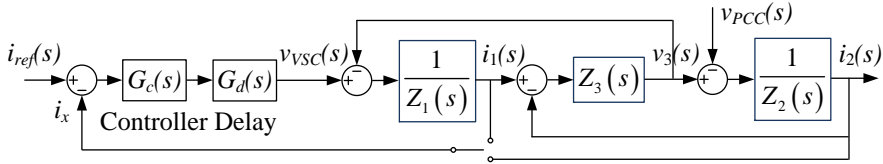


Figure 5.2: Control block diagram of the closed loop system with converter ($x=1$) and grid current feedback ($x=2$) [89].

It includes the current controller (G_c), the delay due to digital computation and PWM (G_d) and the impedance of the passive components. The impedance representation is adopted instead of the simplified representation of the filter given in *Figure 5.1*, for easy adaptation to other high-order passive filters. The delay is responsible for a phase lag in the control system and typically it accounts to about 1.5 of the sampling period, T_s [49]. It can provide stabilizing or destabilizing features to the current control and it have only been recently discussed in the literature [90]–[95].

The current controller (Proportional+Resonant controller is selected for the forthcoming analysis) and control delay can be written as:

$$G_c(s) = k_p + \frac{k_i s}{s^2 + \omega_1^2} \quad (5.1) \quad G_d(s) = e^{-1.5T_s s} \quad (5.2)$$

where k_p and k_i are the current controller proportional and integral gains, selected as function of the desired crossover frequency ω_c and phase margin ϕ_m . The current controller gains and the crossover frequency are defined as [96]:

$$\omega_c = \frac{\pi - \phi_m}{1.5T_s}, \quad k_p \approx \omega_c (L_1 + L_2), \quad k_i \approx k_p \frac{\omega_c}{10} \quad (5.3)$$

For stability analysis, it is suitable to consider only the proportional gain of the current controller [97]. Finally, the open loop current control transfer function can be written as:

$$G_{olv}(s) = G_c(s)G_d(s)Y_{x1}(s) \quad (5.4)$$

where the primary and transfer admittances of the LCL filter can be written respectively, as:

$$Y_{1(LCL)}(s) = A_0 \frac{\frac{s^2}{\gamma_2^2} + 1}{\frac{s^2}{\omega_0^2} + 1} \quad (5.5) \quad Y_{2(LCL)}(s) = A_0 \frac{1}{\frac{s^2}{\omega_0^2} + 1} \quad (5.6)$$

with $\gamma_2^2 = (L_1 C)^{-1}$ and A_0 and ω_0 defined in *Section 3.2.2*.

The bode diagram of the open loop transfer function of the VSC with LCL filter for the converter and grid current feedback is shown in *Figure 5.3* (the chosen LCL filter parameters will be explained in a later section). It has recently been shown, that no damping is required for the grid current control, if the LCL filter resonance frequency is higher than the critical resonance frequency, which is one sixth of the control frequency (for a total time delay of $1.5 T_s$) [90]. If the converter current is controlled, then, the opposite result is obtained [91]. Therefore, to emphasize the influence of damping on the control system, the corresponding diagrams for the LCL filter with a damping resistor connected in series with the filter capacitor, are also illustrated in *Figure 5.3*.

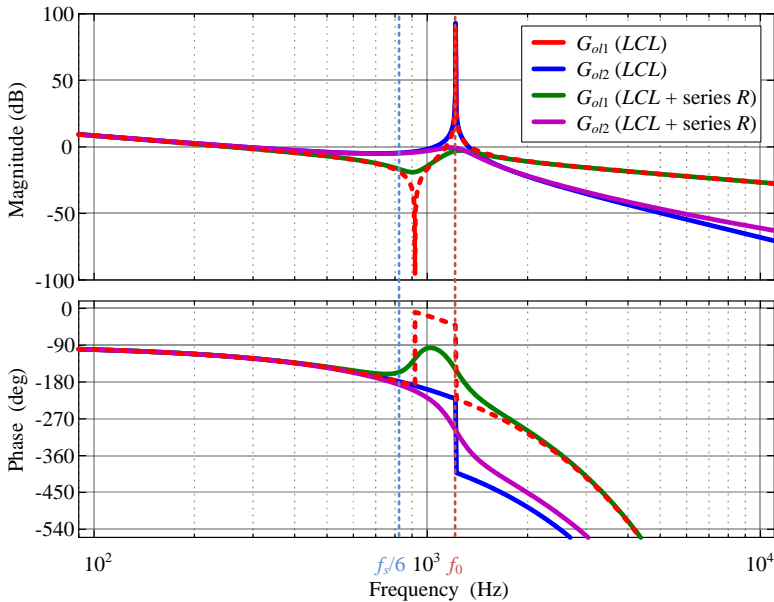


Figure 5.3: Bode diagram of G_{ol1} and G_{ol2} , for $L_1 = 2$ mH (4%), $L_2 = 1.5$ mH (3%), $C = 20$ μ F (10%), $R_d = 1.6$ Ω (0.3%), $k_p = 5$ and $k_i = 250$.

However, the resonance frequency of the filter can be very tedious to be calculated, especially if one has to take into account the detailed model of the filter with all the equivalent resistances. Instead, the characteristic frequency of the filter can be used for stability analysis (which considers zero resistance in the passive filter), which for the *LCL* filter is given by:

$$f_0 = \frac{1}{2\pi} \sqrt{\frac{L_1 + L_2}{L_1 L_2 C}} \quad (5.7)$$

With passive damping, both current control feedbacks are stable, as is illustrated in *Figure 5.3*. However, the converter current control of the *LCL* filter is unstable, according to the Nyquist stability criterion. On the other hand, the grid current control is stable, even if no damping is used, as result of f_0 being larger than $f_s/6$. Based on the placement of the filter characteristic frequency, a set of stability regions can be defined for the converter and grid current control [97] for an extended frequency range, as illustrated in *Figure 5.4*.

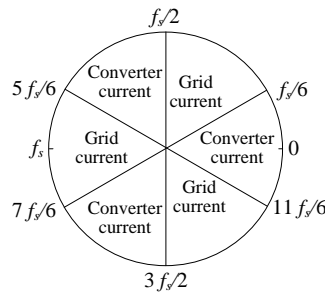


Figure 5.4: Generalized stability regions for VSC with high-order passive filters, provided that $T_d = 1.5 T_s$ [97].

Therefore, if for a given current control feedback, the characteristic frequency of the filter f_0 is placed between the boundaries defined according to *Figure 5.4*, the VSC with passive filter is individually stable. However, the current controller stability may still be influenced by the grid impedance. Additionally, the equivalent damping from the loss of passive components and variation in the filter ratings due to changes in the operating conditions also can influence on the stability regions, since it may shift the frequency of the resonance outside the boundaries.

5.1.2. VSC OUTPUT ADMITTANCE

The open loop transfer function G_{olx} of a grid-connected VSC, is used to design and to evaluate the stability of the VSC controllers with passive filters. That is, it ensures that the VSC is stable by itself [2]. However, to evaluate the stability of the VSC in connection with the varying grid impedance, it is required the VSC output

admittance [2]. Since the coupled internal signals of the VSC make the control block diagram of the VSC rather complicated (see *Figure 5.2*), it may become tedious to derive the canonical form for different control structures [98]. However, a lumped version of the VSC output admittance can be derived, if the control block diagram of the VSC is rearranged into a more complete form, without the coupling signals [99]. The decoupled canonical block diagram for different control structures is illustrated in *Figure 5.5* [99], which is different than the conventional control block diagram from *Figure 5.2*.

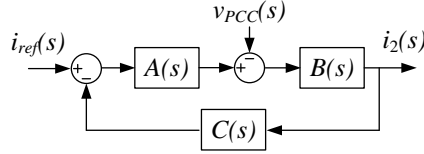


Figure 5.5: The decoupled canonical control block diagram of the closed loop current control [99].

From *Figure 5.5*, the VSC output admittance Y_{clx} can be written as:

$$Y_{clx}(s) = \left. \frac{i_2(s)}{v_{PCC}(s)} \right|_{i_{ref}=0} = \frac{B(s)}{1 + A(s)B(s)C(s)} \quad (5.8)$$

where:

$$\begin{aligned} A(s) &= \frac{Z_3(s)k_p e^{-1.5sT_s}}{Z_1(s) + Z_3(s) + k_p e^{-1.5sT_s}} \\ B(s) &= \frac{Z_1(s) + Z_3(s) + k_p e^{-1.5sT_s}}{Z_1(s)Z_3(s) + Z_1(s)Z_2(s) + Z_2(s)Z_3(s)} \\ C(s) &= \frac{Z_2(s) + Z_3(s)}{Z_3(s)} \end{aligned} \quad (5.9)$$

for the converter current control feedback ($x = 1$), and:

$$\begin{aligned} A(s) &= \frac{Z_3(s)k_p e^{-1.5sT_s}}{Z_1(s) + Z_3(s)} \\ B(s) &= \frac{Z_1(s) + Z_3(s)}{Z_1(s)Z_3(s) + Z_1(s)Z_2(s) + Z_2(s)Z_3(s)} \\ C(s) &= 1 \end{aligned} \quad (5.10)$$

for the grid current control feedback ($x = 2$).

The resulting impedance based model of the VSC with high-order filter is illustrated in *Figure 5.6*, together with the grid impedance.

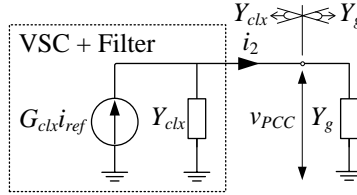


Figure 5.6: Impedance-based equivalent model of the VSC with high-order output filter [99].

To ensure that the control response of the VSC is passive, e.g. it has no negative resistance, an additional set of stability prerequisites must be satisfied [100]:

- $Y_{clx}(s)$ has no Right Half-Plane (RHP) poles.
- $\text{Re}\{Y_{clx}(j\omega)\} \geq 0 \Leftrightarrow \arg\{Y_{clx}(j\omega)\} \in [-90^\circ, 90^\circ], \forall \omega > 0.$

The two conditions are based on the passivity theorem and it ensures the stability of the VSC with the grid impedance, provided that the grid impedance is also passive. The output admittance of the VSC with the specifications and parameters from *Figure 5.3* is illustrated in *Figure 5.7*.

It should be pointed out that, as a result of the closed loop current control of the VSC output admittance, the resonance peaks of the filter admittance are significantly reduced (see *Figure 5.3*). Based on the stability analysis of the VSC output admittance with different grid impedances given in [2], *Figure 5.7* can be interpreted as follows:

- The magnitude of the VSC output admittance shows how the harmonics in the grid may be amplified. Since the magnitude is well below 1 dB, there is no risk of harmonic amplification.
- The resonance frequencies of the passive filter can have no significant influence on the VSC output admittance.
- Since the *LCL* filter with converter current control is unstable and have RHP poles, the VSC output admittance cannot be used for stability evaluation.
- The *LCL* filter with *series resistor* is individually stable for the converter current control feedback. However, due to the non-passive region of the admittance above $f_s/6$ and below f_0 , there is a risk of harmonic destabilization if the magnitude condition $|Y_{clx}| > |Y_g|$ and the negative phase angle crossover condition $\angle Y_{clx} - \angle Y_g = -\pi \pm 2\pi k$ are not satisfied, where k in an integer number, [2].

- Similarly, for the grid current control feedback, the *LCL* filter is stable, but it may destabilize the grid, due to the non-passive region of the admittance below $f_s/6$.
- For the *LCL* filter with *series resistor* and grid current control feedback, there is no risk of harmonic destabilization, provided that Y_g is passive.

Therefore, it becomes possible to design the passive filter stable regardless the grid impedance, by providing appropriate damping to the passive filter.

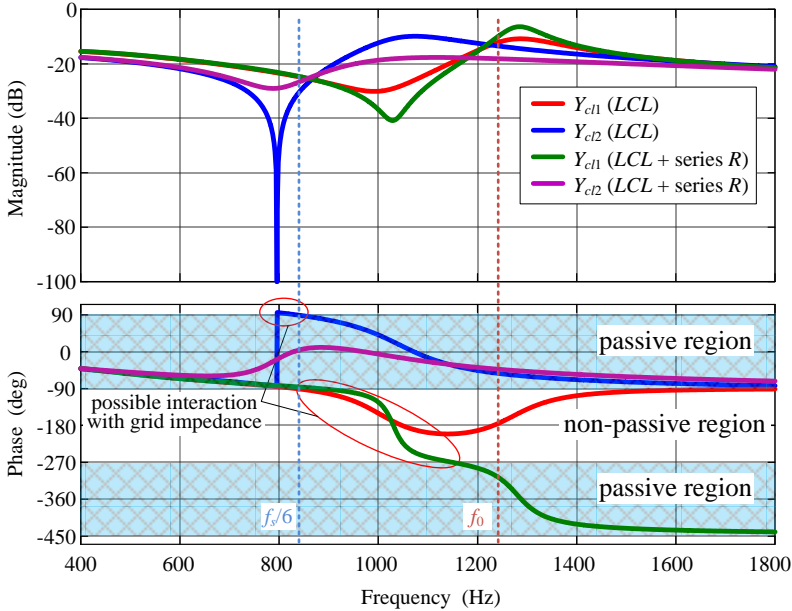


Figure 5.7: Bode diagram of VSC output admittance with different passive filters and current control feedback.

5.2. CONVENTIONAL AND OPTIMAL *LCL* FILTER DESIGN

The design of high-order filters is consistent with the *LCL* filter design in most situations [55]. Therefore, different design criteria are given for the *LCL* filter in the following.

5.2.1. CONVENTIONAL *LCL* FILTER DESIGN

A step-by-step design procedure for an *LCL* filter (see Figure 5.1) was introduced in [19]. It was suggested that the resonance frequency of the filter should be selected between ten times the line frequency and half the switching frequency in

order to ensure effective attenuation of the switching harmonics, and to prevent resonances caused by switching harmonics or low-order harmonics from grid background noise. The design guidelines apply for an operating switching frequency (f_s) of 5~10 kHz [54], [55], [83], [101]–[104]. In addition, the design procedure proposed in [19] enables a relatively fast design of the passive filter with a reduced number of iterations [48]. For example, it can be summarized as:

- Select the converter side inductance L_1 based on desired maximum current ripple in inductor Δi_{1max} .
- Select the filter capacitance C to be no more than 5 % of the base capacitance at rated conditions.
- The total inductance in the filter should be limited to 10 % in order to limit the voltage drop across the inductors.

5.2.2. OPTIMAL LCL FILTER DESIGN WITH MINIMIZATION OF THE STORED ENERGY

The optimization of the filter parameters based on the minimum stored energy with additional considerations on the ripple current, dc link voltage reserve for controllability and attenuation of the filter are given in [17]. An optimal design method of the *LCL* filter to meet the performance criteria can be summarized as follows:

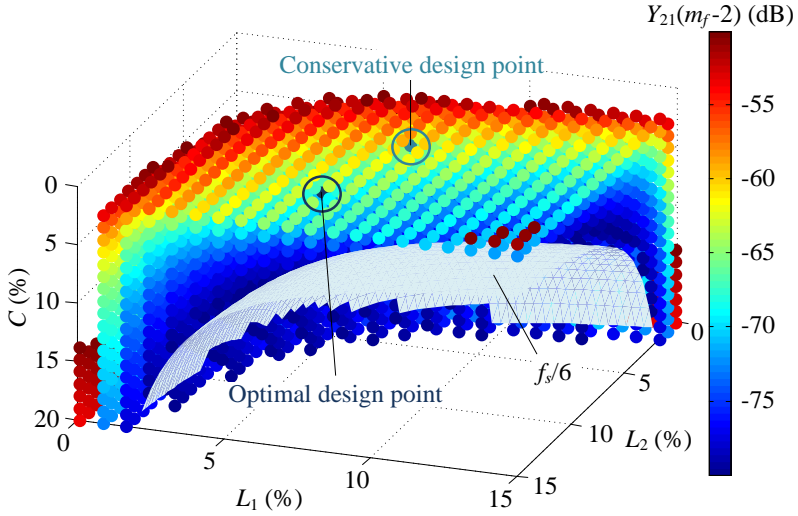
1. Calculate the amplitude of the converter voltage harmonics, $v_{VSC}(h)$ according to the selected PWM method.
2. Calculate the virtual admittance of the harmonic filter (Y_{vhf}) according to the considerations given in *Section 2.5*.
3. Choose the filter components based on the allowable current ripple in the converter side inductance without overrating the VSC, etc. by fulfilling the following admittance attenuation condition:

$$Y_{21}(h) \leq Y_{vhf}(h) \quad (5-11)$$

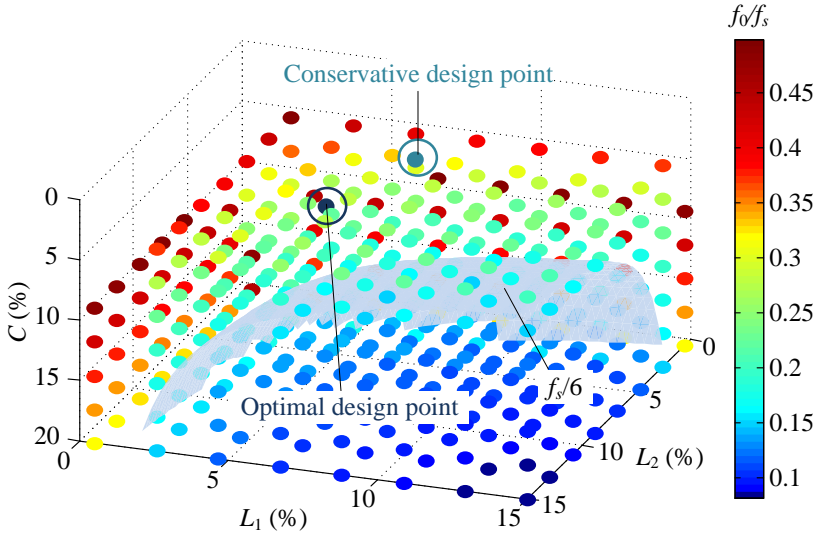
In *Figure 5.8 (a)*, the filter admittance $Y_{21}(h)$ is evaluated for a switching and sampling frequency (f_s) of 5 kHz at the $(m_f - 2)$ harmonic order as function of the variation of reasonable valued *LCL* filter parameters. Assuming that the THI-PWM method is used, then $Y_{vhf}(m_f - 2)$ is around – 65 dB for the IEEE 1574 standard. In *Figure 5.8 (b)* the characteristic frequency of the filter (f_0) is illustrated in order to assess the filter stability based on its placement as function of the $1/6^{\text{th}}$ of f_s .

The results shown in *Figure 5.8* shows that for a 5 kHz VSC, resonance frequencies lower than $\sim 0.2 f_s$ will lead to conservative designs of the passive filter. However, from *Figure 5.8 (a)* exists different solutions in the design space that fulfills the admittance attenuation condition. To reduce the size and cost of the passive filter,

some additional design constraints can be imposed like the limitation of the stored energy in the inductive components [17], [48], [105], [106].



(a)



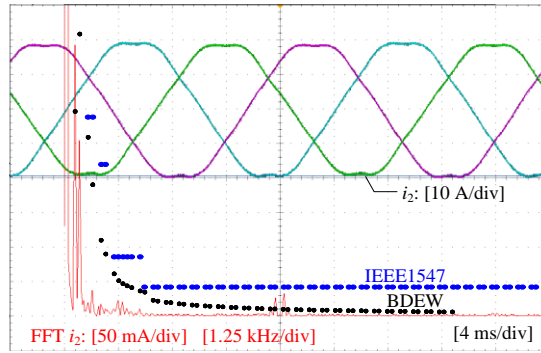
(b)

Figure 5.8: Simulated LCL filter parameters variation ($C_b=199\mu\text{F}$ and $L_b=51\text{mH}$) for $f_s = 5 \text{ kHz}$ as function of: (a) High frequency attenuation, Y_{21} at $(mf - 2)$; (b) Characteristic frequency, f_0 .

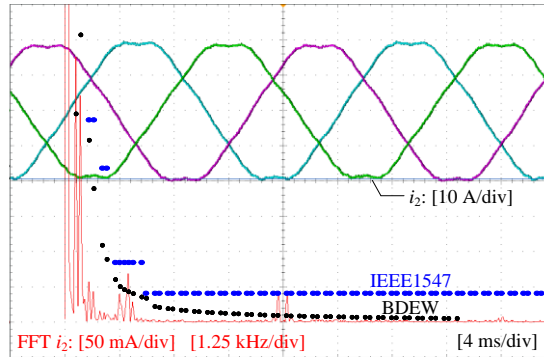
5.2.3. EXPERIMENTAL RESULTS

A 2-level 10 kW VSC with a 5 kHz switching frequency is selected to review the previous two design methods. Assuming about 10 % ripple in L_1 , the resulting inductance is 3.5 mH or 7 %. A 5 % filter capacitance translates to a 9.5 μF capacitance. The grid side inductance L_2 is selected to be 3 % or 1.5 mH. The converter current control is used as feedback variable. Hence, a damping resistor is connected in series with filter capacitor to stabilize the current controller.

The optimal design method considers the minimization of the stored energy in the filter inductors (7% total inductance and 10% capacitance are chosen). The steady-state current waveform and the filter/VSC ratings are shown in *Figure 5.9* for the conservative approach and the optimized filter.



(a) $L_1 = 3.5 \text{ mH}$ (7 %), $L_2 = 1.5 \text{ mH}$ (3 %), $C = 9.5 \mu\text{F}$ (5 %),
 $R_d = 1.4 \Omega$ (0.13 %), $P_d = 0.03 \%$, $k_p = 8.5$, $k_i = 450$



(b) $L_1 = 2 \text{ mH}$ (4 %), $L_2 = 1.5 \text{ mH}$ (3 %), $C = 20 \mu\text{F}$ (10 %),
 $R_d = 1.6 \Omega$ (0.3 %), $P_d = 0.4 \%$, $k_p = 5$, $k_i = 250$

Figure 5.9: Measurements for a designed LCL filter showing the output current harmonics response compared with IEEE 1547 and BDEW limits for a 10 kVA VSC with converter current control and $V_{dc} = 700 \text{ V}$, $f_s = 5 \text{ kHz}$: (a) Conservative approach; (b) Optimized filter.

The size of the filter for the optimized scenario results in decreased size/cost of the filter by roughly 35 %. However, the power losses in the damping resistor used to avoid oscillations are increased by a factor of 13 due to the increased capacitance and increased harmonic current in the filter. Consequently, the low order harmonics are more severe (measurements are made under same grid condition).

The given example is only to illustrate some possible design scenarios. For the elevated switching frequency, the conservative design approach will lead to an increased size compared to the given example. The design of the filters fulfills the IEEE 1547 standard. The more stringent recommendations such as VDE or BDEW imply the use of increased component ratings to fulfill the grid connection requirement. Additionally, no damping is required if the grid current is used for control feedback and damping loss can be avoided, as long as the resonance of the filter is higher than $1/6^{\text{th}}$ of the sampling period.

5.3. OPTIMAL DESIGN OF TRAP FILTERS

The use of *single* or *multi-tuned traps* in the shunt branch of the passive filter makes it possible to reduce the filter size and cost considerably [107]. The *tuned traps* attenuate the switching harmonics selectively, but the overall filter design becomes more challenging due to increased number of passive components. The per-phase schematic of *multi-tuned trap* filter is illustrated in *Figure 5.10*.

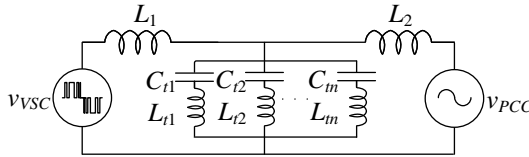


Figure 5.10: Per phase schematics of a multi-tuned trap filter.

5.3.1. CONVENTIONAL DESIGN OF THE INDIVIDUAL TRAPS BASED ON THE TRAP QUALITY FACTOR

One criteria to design the individual traps in a multi-tuned *trap* filter are the tuned frequency $\omega_{t(x)}$ and the quality factor of the individual traps [56]. The later, should be in the range of $10 \leq Q_{t(x)} \leq 50$ [55], [56]. Both the tuned frequency and quality factor of the x -tuned trap are given as:

$$\omega_{t(x)} = \sqrt{L_{t(x)} C_{t(x)}}^{-1}, \quad Q_{t(x)} = \frac{1}{R_{t(x)}} \sqrt{\frac{L_{t(x)}}{C_{t(x)}}} \quad (5-12)$$

where $L_{t(x)}$ is the tuned inductor, $C_{t(x)}$ is the tuned capacitor and $R_{t(x)}$ is the equivalent resistor of the tuned trap, mainly given by the *ESR* of the inductor and wiring resistance in the tuned trap. Therefore, assuming a fixed trap inductance, the quality factor varies only with the tuned capacitance or vice versa. The impedance of a tuned trap is illustrated in *Figure 5.11* for two different capacitances together with the definition of the bandwidth parameter (B_w) which describes how broad is the filtering action.

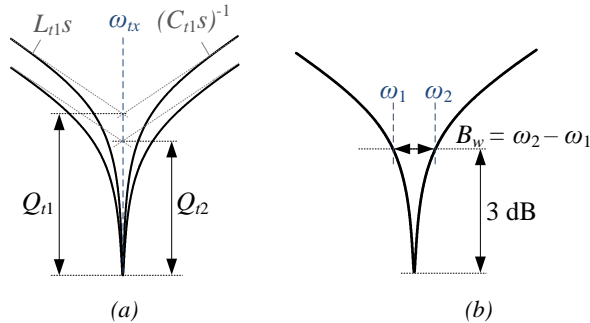


Figure 5.11: Characteristic impedance of the series tuned traps: (a) Provided same inductance/resistance and $Q_{t1} = 50$, $Q_{t2} = 25$; (b) Definition of the bandwidth parameter.

Therefore, with the bandwidth and quality factor information it becomes easier to design the tuned traps. However, both the bandwidth and quality factor implies complete knowledge of the trap resistance, which is more difficult to be calculated accurately.

Furthermore, values of the quality factor as recommended in [55], [56] typically applies for series tuned traps used to compensate individual low order harmonics that are presented in the grid. For a grid connected VSC, the tuned trap is responsible to reduce the entire spectrum of dominant sideband harmonics around the switching frequency or multiples.

The admittance of the *trap* filter, tuned around the switching frequency of the VSC is shown in *Figure 5.12* with varying the trap resistance. The virtual harmonic admittance of the filter considering the IEEE1547 standard and calculated for the sidebands harmonics $m_f \pm 2$, $m_f \pm 4$, $m_f \pm 8$, etc. is also illustrated in *Figure 5.12*. It can help to identify that the choice of the trap resistance value (and therefore the quality factor) does not significantly influence on the attenuation of dominant harmonics. Therefore, a design procedure with the quality factor/bandwidth in mind could turn tedious, especially if more than one trap is used.

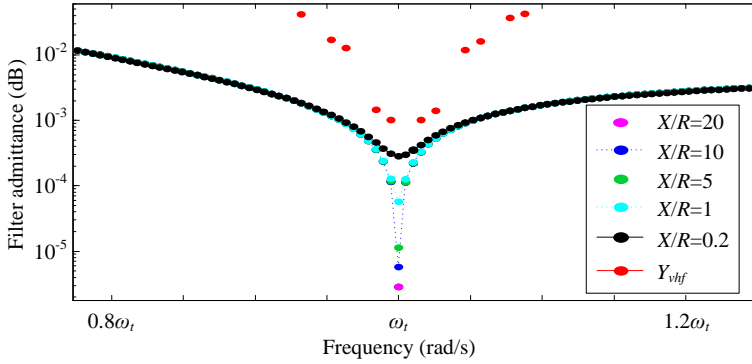


Figure 5.12: Filter admittance around the tuned frequency of the first trap for different X/R values (or Q factors).

5.3.2. IMPROVED DESIGN METHOD BASED ON INDIVIDUAL FUNCTIONS OF THE MULTI-SPLIT CAPACITORS

It was shown in *Figure 5.11* how the increase of the tuned trap capacitance will lead to an increase in the *trap* filter bandwidth, *i.e.* high attenuation is obtained for a broader range of frequencies. This fact is used to design the multi-tuned traps, by adequately split the filter capacitors such the switching harmonics are effectively reduced. The design problem of the multi-split for an n -*trap* filter is illustrated in *Table 5.1*. In short, the design problem reduces in defining the total filter capacitance and of the split factor (t_x), which defines how many times the capacitance in the trap tuned around the switching frequency is larger than the capacitance of $(x+1)$ – trap tuned around the multiple of the switching frequency.

Table 5.1: Design problem of a multi-tuned trap filter.

Step	Meaning	Multi-tuned trap filter	2 traps filter ($n = 2$)
1	Define the total capacitance	$C_t = \sum_{x=1}^n C_{t(x)}$	$C_t = C_{t1} + C_{t2}$
2	Find the split factor	$t_x \geq \left(\frac{\omega_{t(x+1)}}{\omega_{t1}} \right)^2 \Big _{x=1..n-1}$	$t_1 \geq \left(\frac{\omega_{t2}}{\omega_{t1}} \right)^2 = 4$
3	Find the trap capacitance of first tuned trap	$C_{t1} = \frac{C_t}{1 + \sum_{x=1}^{n-1} \frac{1}{t_x}}$	$C_{t1} = \frac{C_t}{1 + \frac{1}{t_1}} = \frac{t_1}{t_1 + 1} C_t$
4	Find the trap capacitance of first x -tuned trap	$C_{t(x+1)} = \frac{C_t}{1 + \sum_{x=1}^{n-1} \frac{1}{t_x}} \Big _{x=1..n-1}$	$C_{t2} = \frac{C_t}{1 + \frac{1}{t_1}} \frac{1}{t_1} = \frac{1}{t_1 + 1} C_t$

For a 2 *trap* filter, which is designed to attenuate the harmonics around the switching and twice the switching frequency, the previous precondition leads to the conservative limit of the split factor given by $t_1 \geq 4$. This ensures that the bandwidth of the second trap does not exceed the bandwidth of the first trap. The choice of the split factor is critical because it specifies how the two individual traps suppress the switching harmonics. For example, in [56], [107], relatively close values of the trap capacitors have been suggested for the multi-tuned *trap* filter ($1 \leq t_1 \leq 2$). Another solution is to adopt the conservative limit, *i.e.* $t_1=4$ as was also used for the *LTCL* filter in [56], which ensures the same bandwidth for the two traps. However, both solutions will not result in the most desirable solution since the second trap will have a broader attenuation compared with the first trap. This is equivalent to a larger capacitance than actually needed, which finally result into a larger fundamental current in the inductor since with higher capacitance, the fundamental current increases in the second trap.

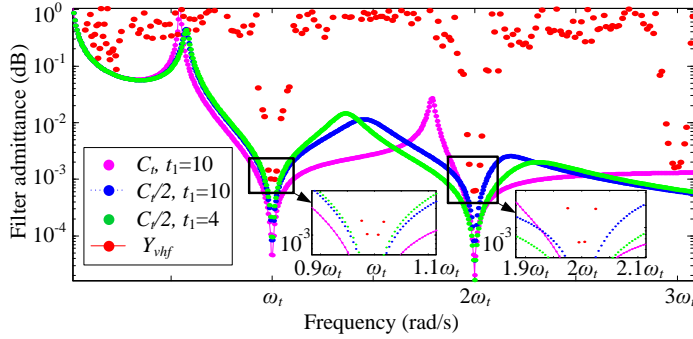
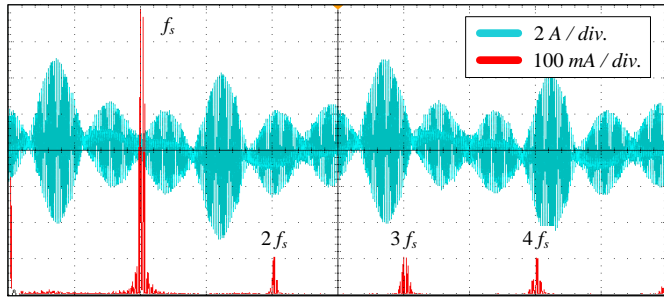


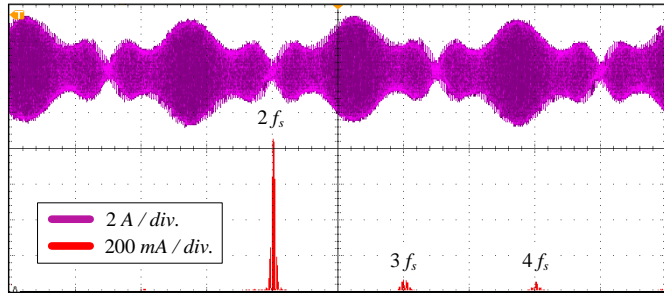
Figure 5.13: Examples of a 2 trap filter admittances Y_{21} for different trap capacitances (C_i) and split factors (t_1).

In the proposed design method, a split factor that ensures similar attenuation of the switching harmonics in the tuned traps is suggested, *i.e.* the tuned traps must have about the same broader attenuation around the most dominant harmonics. In *Figure 5.13*, the 2 *trap* filter admittance is illustrated for different split factors by varying the total capacitance. It reveals that once the split factor is properly designed, changing the total trap capacitance influences in the same way the attenuation of individual traps, so adjustments of the split factor are not necessary by changing the filter capacitance.

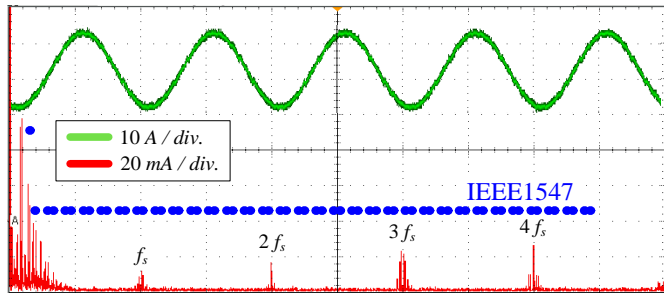
For a given total capacitance of the filter, the split factor can be calculated from Y_{vhf} , while the total capacitance can be adjusted afterwards based on the required attenuation of the filter, susceptibility of the filter towards the tolerances in the passive components, variation of the grid impedance, etc.



(a)



(b)



(c)

Figure 5.14: Measured current waveforms and harmonic spectrum of 2 trap filter with the proposed design method: (a) First trap; (b) Second trap; (c) Grid current.

The current waveforms of a 2 trap filter designed with the proposed method are illustrated in Figure 5.14. The filter is designed for a 10 kW VSC and 10 kHz switching frequency, with the main parameters of the filter given in Table 5.2.

5.4. OPTIMAL DESIGN OF PASSIVE DAMPERS

The design of passive dampers required to limit the resonances of high-order filters, result in a large range of available solutions for the choice of filter parameters [49], [75], similar as for the *LCL* filter design. However, by inspection of the filter behavior with different passive dampers, it is possible to limit the range of available solutions, similarly as with passive damped filters used in dc-dc converters [24]. In short, the optimization and design problem reduces to the proper selection of the multi-split capacitors or inductors in the high-order filter. However, the approach is different than that of the multi-tuned *trap* filter, as the aim here is to optimize the resonance damping. Several passive filters with multi-split capacitors or inductors are illustrated in *Figure 5.15*.

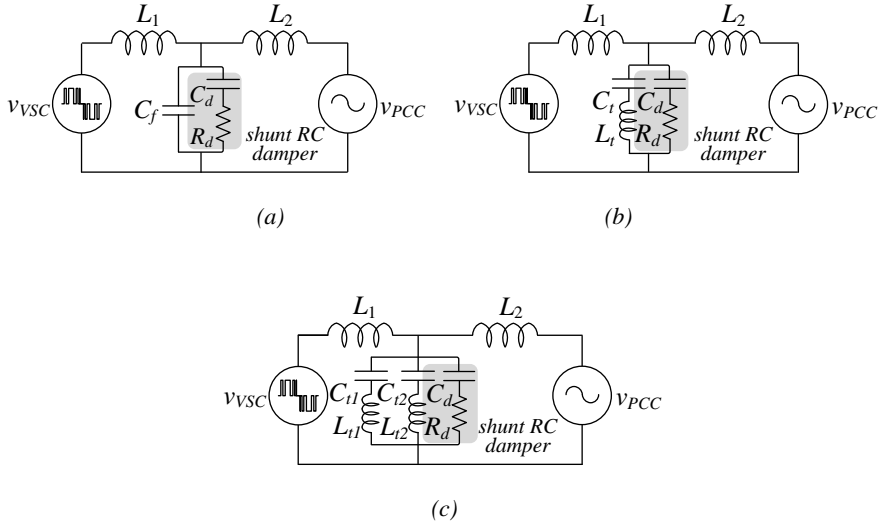


Figure 5.15: Passive filter configurations with multi-split capacitors and/or inductors: (a) LCL with shunt RC damper; (b) Trap with shunt RC damper; (c) 2 traps with shunt RC damper.

5.4.1. PROPOSED DESIGN METHOD

In the following, an optimal design method of passive dampers is given for the passive filters illustrated in *Figure 5.15*. However, it can be equally applied to other passive filters that use multi-split capacitors or inductors.

The principle of optimum damping is illustrated in *Figure 5.16*. It can be seen that a very low value of the damping resistor (low quality factor of $Q \approx 0$) or high value of the resistor (high quality factor of $Q \approx \infty$) lead to increased resonances in the filter at different frequencies defined in [69]. Then, there is only one value of the

damping resistor which causes the filter admittance to be minimum and this occurs at an optimum frequency ω_{opt} [24].

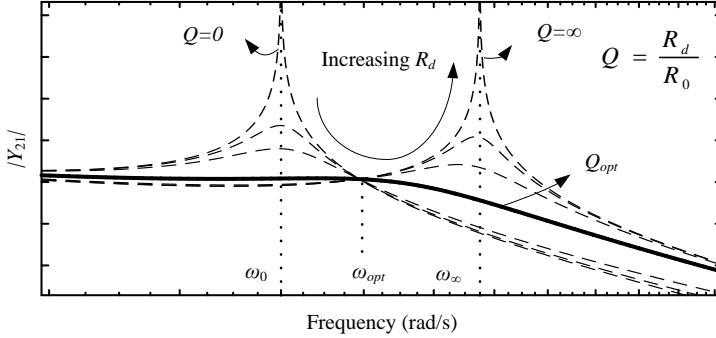


Figure 5.16: Optimum quality factor and frequency for passive filters with split capacitors and/or inductors.

Equating the passive filter transfer admittance when the damping resistor is zero and infinite respectively, ω_{opt} can be obtained from the equality condition:

$$\left| Y_{21}(s) \right|_{R_d=0} \Big|_{s=j\omega_{opt}} = \left| Y_{21}(s) \right|_{R_d=\infty} \Big|_{s=j\omega_{opt}} \quad (5-13)$$

For example, solving for the *LCL* filter with shunt *RC* damper, it will explicitly result in the following equality and ω_{opt} [69]:

$$Y_{21(LCL+RC)} = A_0 \frac{\frac{nQ_{opt}}{n+1} \frac{s}{\omega_0} + 1}{\frac{nQ_{opt}s^3}{(n+1)^2 \omega_0^3} + \frac{s^2}{\omega_0^2} + \frac{nQ_{opt}}{n+1} \frac{s}{\omega_0} + 1} \quad (5-14)$$

$$\left| \frac{s^2}{\omega_0^2} + 1 \right|_{s=j\omega_{opt}} = \left| \frac{s^2}{(n+1)\omega_0^2} + 1 \right|_{s=j\omega_{opt}} \rightarrow \omega_{opt} = \omega_0 \sqrt{\frac{2(n+1)}{n+2}} \quad (5-15)$$

where $n = C_d/C_f$. Then, the optimum quality factor which causes the filter admittance to be minimum, can be obtained from the derivative of the filter transfer admittance [69]:

$$\left[\frac{d}{d(x^2)} |Y_{21}|^2 \right]_{\substack{s=j\omega_{opt} \\ x = \frac{\omega_{opt}}{\omega_0} = \sqrt{\frac{2(n+1)}{n+2}}}} = 0 \quad (5-16)$$

$$\rightarrow Q_{opt} = \sqrt{\frac{(5n+4)(n+2)(n+1)}{2n^2(-n+4)}} \quad \text{for } n \in (0, 1.3]$$

The variation of the optimal quality factor as a function of the filter capacitors and/or inductor ratio is illustrated in *Figure 5.17* for the *LCL* filter and *trap* filter with shunt *RC* damper. For the *trap* filter, the quality factor depends also on the ratio between the trap inductance and filter inductance as given by:

$$a = \frac{L_1 + L_2}{L_1 L_2 \sum_{x=1}^n \frac{1}{L_{t(x)}}} \quad (5-17)$$

The proposed passive damping design can be simplified as follows:

1. Design the main passive filter parameters without additional damping.
2. By adding the damping circuit, find the optimum frequency (ω_{opt}) and quality factor (Q_{opt}) of the filter, which minimizes the peak in the filter attenuation admittance.
3. Choose the ratio of the split capacitors and/or inductors and decide the final value of the quality factor as a trade-off between damping performance (attenuation of the resonance peak), power losses in the damping resistor and decrease of high frequency attenuation.

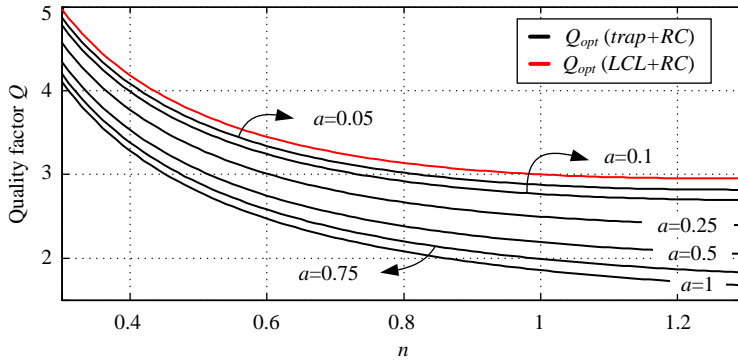


Figure 5.17: Optimal quality factor of the LCL filter and trap filter with shunt RC damper.

With the proposed design method, the damping circuit parameters depend only on the ratio between the split capacitors and/or inductors, which further depends on the conventional filter parameters without passive damping. The method further ensures low ratings of the passive components in the damping circuit [24].

5.4.2. ROBUST PASSIVE DAMPING DESIGN

It was shown in *Section 3.4.2*, how the actual impedance of the inductors can influence the frequency response of the passive filter. For robustness analysis of the filter design, the following considerations are made:

1. An inductive grid impedance is considered with an equivalent inductance in the range of 0.6 – 5 % (calculated from the base inductance of the VSC);
2. The percent permeability of the filter inductors is 70 % (in low load condition the inductance is 130 %);
3. The tolerances of the passive components are $\pm 30\%$ for the inductors and $\pm 20\%$ for the filter capacitors.

Therefore, a worst case of filter parameters can be included in the filter design, mainly given by the low load condition, high-grid impedance and increased tolerances in the passive components. Is resulting a value of 170 % of the designed filter inductors and 120 % of the filter capacitance [69] as a worst case scenario. In *Figure 5.18*, the root loci of the closed loop current control with the proposed passive filter design is shown for ideal and worst case operating conditions.

For the worst case parameter drift of the filter or grid inductance, adopting no damping resistor will result in harmonic instability whatever tuning of the current controllers. Finally, the choice of the split ratio of the capacitors as a trade-off between damping losses, resonance peak and harmonic attenuation is shown in *Figure 5.19*. It should be pointed out that if the obtained results are not satisfactory, then it is possible to increase or decrease the capacitance of the filter. For this case, there is an optimum point for $n \approx 1$, which ensures the required attenuation of the switching harmonics (0.3 % limit based on IEEE 1547), while keeping the damping losses low. The resonance peak in the open loop transfer function is limited to -6 dB. The optimization is performed for a 10 kW VSC (10 kHz switching frequency).

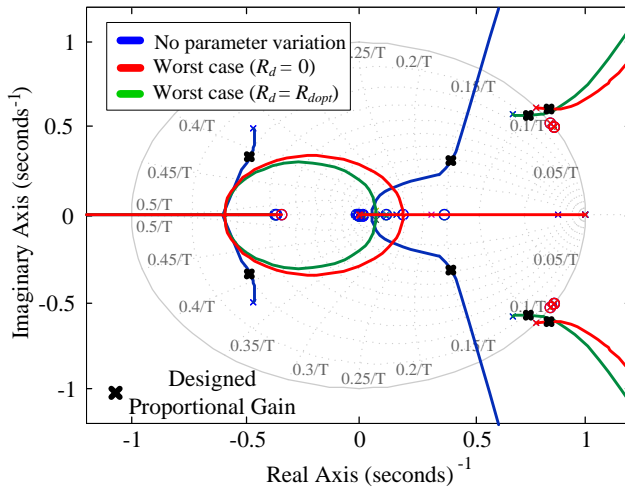


Figure 5.18: Root loci of the closed loop current control under ideal and worst case conditions for the trap filter with shunt RC damper (grid current control feedback)

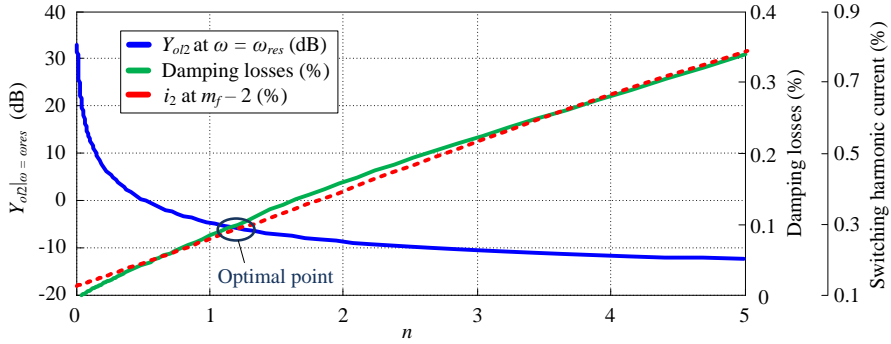


Figure 5.19: Optimal selection of the capacitors ratio for an LCL filter with shunt RC damper as a trade-off between the resonance peak, damping losses and grid current harmonics at the most dominant harmonic frequency.

The final ratings of the filters in the case of a robust design are shown in Table 5.2. The performances of the passive filters are shown in Table 5.3 based on real test results. Low total loss and around half size are obtained by adopting the 2 trap filter. The associated loss due to high ripple in the converter side inductance is reduced by changing the magnetic core from Fe-Si powder (which is used for the LCL filter and trap filter) to Sendust. Hence, lower total losses are obtained for the 2 trap filter.

Table 5.2: Filter ratings based on the proposed designed method (Per Phase)

Filter	Passive Device	Peak Rating	L/C/R	LI^2 (HA ²)	Volume (cm ³)
LCL + RC	L_1	23 A	1.5 mH	1.06	513
	L_2	21 A	0.7 mH		
	C_d, C_t	330 V	4.7 μ F		
	R_d	17 W	17 Ω		-
Trap + RC	L_1	23 A	1.5 mH	0.89	513
	L_2	21 A	0.3 mH		
	C_d, C_t	330 V	4.7 μ F		
	L_t	3 A	0.05 mH		
	R_d	14 W	13 Ω		-
2 traps + RC	L_1	25 A	0.8 mH	0.59	200
	L_2	21 A	0.2 mH		
	C_d, C_t	330 V	4.7 μ F		
	L_t	5 A	0.05 mH		
	C_{r2}	330 V	0.44		
	L_{r2}	2.5 A	0.14 mH		
	R_d	17 W	7.7 Ω		-

Table 5.3: Measured power losses and power quality indices (%)

Description	<i>LCL+RC</i>	<i>Trap+RC</i>	<i>2 traps+RC</i>
Total Losses	1	1	0.95
Damping Losses	0.075	0.071	0.053
<i>THD_{vPCC}</i>	0.45	0.45	0.39
<i>THD_{iPCC}</i>	1.27	1.12	2.67
<i>i_{2(mf-2)}</i>	0.083	0.0083	0.0328

5.4.3. LOSS OPTIMIZED PASSIVE DAMPING DESIGN

The previous analysis was performed for a fixed switching frequency in the filter design (10 kHz). In addition, the design of the passive filter accounted for large variation in the filter parameters, which may not be likely to occur in practice. Considering the same stability margins for several passive filters, a loss optimized passive damping design can be performed. To ensure the same stability margins from the filter and control system, the Maximum Peak Criterion (MPC) is adopted in the filter design.

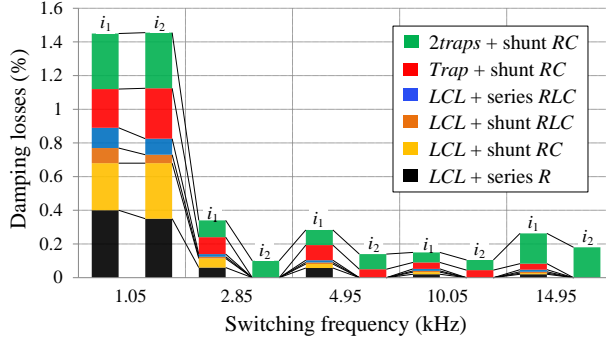
MPC makes use of the sensitivity indicator (M_s), which denotes the amount of resonance (i.e. maximum peaking) in the sensitivity transfer function $S(s)$ of the control system. $S(s)$ and M_s for the current control feedback are defined as [108]:

$$\begin{cases} S_x(s) = \frac{1}{1+Y_{olx}(s)}, & x = \overline{1,2} \\ M_{Sx} = \max |S_x(j\omega)| \end{cases} \quad (5-18)$$

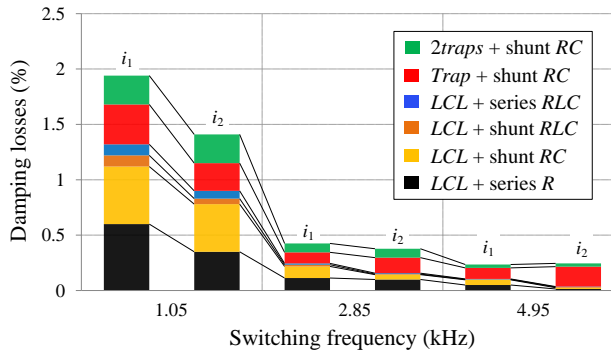
where x is the number of controlled current variable ($x = 1$ for converter current control and $x = 2$ for grid current control). The inverse of the maximum sensitivity gain, $(M_s)^{-1}$ gives the closest distance between the critical point $(-1,0)$ and the open loop transfer function.

In *Figure 5.20*, the damping losses are shown for different passive filters as a function of the switching frequency, controlled current variable or different attenuation requirements. Relatively low damping losses are obtained with the proposed design method, especially if the switching frequency of the VSC is higher than 2.5 kHz. The *2 traps* filter has relatively high losses at high frequencies, as a consequence of significant size reduction, which leads to a high harmonic current flow in the filter (due to high ripple in the converter side inductance). The shunt or series *RLC* damper circuits provide low losses (up to 0.1 %) for the entire simulated frequency range (1-15 kHz). In the filter design procedure, the damping losses are

calculated analytically using the methodology described in [72], while the final results shown in *Figure 5.20* are obtained using PLECS circuit simulator and Matlab Simulink.



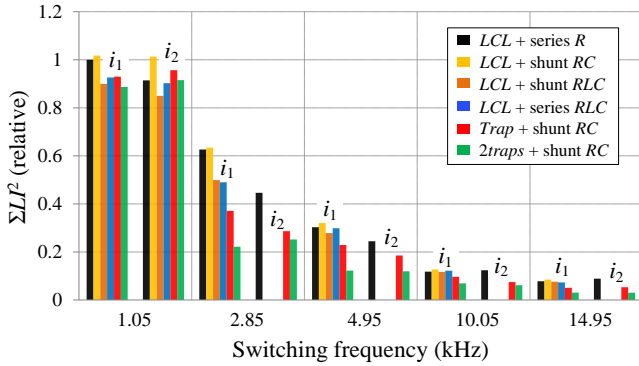
(a) IEEE 1547



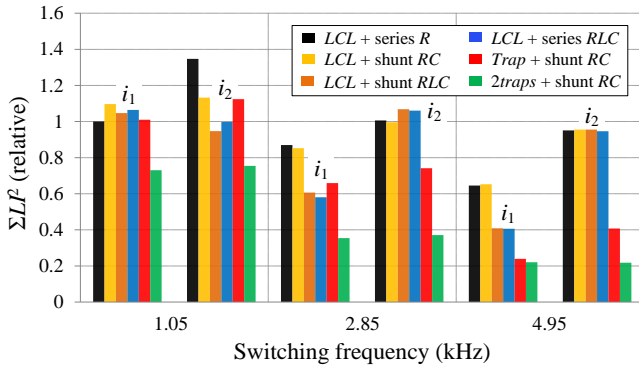
(b) BDEW

Figure 5.20: Damping losses in the filter at rated current as function of switching frequency for converter (i_1) and grid current control (i_2).

The size evaluation of the passive filters is shown in *Figure 5.21* by the total energy stored in inductors. The size is relative to the *LCL* filter with a *series resistor* working at 1.05 kHz. Adopting single or multi-tuned traps can reduce the size of the passive filter by a factor of 3 depending on the operating switching frequency, number of tuned traps or adopted attenuation recommendations. However, the use of passive damping in addition to the tuned traps may lead to significant damping losses as shown in *Figure 5.20*. For stringent harmonic recommendations, it is not possible a significant decrease in the filter size by increasing the switching frequency (IEEE 1547 vs. BDEW).



(a) IEEE 1547



(b) BDEW

Figure 5.21: Filter size evaluation for converter (i_1) and grid current control (i_2) by total relative stored energy in inductors (relative to the LCL + series R damper working at $f_s = 1.05$ kHz).

5.5. IMPROVED PASSIVE DAMPED TRAP FILTER

Since the use of single or multi-tuned traps in the filter increases the harmonic current in the filter because of increased current ripple in the converter side inductance, conventional passive damping solutions lead to relatively high losses. Therefore, a new passive damped filter topology is presented, which offers a good trade-off in terms of size and damping losses compared with the traditional LCL filter and the single-tuned trap filter. The proposed filter replaces the capacitor of the LCL filter with a C-type filter as presented in Figure 5.22. C-type filters are used to reduce multiple harmonic frequencies, especially above the tuning frequency of the filter given by the two capacitors and the tuned inductor, where the tuning frequency is typically the most dominant harmonic frequency [109]. Additionally, the tuned circuit nC_f-L_f is tuned at the fundamental frequency in order

to bypass the fundamental losses in the resistor. Therefore, the *C-type* filter can provide low damping losses and good harmonic attenuation compared to more conventional passive filters.

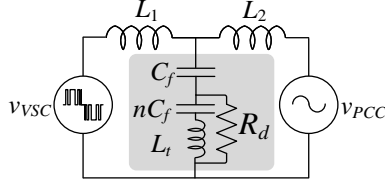


Figure 5.22: Proposed passive damped filter topology, which is a *C-type* filter.

5.5.1. OPERATING PRINCIPLE OF THE PROPOSED FILTER

The functionalities of the proposed *C-type* filter are slightly different from the conventional design. Depending on how the damping resistor is selected, the behavior of the proposed filter will be either towards the conventional *LCL* filter or towards the *trap* filter. For example, when the resistor is zero, then the tuned circuit nC_f-L_t is short-circuited and the filter behavior is identical to the *LCL* filter. If the damping resistor is very large, then the current will flow only into the tuned circuit omitting the resistor and the filter behaving like a *trap* filter.

The quality factor of the filter, that gives the damping effect in the circuit and whose value depends of the whole filter components can be written as:

$$Q = \frac{R_0}{R_d} \quad (5-19)$$

where R_0 denotes the characteristic resistance of the filter, that is the resistance of the filter when the damping resistor is zero and whose value is $R_0 = \sqrt{L_1 L_2 / [(L_1 + L_2) C_f]}$.

In Figure 5.23, a typical harmonic attenuation profile of the proposed filter is illustrated together with the *LCL* and *trap* filters, respectively. The proposed filter has the benefits off the both *LCL* and *trap* filters in that the switching harmonics are attenuated more selectively. In addition, a good damping performance is obtained.

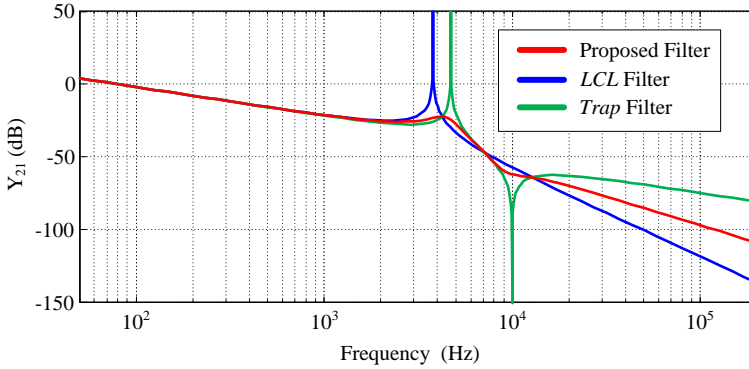


Figure 5.23: Transfer admittance of the proposed filter with optimum damping resistor (red line), zero damping resistor (LCL filter) and infinite damping resistor (trap filter).

5.5.2. DESIGN OF THE PROPOSED PASSIVE DAMPED FILTER

The *C-type* filter is tuned in such a way that the switching harmonics are to be attenuated by the equivalent tuned circuit of the filter (neglecting the damping resistor).

The choice of the tuned capacitor C_t is dictated by the amount of damping that is required. For high resonance damping attenuation, C_t is required to be in the same range as the filter capacitor C_f or smaller. With a larger C_t , the damping of the filter becomes very limited. The tuned capacitor can be written as:

$$C_t = nC_f \quad (5-20)$$

The filter capacitor and tuned capacitor are selected equal ($n = 1$), which would ensure that the total damping can be achieved in the control to output admittance is well below 0 dB. The actual damping effect depends also on the value of the damping resistor.

The tuned inductor is selected in such a way that harmonics at the switching frequency ω_{sw} should be cancelled. This implies that:

$$\omega_{sw} = \sqrt{\frac{(n+1)}{nL_t C_f}} \quad (5-21)$$

Therefore, the tuned inductor can be written as:

$$L_t = \frac{n+1}{nC_f \omega_{sw}^2} \quad (5-22)$$

The value of the damping resistor can be found in the same way as it was shown in the previous section, i.e. by finding the quality factor of the filter, which minimizes the filter admittance magnitude. Then, the damping resistor can be found from the optimum quality factor. Additionally, the damping losses can be selectively eliminated if the tuned frequency ω_t of the nC_f-L_t branch is selected at the dominant harmonic order according to:

$$\omega_t = \frac{\omega_{sw}}{\sqrt{(n+1)}} \quad (5-23)$$

It follows that if the fundamental losses are to be cancelled as in the case of a conventional *C-type* filter, then this would imply that n should be very large. However, a large n means reduced damping effect from the filter. On the other hand, in PWM converters, the most dominant harmonics occur at the switching frequency. Therefore, n can be selected low and the tuned frequency of the nC_f-L_t branch can be selected close to the switching frequency. In Figure 5.24, the measured grid current waveform for the proposed filter is illustrated. The results are comparable with the *trap* filter with *shunt RC damper* illustrated in Table 5.3.

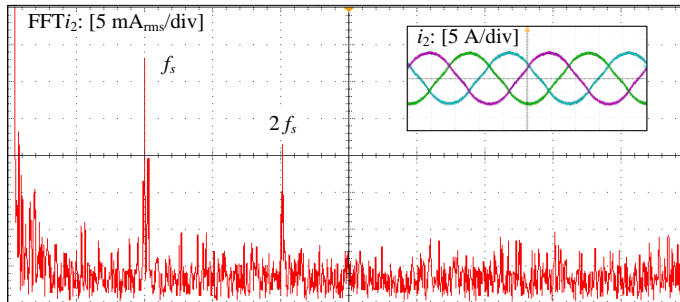


Figure 5.24: Measured grid current waveforms and harmonic spectrum of the proposed filter, with $L_1 = 1.5 \text{ mH}$ (3 %), $L_2 = 0.5 \text{ mH}$ (1 %), $C_f = 4.7 \text{ }\mu\text{F}$ (2.3 %), $P_d = 0.07 \%$ ($S_{VSC} = 10 \text{ kVA}$, $f_{sw} = 10 \text{ kHz}$).

5.6. SUMMARY

A stability evaluation of grid-connected VSCs with high-order passive filters has been presented in this chapter. By placing the resonance frequency according to the critical frequency given by the sampling delay, either of the converter or grid current control is inherently stable without any damping. However, it creates a negative resistance in the control response of the output admittance of the VSC, which may interact with the grid impedance. By adopting passive damping, the VSC output admittance can be made passive, which means that harmonic

interactions between the VSC and grid impedance are avoided (provided the grid impedance is passive as well).

A review of the conventional design methods of the *LCL* filter reveals that by reducing the inductor size in order to minimize the filter size, the harmonic current flow in the filter increases, especially at low frequencies. In these situations, adopting passive damping methods can result in excessive losses in the filter. Therefore, an optimal design method of the passive dampers is proposed, which simplifies the passive damping design and which can ensure the maximum damping performance by using lower rated damping components. Further, it can find the best trade-offs between different features of the passive filters, such as the harmonic attenuation, power losses in the resistor or the amount of the resonance damping, given by the quality factor.

To differentiate between the features of the different passive filter topologies, an in-depth comparison is completed. Passive damped filters with *RLC* dampers in different configurations can be tuned in such a way to obtain very low losses over a wide range of operating conditions. On the other hand, the use of multi-tuned traps makes it possible to reduce the overall filter size significantly, at a price of increased component count and complexity. However, reduced filter size translates into high harmonic current flow in the filter, and excessive power loss may not be avoided. Therefore, a new passive damped filter is presented which offers a good trade-off in terms of size and loss compared with the traditional *LCL* filter and the single-tuned *trap* filter.

CHAPTER 6. CONCLUSIONS

This chapter summarizes the main conclusions of this research and points out the main findings. Future expectations and developments in the field of power filters are also discussed.

6.1. SUMMARY

The main goal of this project was to investigate the stability of grid-connected VSCs seen from the power filter design point of view. To deal with all aspects of the passive filter design, the content of the report has been structured as follows.

The introductory chapter includes project motivation, background in harmonic filtering, a short review of stability interactions related to VSCs, problem formulation, project objectives and limitations of this work.

In *Chapter 2*, several specifications and requirements for passive filters were given at a system level. By considering the passive filter as a black-box model, it is possible to establish a set of filter design prerequisites by inspection of the filter behavior from the converter side and grid side, independently. For instance, the dependencies of the output harmonic voltage of the converter with different operation modes of the VSC are considered. Then, the influence of the worst case harmonic grid impedance on the filter and some methods to describe the frequency dependent grid impedance are given. The concept of the filter virtual admittance is introduced afterwards, which can facilitate the choice of suitable passive filter topologies.

In *Chapter 3*, several passive filters and a comprehensive selection of passive damping circuits for use in VSC applications are categorized together with their advantages. It is shown how a high-order filter, like the *LCL* or *trap* filters can provide reduced size as consequence of higher filtering attenuation. However, the drawback denoted by the presence of resonances in the filter frequency response, may require the use of an additional damping circuit. Different passive filter solutions to damp the filter resonances are given. However, the best suited topology is to be decided depending on the intended application since with passive damping, there is no significant influence on the low and high frequency behavior of the filter. It is also shown, how the winding resistance of the inductors can contribute to the damping of the filter and can significantly reduce the resonant peaks in the frequency response. The inductance dependence with current plays a role in lowering the filter resonance frequency with decreasing the operating current.

As main part of the passive filters, the inductive components are characterized in *Chapter 4*. It is shown how in a high-order filter, the inductor on the converter side of the VSC is the limiting factor, when it has to be decided about the passive filter size, cost and efficiency. Several magnetic materials are compared in terms of power losses and their non-linear characteristics are fully explored. The role of the inductors in shunt filters or in the grid side of the filters are also highlighted, together with corresponding sizing considerations.

The stability evaluation of grid-connected VSCs with high-order passive filters is presented in *Chapter 5*. By placing the resonance frequency according to the critical frequency given by the sampling delay in the VSC, either of the converter or grid current control is inherently stable without any damping. However, it creates a negative resistance in the control response of the output admittance of the VSC, which may interact with the grid impedance. By adopting passive damping, the VSC output admittance can be made passive, which means that harmonic interactions between the VSC and grid impedance are avoided. An optimal design method of several passive dampers is proposed, which simplifies the passive damping design and can ensure the maximum damping performance by using lower rated damping components. Further, it can find the best trade-offs between different features of the passive filters, such as the harmonic attenuation, power losses in the resistor or the amount of the resonance damping, given by the quality factor. An in-depth comparison of several passive damped filters is completed. Passive filters with *RLC* dampers in different configurations can be tuned in such a way to obtain very low losses over a wide range of operating conditions. On the other hand, the use of multi-tuned traps makes possible to reduce the overall filter size significantly, at a price of increased component count and complexity. However, reduced filter size translates into high harmonic current flow in the filter, and extra power losses may not be avoided. Therefore, a new passive damped filter is presented, which offers a good trade-off in terms of size and loss compared with the traditional *LCL* filter and the single-tuned *trap* filter.

6.2. MAIN CONTRIBUTIONS

The main contributions of this work can be summarized as follow:

- Stability analysis of grid-connected VSC with high-order passive filters: the influence of the converter and grid current control feedback on the VSC output admittance is investigated. While both control feedbacks can be inherently stable, they introduce a negative resistance in control response of the VSC, which may interfere with the grid impedance. With the proposed method, it becomes apparently easy to design the VSC with the passive filter stable for a wide range of grid impedances.

- In-depth core loss evaluation of inductors: Several magnetic materials are compared in terms of power losses and their non-linear characteristics. It provides more details about the equivalent loss in inductors, which greatly influence on the overall passive filter efficiency, cost and size.
- New optimal design method for passive-damped filters: the conventional design method of second-order passive damped filters used in dc-dc converters and developed by Middlebrook is extended to high-order filters used in grid-connected VSC applications. It provides a straightforward design approach in finding the resonance frequency of the filter, quality factor and optimal damping parameters which otherwise are impossible to be found. It can find the best trade-offs between different features of the passive filters, such as the harmonic attenuation, power losses in the resistor or the amount of the resonance damping.
- Review of high-order passive filters for grid-connected VSC: the most common passive filter topologies are reviewed and evaluated in terms of damping capability, stored energy in the passive components and power loss in the damping circuit. Additionally, the influences of different switching frequencies of power converters on the passive filter design are also discussed in the frequency range of 1-15 kHz. For specific topologies, the results show that it is possible to limit the damping loss below 0.1 % over a wide range of operating conditions.
- New passive filter topology for VSC: a passive damped filter is proposed, which can offer a good trade-off between the conventional *LCL* or *trap* filter. It can provide additional benefits compared with more conventional filter topologies: decreased VAR ratings, lower damping losses, less susceptible to component tolerances, decreased risk of harmonic amplification, etc.

6.3. FUTURE WORK

As part of the outcome of this work is that new research questions related to the filter design can be defined:

- ▶ Optimization of the converter side inductor, by harmonization between core loss of different magnetic materials and PWM method: the core loss is highly influenced by duty cycle and magnetic properties of the core. Hence, it is possible to obtain better designs trade-offs for the converter side inductance of high-order passive filters.
- ▶ Aggregation of multiple VSC with passive filters, to model the equivalent damping between the converters and to model the corresponding harmonic interaction: for applications with multiple paralleled VSCs, it is possible to reduce the required filtering, if one could account for the interactions between the converters.

- ▶ Passivity based design with reduced passive filter size: passivity based theorem can ensure that the grid impedance does not destabilize the VSC. However, is not yet clear how conservative is the passivity based design and how it will limit the performance of the VSC. In addition, it is required to determine how the size of passive components can be minimized in the case of stable and robust VSC.
- ▶ Clarification of harmonic standards for VSC connection to the utility grids: the applicability of harmonic standards for frequencies above 2 kHz is not very clear and passive filter design to meet performance criteria is questionable. To what extent, the filtering of high frequency harmonics is adequate?
- ▶ Simulation and also the test of a more complete utility grid with particular configuration, in order to find the worst case grid impedance parameters. One reason is to find the contribution of the grid impedance to harmonic filtering. Or in other words, how to find the optimum selection of the shunt capacitor and grid side inductance of high order filters? It is interesting to determine whether there is a significant decrease or increase in the filter size with the consideration of the grid impedance for a particular grid configuration.
- ▶ Optimization of current controller design with accurate characterization of the passive components: the non-linear characteristics of the passive filter challenges the current controller design. A better coordination between the current controller design and detailed knowledge of the passive filter is possible and would improve the performance of a grid-connected VSC.
- ▶ Multi-tuned trap filters in combination with EMI filters: the use of multi-tuned trap filters implies a relatively reduced high frequency attenuation of the filter. Therefore, it is required to combine trap filters with additional filter arrangements in order to ensure an effective filtering solution, especially for higher frequencies where the trap filter is not effective.

REFERENCES

- [1] M. H. J. Bollen and K. Yang, “Harmonic aspects of wind power integration,” *J. Mod. Power Syst. Clean Energy*, vol. 1, no. 1, pp. 14–21, Jul. 2013.
- [2] C. Yoon, H. Bai, R. Beres, X. Wang, C. Bak, and F. Blaabjerg, “Harmonic Stability Assessment for Multi-Paralleled, Grid-Connected Inverters,” *IEEE Trans. Sustain. Energy*, no. Early Access, 2016.
- [3] M. Cespedes and J. Sun, “Impedance modeling and analysis of grid-connected voltage-source converters,” *IEEE Trans. Power Electron.*, vol. 29, no. 3, pp. 1254–1261, 2014.
- [4] J. Sun, “Impedance-Based Stability Criterion for Grid-Connected Inverters,” *IEEE Trans. Power Electron.*, vol. 26, no. 11, pp. 3075–3078, Nov. 2011.
- [5] J. Muhlethaler, M. Schweizer, R. Blattmann, J. W. Kolar, and A. Ecklebe, “Optimal Design of LCL Harmonic Filters for Three-Phase PFC Rectifiers,” *IEEE Trans. Power Electron.*, vol. 28, no. 7, pp. 3114–3125, Jul. 2013.
- [6] N. Flourentzou, V. G. Agelidis, and G. D. Demetriades, “VSC-Based HVDC Power Transmission Systems: An Overview,” *IEEE Trans. Power Electron.*, vol. 24, no. 3, pp. 592–602, Mar. 2009.
- [7] J. M. Carrasco, L. G. Franquelo, J. T. Bialasiewicz, E. Galvan, R. C. PortilloGuisado, M. A. M. Prats, J. I. Leon, and N. Moreno-Alfonso, “Power-Electronic Systems for the Grid Integration of Renewable Energy Sources: A Survey,” *IEEE Trans. Ind. Electron.*, vol. 53, no. 4, pp. 1002–1016, Jun. 2006.
- [8] F. Blaabjerg, Z. Chen, and S. B. Kjaer, “Power Electronics as Efficient Interface in Dispersed Power Generation Systems,” *IEEE Trans. Power Electron.*, vol. 19, no. 5, pp. 1184–1194, Sep. 2004.
- [9] B. Singh, B. N. Singh, A. Chandra, K. Al-Haddad, A. Pandey, and D. P. Kothari, “A review of single-phase improved power quality ac~dc converters,” *IEEE Trans. Ind. Electron.*, vol. 50, no. 5, pp. 962–981, Oct. 2003.
- [10] C. Ruester, S. Hoppert, and J. Blum, “Power Quality and Stability Issues in Modern Distribution Grids: Identification and Mitigation,” in *Proc. of*

- CIREC Workshop*, 2014, no. 358, pp. 1–5.
- [11] “IEEE Guide for Application and Specification of Harmonic Filters,” *IEEE Std 1531-2003*, 2003.
- [12] J. C. Das, “Passive Filters—Potentialities and Limitations,” *IEEE Trans. Ind. Appl.*, vol. 40, no. 1, pp. 232–241, Jan. 2004.
- [13] B. Singh, V. Verma, A. Chandra, and K. Al-Haddad, “Hybrid filters for power quality improvement,” *IEE Proc. - Gener. Transm. Distrib.*, vol. 152, no. 3, p. 365, 2005.
- [14] “Guide to the Specification and Design Evaluation of AC Filters for HVDC systems,” *CIGRE Work. Gr. 14.30*, 1999.
- [15] “Benchmark Systems for Network Integration of Renewable and Distributed Energy Resources,” *CIGRE Task Force C6.04*, 2014.
- [16] R. Teichmann, M. Malinowski, and S. Bernet, “Evaluation of Three-Level Rectifiers for Low-Voltage Utility Applications,” *IEEE Trans. Ind. Electron.*, vol. 52, no. 2, pp. 471–481, Apr. 2005.
- [17] K. Jalili and S. Bernet, “Design of LCL Filters of Active-Front-End Two-Level Voltage-Source Converters,” *IEEE Trans. Ind. Electron.*, vol. 56, no. 5, pp. 1674–1689, May 2009.
- [18] A. M. Hava, T. A. Lipo, and W. L. Erdman, “Utility interface issues for line connected PWM voltage source converters: a comparative study,” in *Proc. of IEEE Applied Power Electronics Conference and Exposition*, 1995, pp. 125–132.
- [19] M. Liserre, F. Blaabjerg, and S. Hansen, “Design and Control of an LCL-Filter-Based Three-Phase Active Rectifier,” *IEEE Trans. Ind. Appl.*, vol. 41, no. 5, pp. 1281–1291, Sep. 2005.
- [20] R. N. Beres, X. Wang, M. Liserre, F. Blaabjerg, and C. L. Bak, “A Review of Passive Power Filters for Three-Phase Grid-Connected Voltage-Source Converters,” *IEEE J. Emerg. Sel. Top. Power Electron.*, vol. 4, no. 1, pp. 54–69, Mar. 2016.
- [21] T. Shimizu and S. Iyasu, “A practical iron loss calculation for AC filter inductors used in PWM inverters,” *IEEE Trans. Ind. Electron.*, vol. 56, no. 7, pp. 2600–2609, 2009.

- [22] H. Matsumori, T. Shimizu, K. Takano, and H. Ishii, "Evaluation of Iron Loss of AC Filter Inductor Used in Three-Phase PWM Inverters Based on an Iron Loss Analyzer," *IEEE Trans. Power Electron.*, vol. 31, no. 4, pp. 3080–3095, Apr. 2016.
- [23] E. W. Kimbark, *Direct Current Transmission, Volume I*. Wiley-Interscience, 1971.
- [24] R. D. Middlebrook, "Design Techniques for Preventing Input-Filter Oscillations in Switched-Mode Regulators," in *Proc. of Power Convers. Conf., 1978*, pp. A3.1–A3.16.
- [25] "China Wind Power Center (CWPC)," 2014. [Online]. Available: <http://www.cwpc.cn/cwpp/files/1314/1050/5552/6.-.pdf>.
- [26] I. Shumkov, "Dong's Anholt Offshore Wind Farm shuts down due to new cable fault," *Wind Energy News*, 2015. [Online]. Available: <https://www.wind-watch.org/news/2015/02/24/dongs-anholt-offshore-wind-farm-shuts-down-due-to-new-cable-fault/>. [Accessed: 23-May-2016].
- [27] J. H. R. Enslin and P. J. M. Heskes, "Harmonic interaction between a large number of distributed power inverters and the distribution network," *IEEE Trans. Power Electron.*, vol. 19, no. 6, pp. 1586–1593, 2004.
- [28] E. Kimbark, *Power System Stability: 1. Elements of Stability Calculations*. John Wiley & Sons, 1948.
- [29] Anatol I. Zverev, *Handbook of Filter Synthesis*. John Wiley & Sons, 1967.
- [30] R. D. Middlebrook, "Input Filter Considerations in Design and Application of Switching Regulators," in *Proc. of IEEE IAS Annual Meeting*, 1976, pp. 366–382.
- [31] M. Liserre, F. Blaabjerg, and S. Hansen, "Design and control of an LCL-filter based three-phase active rectifier," in *Proc. of IEEE Industry Applications Conference. 36th IAS Annual Meeting*, 2001, vol. 1, no. C, pp. 299–307.
- [32] J. Muhlethaler, M. Schweizer, R. Blattmann, J. W. Kolar, and A. Ecklebe, "Optimal design of LCL harmonic filters for three-phase PFC rectifiers," in *Proc. of IECON 2011 - 37th Annual Conference of the IEEE Industrial Electronics Society*, 2011, pp. 1503–1510.
- [33] T. Shimizu, K. Mishima, and K. Ishii, "Mitigation of Inductor Loss Based

- on Minor-Loop Hysteresis Characteristics,” in *Proc. of The 25th International Telecommunications Energy Conference, 2003. INTELEC '03.*, 2003, pp. 834–839.
- [34] S. Iyasu, T. Shimizu, and K. Ishii, “A novel iron loss calculation method on power converters based on dynamic minor loop,” in *Proc. of European Conference on Power Electronics and Applications*, 2005, p. P.1–P.10.
- [35] M. Liserre, F. Blaabjerg, and S. Hansen, “Design and Control of an LCL-Filter-Based Three-Phase Active Rectifier,” *IEEE Trans. Ind. Appl.*, vol. 41, no. 5, pp. 1281–1291, Sep. 2005.
- [36] “IEEE Recommended Practice and Requirements for Harmonic Control in Electric Power Systems,” IEEE Std 519-2014 (Revision of IEEE Std 519-1992),” 2014.
- [37] “IEC 61000-3-2: Limits for harmonic current emissions,” *IEC Stand.*, 2004.
- [38] “IEC 61000-3-12: Limits for harmonic current produced by equipment connected to public low voltage systems with input current $> 16\text{A}$ and $\leq 75\text{A}$ per phase,” *IEC Stand.*, 2005.
- [39] “VDE-AR-N 4105: Power generation systems connected to the low-voltage distribution network - Technical minimum requirements for the connection to and parallel operation with low-voltage distribution networks,” *VDE Stand.*, 2011.
- [40] “Generating Plants Connected to the Medium-Voltage Network,” *BDEW Stand.*, 2008.
- [41] “IEEE Standard for Interconnecting Distributed Resources with Electric Power Systems,” *IEEE Stand. 1547.2-2008*, 2009.
- [42] “IEC 61727: Photovoltaic (PV) systems - Characteristic of the utility interface,” *IEC Stand.*, 2004.
- [43] “UL1741 - Inverters, Converters, and Controllers for Use in Independent Power Systems,” *UL Stand.*, 2001.
- [44] “IEC 61000-4-30: Testing and Measurement Techniques–Power Quality Measurement Methods,” *IEC Stand.*, 2003.
- [45] “IEC 61000-4-7: Testing and measurement techniques – General guide on harmonics and interharmonics measurements and instrumentation, for power

- supply systems and equipment connected thereto,” *IEC Stand.*, 2002.
- [46] A. A. Rockhill, M. Liserre, R. Teodorescu, and P. Rodriguez, “Grid-Filter Design for a Multimegawatt Medium-Voltage Voltage-Source Inverter,” *IEEE Trans. Ind. Electron.*, vol. 58, no. 4, pp. 1205–1217, Apr. 2011.
- [47] J. Rocabert, A. Luna, F. Blaabjerg, and P. Rodriguez, “Control of Power Converters in AC Microgrids,” *IEEE Trans. Power Electron.*, vol. 27, no. 11, pp. 4734–4749, Nov. 2012.
- [48] L. Shen, G. Asher, P. Wheeler, and S. Bozhko, “Optimal LCL filter design for 3-phase Space Vector PWM rectifiers on variable frequency aircraft power system,” in *Proc. of 2013 15th European Conference on Power Electronics and Applications (EPE)*, 2013, pp. 1–8.
- [49] M. Liserre, F. Blaabjerg, and A. Dell’Aquila, “Step-by-step design procedure for a grid-connected three-phase PWM voltage source converter,” *Int. J. Electron.*, vol. 91, no. 8, pp. 445–460, Aug. 2004.
- [50] R. Teodorescu, M. Liserre, and P. Rodríguez, *Grid Converters for Photovoltaic and Wind Power Systems*. Wiley-IEEE Press, 2011.
- [51] M. Jordan, H. Langkowski, T. Do Thanh, and D. Schulz, “Frequency dependent grid-impedance determination with pulse-width-modulation-signals,” in *Proc. of 7th International Conference-Workshop Compatibility and Power Electronics (CPE)*, 2011, pp. 131–136.
- [52] “AC harmonic filters and reactive compensation for HVDC with particular reference to non-characteristic harmonics,” *Cigre Work. Gr. 14.03*, 1990.
- [53] J.C. Das, *Power System Harmonics and Passive Filter Designs*. Wiley-IEEE Press, 2015.
- [54] Y. Tang, P. C. Loh, P. Wang, F. H. Choo, and K. K. Tan, “Improved one-cycle-control scheme for three-phase active rectifiers with input inductor-capacitor-inductor filters,” *IET Power Electron.*, vol. 4, no. 5, pp. 603–614, 2011.
- [55] W. Wu, Y. He, and F. Blaabjerg, “An LLCL Power Filter for Single-Phase Grid-Tied Inverter,” *IEEE Trans. Power Electron.*, vol. 27, no. 2, pp. 782–789, Feb. 2012.
- [56] J. Xu, J. Yang, J. Ye, Z. Zhang, and A. Shen, “An LTCL Filter for Three-Phase Grid-Connected Converters,” *IEEE Trans. Power Electron.*, vol. 29,

- no. 8, pp. 4322–4338, Aug. 2014.
- [57] W. Guo, T. Mingxing, and R. Enen, “Structure design and its parameter optimization of output filter in current balance compensation inverter for electrified railway,” in *Proc. of the 2nd International Symposium on Power Electronics for Distributed Generation Systems*, 2010, pp. 791–795.
- [58] F. Feng, “Optimal Damping of EMI Filter Input Impedance,” *IEEE Trans. Ind. Appl.*, vol. 47, no. 3, pp. 1432–1440, May 2011.
- [59] Y. Tang, P. C. Loh, P. Wang, F. H. Choo, F. Gao, and F. Blaabjerg, “Generalized Design of High Performance Shunt Active Power Filter With Output LCL Filter,” *IEEE Trans. Ind. Electron.*, vol. 59, no. 3, pp. 1443–1452, Mar. 2012.
- [60] M. A. Abusara and S. M. Sharkh, “Design and control of a grid-connected interleaved inverter,” *IEEE Trans. Power Electron.*, vol. 28, no. 2, pp. 748–764, 2013.
- [61] A. Lesnicar and R. Marquardt, “An innovative modular multilevel converter topology suitable for a wide power range,” in *Proc. IEEE Power Tech Conference*, 2003, vol. 3, pp. 272–277.
- [62] D. O. Boillat, F. Krismer, and J. W. Kolar, “Design Space Analysis and Pareto Optimization of Output Filters for Switch-Mode AC Power Sources,” *IEEE Trans. Power Electron.*, vol. 30, no. 12, pp. 6906–6923, Dec. 2015.
- [63] A.-S. A. Luiz and B. J. Cardoso Filho, “Analysis of passive filters for high power three-level rectifiers,” in *Proc. of 34th Annual Conference of IEEE Industrial Electronics*, 2008, pp. 3207–3212.
- [64] Y. Patel, D. Pixler, and A. Nasiri, “Analysis and design of TRAP and LCL filters for active switching converters,” in *Proc. of 2010 IEEE International Symposium on Industrial Electronics*, 2010, pp. 638–643.
- [65] A. M. Cantarellas, E. Rakhshani, D. Remon, and P. Rodriguez, “Grid connection control of VSC-based high power converters for wave energy applications,” in *Proc. of IECON 2013 - 39th Annual Conference of the IEEE Industrial Electronics Society*, 2013, pp. 5092–5097.
- [66] F. Li, X. Zhang, H. Zhu, H. Li, and C. Yu, “An LCL-LC Filter for Grid-Connected Converter: Topology, Parameter, and Analysis,” *IEEE Trans. Power Electron.*, vol. 30, no. 9, pp. 5067–5077, Sep. 2015.

- [67] G. Gohil, L. Bede, R. Teodorescu, T. Kerekes, and F. Blaabjerg, "Line Filter Design of Parallel Interleaved VSCs for High-Power Wind Energy Conversion Systems," *IEEE Trans. Power Electron.*, vol. 30, no. 12, pp. 6775–6790, Dec. 2015.
- [68] Y. S. Noh, Y. H. Ji, S. H. Song, Y. C. Jung, and C. Y. Won, "Design of trap-CL filter of single-phase flyback inverter for photovoltaic microinverter," in *Proc. of 2012 IEEE 7th International Power Electronics and Motion Control Conference - ECCE Asia, IPEMC 2012*, 2012, vol. 2, pp. 1413–1417.
- [69] R. N. Beres, X. Wang, F. Blaabjerg, M. Liserre, and C. L. Bak, "Optimal Design of High-Order Passive-Damped Filters for Grid-Connected Applications," *IEEE Trans. Power Electron.*, vol. 31, no. 3, pp. 2083–2098, Mar. 2016.
- [70] B. Bolsens, K. De Brabandere, J. Van Den Keybus, J. Driesen, and R. Belmans, "Model-Based Generation of Low Distortion Currents in Grid-Coupled PWM-Inverters Using an LCL Output Filter," *IEEE Trans. Power Electron.*, vol. 21, no. 4, pp. 1032–1040, 2006.
- [71] K. H. Ahmed, S. J. Finney, and B. W. Williams, "Passive Filter Design for Three-Phase Inverter Interfacing in Distributed Generation," in *Proc. of Compatibility in Power Electronics*, 2007, pp. 1–9.
- [72] P. Channegowda and V. John, "Filter Optimization for Grid Interactive Voltage Source Inverters," *IEEE Trans. Ind. Electron.*, vol. 57, no. 12, pp. 4106–4114, Dec. 2010.
- [73] T. C. Y. Wang, Z. Ye, G. Sinha, and X. Yuan, "Output filter design for a grid-interconnected three-phase inverter," in *Proc. of IEEE 34th Annual Conference on Power Electronics Specialist, 2003. PESC '03.*, 2003, vol. 2, pp. 779–784.
- [74] Lei Xing, F. Feng, and Jian Sun, "Optimal Damping of EMI Filter Input Impedance," *IEEE Trans. Ind. Appl.*, vol. 47, no. 3, pp. 1432–1440, May 2011.
- [75] W. Wu, Y. Sun, M. Huang, X. Wang, H. Wang, F. Blaabjerg, M. Liserre, H. S. Chung, and S. Member, "A Robust Passive Damping Method for LLCL-Filter-Based Grid-Tied Inverters to Minimize the Effect of Grid Harmonic Voltages," *IEEE Trans. Power Electron.*, vol. 29, no. 7, pp. 3279–3289, Jul. 2014.

- [76] M. L. Heldwein, "EMC Filtering of Three-Phase PWM Converters," ETH Zurich, 2008.
- [77] B. C. Parikshith and V. John, "Higher Order Output Filter Design for Grid Connected Power Converters," in *Proc. of Fifteenth National Power Systems Conference (NPSC), IIT Bombay*, 2008, pp. 614–619.
- [78] T. Shimizu, K. Kakazu, K. Takano, and H. Ishii, "Loss evaluation of AC filter inductor core on a PWM converter," in *Proc. of 8th International Conference on Power Electronics - ECCE Asia*, 2011, pp. 1047–1052.
- [79] K. Park, F. Kieferndorf, U. Drofenik, S. Pettersson, and F. Canales, "Weight minimization of LCL filters for high power converters," in *Proc. of 9th International Conference on Power Electronics and ECCE Asia (ICPE-ECCE Asia)*, 2015, pp. 142–149.
- [80] L. Wei, Y. Patel, and C. S. N. Murthy, "Evaluation of LCL filter inductor and active front end rectifier losses under different PWM method," in *Proc. of IEEE Energy Conversion Congress and Exposition*, 2013, pp. 3019–3026.
- [81] "Magnetic Powder Cores," *CSC Cat. ver. 13*, 2015.
- [82] M. S. Rylko, K. J. Hartnett, J. G. Hayes, and M. G. Egan, "Magnetic Material Selection for High Power High Frequency Inductors in DC-DC Converters," in *Proc. of IEEE Applied Power Electronics Conference and Exposition*, 2009, pp. 2043–2049.
- [83] Y. Jiao and F. C. Lee, "LCL Filter Design and Inductor Current Ripple Analysis for a Three-Level NPC Grid Interface Converter," *IEEE Trans. Power Electron.*, vol. 30, no. 9, pp. 4659–4668, Sep. 2015.
- [84] D. G. Holmes, "A general analytical method for determining the theoretical harmonic components of carrier based PWM strategies," in *Proc. of 1998 IEEE Industry Applications Conference. Thirty-Third IAS Annual Meeting*, 1998, vol. 2, no. 2.
- [85] D. G. Holmes and T. A. Lipo, *Pulse Width Modulation for Power Converters: Principles and Practice*. John Wiley & Sons, 2003.
- [86] A. Van Den Bossche and V. C. Valchev, *Inductors and Transformers for Power Electronics*. Taylor & Francis, 2005.
- [87] T. Shimizu, K. Kakazu, K. Takano, and H. Ishii, "Verification of Iron Loss Calculation Method Using a High-Precision Iron Loss Analyzer," *Electr.*

- Eng. Japan*, vol. 192, no. 4, pp. 51–63, Sep. 2015.
- [88] X. Wang, Y. W. Li, F. Blaabjerg, and P. C. Loh, “Virtual-Impedance-Based Control for Voltage-Source and Current-Source Converters,” *IEEE Trans. Power Electron.*, vol. 30, no. 12, pp. 7019–7037, Dec. 2015.
- [89] Y. Tang, P. C. Loh, P. Wang, F. H. Choo, and F. Gao, “Exploring Inherent Damping Characteristic of LCL-Filters for Three-Phase Grid-Connected Voltage Source Inverters,” *IEEE Trans. Power Electron.*, vol. 27, no. 3, pp. 1433–1443, Mar. 2012.
- [90] S. G. Parker, B. P. McGrath, D. G. Holmes, S. Member, B. P. McGrath, and D. G. Holmes, “Regions of Active Damping Control for LCL Filters,” *IEEE Trans. Ind. Appl.*, vol. 50, no. 1, pp. 424–432, Jan. 2014.
- [91] C. Zou, B. Liu, S. Duan, and R. Li, “Influence of Delay on System Stability and Delay Optimization of Grid-Connected Inverters with LCL Filter,” *IEEE Trans. Ind. Informatics*, vol. 10, no. 3, pp. 1775–1784, 2014.
- [92] L. Harnefors, A. G. Yepes, A. Vidal, and J. Doval-Gandoy, “Passivity-Based Stabilization of Resonant Current Controllers With Consideration of Time Delay,” *IEEE Trans. Power Electron.*, vol. 29, no. 12, pp. 6260–6263, Dec. 2014.
- [93] L. Harnefors, A. G. Yepes, A. Vidal, and J. Doval-Gandoy, “Passivity-Based Controller Design of Grid-Connected VSCs for Prevention of Electrical Resonance Instability,” *IEEE Trans. Ind. Electron.*, vol. 62, no. 2, pp. 702–710, Feb. 2015.
- [94] L. Harnefors, X. Wang, A. G. Yepes, and F. Blaabjerg, “Passivity-Based Stability Assessment of Grid-Connected VSCs—An Overview,” *IEEE J. Emerg. Sel. Top. Power Electron.*, vol. 4, no. 1, pp. 116–125, Mar. 2016.
- [95] J. Wang, J. D. Yan, L. Jiang, and J. Zou, “Delay-Dependent Stability of Single-Loop Controlled Grid-Connected Inverters with LCL Filters,” *IEEE Trans. Power Electron.*, vol. 31, no. 1, pp. 743–757, Jan. 2016.
- [96] D. G. Holmes, T. A. Lipo, B. P. McGrath, and W. Y. Kong, “Optimized Design of Stationary Frame Three Phase AC Current Regulators,” *IEEE Trans. Power Electron.*, vol. 24, no. 11, pp. 2417–2426, Nov. 2009.
- [97] Y. Tang, C. Yoon, R. Zhu, and F. Blaabjerg, “Generalized stability regions of current control for LCL-filtered grid-connected converters without passive or active damping,” in *Proc. of IEEE Energy Conversion Congress*

- and Exposition (ECCE)*, 2015, pp. 2040–2047.
- [98] Y. Tang, P. C. Loh, P. Wang, F. H. Choo, and F. Gao, “Exploring Inherent Damping Characteristic of LCL-Filters for Three-Phase Grid-Connected Voltage Source Inverters,” *IEEE Trans. Power Electron.*, vol. 27, no. 3, pp. 1433–1443, Mar. 2012.
- [99] X. Wang, R. Beres, F. Blaabjerg, and P. C. Loh, “Passivity-based design of passive damping for LCL-filtered voltage source converters,” in *Proc. of IEEE Energy Conversion Congress and Exposition (ECCE)*, 2015, pp. 3718–3725.
- [100] O. Brune, “Synthesis of a Finite Two-terminal Network whose Driving-point Impedance is a Prescribed Function of Frequency,” *J. Math. Phys.*, vol. 10, no. 1–4, pp. 191–236, Apr. 1931.
- [101] Yongqiang Lang, Dianguo Xu, S. R. Hadianamrei, and Hongfei Ma, “A Novel Design Method of LCL Type Utility Interface for Three-Phase Voltage Source Rectifier,” in *Proc. of IEEE 36th Conference on Power Electronics Specialists, 2005.*, 2005, pp. 313–317.
- [102] S. Jung, Y. Bae, S. Choi, and H. Kim, “A Low Cost Utility Interactive Inverter for Residential Fuel Cell Generation,” *IEEE Trans. Power Electron.*, vol. 22, no. 6, pp. 2293–2298, Nov. 2007.
- [103] S. V. Araujo, A. Engler, B. Sahan, and F. L. M. Antunes, “LCL filter design for grid-connected NPC inverters in offshore wind turbines,” in *Proc. of 7th International Conference on Power Electronics*, 2007, pp. 1133–1138.
- [104] A. Reznik, M. G. Simoes, A. Al-Durra, and S. M. Muyeen, “LCL Filter Design and Performance Analysis for Grid-Interconnected Systems,” *IEEE Trans. Ind. Appl.*, vol. 50, no. 2, pp. 1225–1232, Mar. 2014.
- [105] G. Zeng, T. W. Rasmussen, and R. Teodorescu, “A novel optimized LCL-filter designing method for grid connected converter,” in *Proc. of International Symposium on Power Electronics for Distributed Generation Systems*, 2010, vol. 2, pp. 802–805.
- [106] J. Verwecken, J. F. Silva, and J. Driesen, “Optimal analytic LCL filter design for grid-connected voltage-source converter,” in *Proc. of Eurocon 2013*, 2013, no. July, pp. 823–830.
- [107] J. M. Bloemink and T. C. Green, “Reducing Passive Filter Sizes with Tuned Traps for Distribution Level Power Electronics,” in *Proc. of 14th European*

Conference on Power Electronics and Applications (EPE 2011), vol., no., pp.1-9, Aug. 30 2011-Sept. 1 2011.

- [108] S. Vesti, T. Suntio, J. a. Oliver, R. Prieto, and J. a. Cobos, "Impedance-based stability and transient-performance assessment applying maximum peak criteria," *IEEE Trans. Power Electron.*, vol. 28, no. 5, pp. 2099–2104, 2013.

- [109] R. Dugan, M. McGranaghan, S. Santoso, and H. Beaty, *Electrical power systems quality*. McGraw-Hill, 2002.



CV

Name Remus Narcis Beres

Date of Birth 23rd January 1984

Place of Birth Sfântu Gheorghe, Covasna (Romania)

Citizen of Romania

Education 2006–2010 B.Sc. in Electrical Engineering, Specialization: Energy Management, Transilvania University of Braşov, Romania

2010–2012 M.Sc. in Electrical Engineering, Specialization: Advanced Electrical Systems, Transilvania University of Braşov, Romania

2011–2013 M.Sc. in Electrical Engineering, Specialization: Wind Power Systems, Aalborg University, Denmark

2013–2016 Ph.D. Studies at Aalborg University, Denmark

Work 2010–2011 Electrical Technician, Electrica Transilvania Sud, Braşov

2012–2013 Researcher at Aalborg University, Department of Energy Technology

ISSN (online): 2246-1248
ISBN (online): 978-87-7112-712-6

AALBORG UNIVERSITY PRESS